Particle Sensors Based on Amplified Quenching of Conjugated Polymers for Biosensing Applications

by

Jessica Huien Liao

B.S. Biomedical Engineering
Rutgers, the State University of New Jersey, 2002

SUBMITTED TO THE DEPARTMENT OF MATERIALS SCIENCE AND ENGINEERING IN PARTIAL FULFILLMENT OF THE REQUIREMENTS FOR THE DEGREE OF

DOCTOR OF PHILOSOPHY IN MATERIALS SCIENCE AND ENGINEERING
AT THE
MASSACHUSETTS INSTITUTE OF TECHNOLOGY

JUNE 2007

Signature of Author: _____
Department of Materials Science and Engineering
May 16, 2007

Certified by: _____
Timothy M. Swager
John D. MacArthur Professor of Chemistry
Thesis Advisor

_____
Michael F. Rubner
TDK Professor of Materials Science and Engineering
Thesis Co-Advisor

Accepted by: _____
Samuel M. Allen
POSCO Professor of Physical Metallurgy
Chair, Departmental Committee on Graduate Students

Dedicated to my family for their love, support, and encouragement

Particle Sensors Based on Amplified Quenching of Conjugated Polymers for Biosensing Applications

by

Jessica Huien Liao

Submitted to the Department of Materials Science and Engineering
on May 16, 2007 in Partial Fulfillment of the
Requirements for the Degree of Doctor of Philosophy in
Materials Science and Engineering

ABSTRACT

Conjugated polymers (CP)s display unique material properties that allow for implementation as sensors. For sensors to operate in complex biological environments, it is important to address the issues of sensitivity and specificity. To develop these attributes in a biosensor design, CP-based core-shell particles have been investigated as potential material platforms to detect protease activity. CP-based particles have greater sensitivity versus CPs in solution due to interchain and intrachain interactions afforded in the solid state. The CP core of the particle can be made using layer-by-layer assembly, a versatile technique that forms uniform polymeric films through non-covalent interactions. To measure the response of CP core particles in aqueous environments, a quantitative ratiometric approach was developed to account for system fluctuations encountered with particle dispersions. This method can help assess the molecular design of polymers and quenchers in a systematic approach. CP core particles, because of their electrostatic charge, suffer from nonspecific interactions with other charged species, and thus encapsulating CP particles with a hydrogel shell should create sensor materials with higher specificity. To illustrate this concept, CP-particle containing hydrogel films were created to permit selective interactions with designed quenchers. The encapsulation of the individual CP-core particles was accomplished through atom transfer radical polymerization (ATRP) of functional monomers from the surface, and the choice of reactive group on the monomer allows for bioconjugation on the particle shell. Future core-shell materials can also be developed with ATRP, and give prospects to new schemes for CP-based biosensing.

Thesis Supervisor: Timothy M. Swager
Title: John D. MacArthur Professor of Chemistry

Table of Contents

List of Figures

Chapter 7

List of Tables

Chapter 1:

Introduction

1.1 The need for biosensors

One of the earlier known examples of a biological sensor, or a biosensor, was the canary in a cage, to warn coal miners of the presence of methane gas.[1] While a rather low-tech solution, it was however extremely effective in alerting miners to evacuate and avoid being caught in an explosion. Understanding how to utilize the canary's acute senses had a huge impact on helping populations of miners monitor their conditions and escape from tragedy.

In our present information-driven and knowledge-based society, there is stimulated interest in creating technological solutions for monitoring biological systems that parallel our progress in computation and informatics. Biosensors are critically important for monitoring real-time events for medical diagnostics for both home and point-of-care, biotechnology/drug discovery, food safety, the environment, defense, and a fundamental understanding of biochemical processes. The estimated $2.7 billion world market of biosensors in 2006[2] exemplifies their impact. Despite this large opportunity, only the glucose sensor, however, has experienced widespread commercial success for home diagnostics.

It is posited that nanotechnology will yield a myriad of biosensing solutions in the next decade.[3-6] Still, commercialization of most technologies continues to lag behind research by several years due to the costs associated with development. New devices are needed that not only have the laboratory attributes of high sensitivity and specificity, but also have the form factor and capacity to be easily scalable and mass-produced for high-throughput applications. In addition, multiplexing analyte detection is advantageous in increasing sensor throughput and providing ensemble information, and therefore bringing commercial value. Interdisclipinary efforts comprised of chemistry, materials science, and medicine are critical for the implementation of nanotechnology for real-use clinical diagnostics.

1.2 Many modalities for biosensors

Table 1.1 highlights some of the potential modalities available for biosensors. A recent review by Rosi and Mirkin outlines the current progress and some of the fundamental properties of nanostructures in biodiagnostics.[7] It is important to understand that each application for screening has its respective requirements, and thus different modalities operate in different scenarios.

Optical	Surface plasmon resonance[8] Fiber optic[9] Absorbance[10] Fluorescence[11,12]
Magnetic	Magnetic relaxation detection[13]
Electrical	Nanowires[14] Nanotubes[15]
Piezoelectric	Quartz crystal microbalance[16]
Electrochemical	Potentiometric[17,18]
Electromechanical	Microcantilevers[19]

Table 1.1. Classification of biosensors with representative examples.

For example, the fiber optic technology developed by Walt[9] is excellent for creating DNA microarrays due to its amenable nature for multiplexing, and provides a powerful biosensor for high-throughput *in vitro* diagnostics. *In vivo* biosensors require methods for high image contrast in tissue, and Weissleder's group at MGH[13] has pioneered the development of iron-oxide nanoparticles for magnetic relaxation detection to meet this need. An understanding of the system and the desired output is thus required for evaluating and identifying different technologies.

1.3 Advantages of fluorescent biosensors

With the diversity of modalities possible for constructing biosensors, there are inherent advantages for fluorescent biosensors. Fluorescence is one of the most widely used optical techniques due to its high level of sensitivity and ease of measurement. Despite these attributes, the demonstration of its full potential has not been observed in biosensors. Both researchers and clinicians understand the technique, and often this user familiarity is a large contributing factor for mass adoption of technology. In addition to monitoring, fluorescence provides imaging capability, and thus essential information can be gained through visualization of real-time events. Furthermore, instrumentation and measurement of fluorescence is relatively low cost and well-defined, with the possibility for resource-efficient and miniaturized systems[20] using current off-the-shelf components. Finally, a broad range of emission wavelengths is accessible with fluorophores, providing avenues for multiplexing sensor formats.

1.3.1 General design of fluorescent biosensors

A general scheme for biosensors is shown in Figure 1.1. A biosensor consists of a biological target, in close contact with the transducer. For fluorescent biosensors, the transducer consists of the fluorophore, and a modulator, which produces a change in the fluorophore photophysical properties. Activation of the target causes the selective transduction, and monitoring the event proceeds via excitation by light source and collecting the response in a detector. How the sensor performs in its surroundings is critically important. This will be described for biosensors in Section 1.4 in further detail.

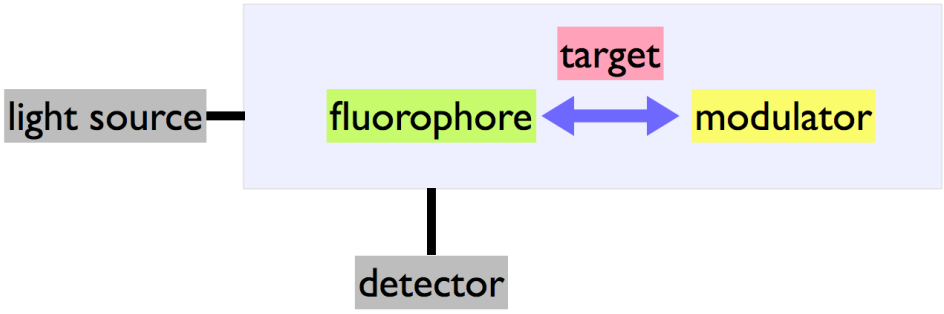

Figure 1.1. General design of fluorescent biosensors.

1.4 Challenges for designing robust biosensors

The two most important properties of any proposed biosensor are (1) its sensitivity towards the target analyte(s) and (2) its specificity.[21] Sensitivity of the integrated device is dependent on both the biological component and the transduction mechanism because there must be a significant biomolecule-analyte interaction and a high efficiency of subsequent detection of this reaction by the transducer. Often it is easy to design a highly sensitive system in one environment, but when translating into other environments, the efficiency of the detection may be reduced. Overall sensitivity of the system determines the limit of detection and the relative signal-to-background that the sensor can achieve. Specificity is generally achieved as a direct result of biomolecular recognition, such as antibody-antigen interactions, that results in less cross-reactivity versus chemical sensors. This high level of specificity can only be successful if there is highly efficient coupling between the biological and transducer components. The transduction scheme must be selective only to the biological interaction of interest, reducing interactions with species in the environment that produce false responses in the system. These negative interactions can easily be understood with the polymer shown in

Figure 1.2, in which there are designed receptors for a particular target, but a "false positive" results due to nonspecificity. Understanding how to address these issues will prove for a more reliable biosensor.

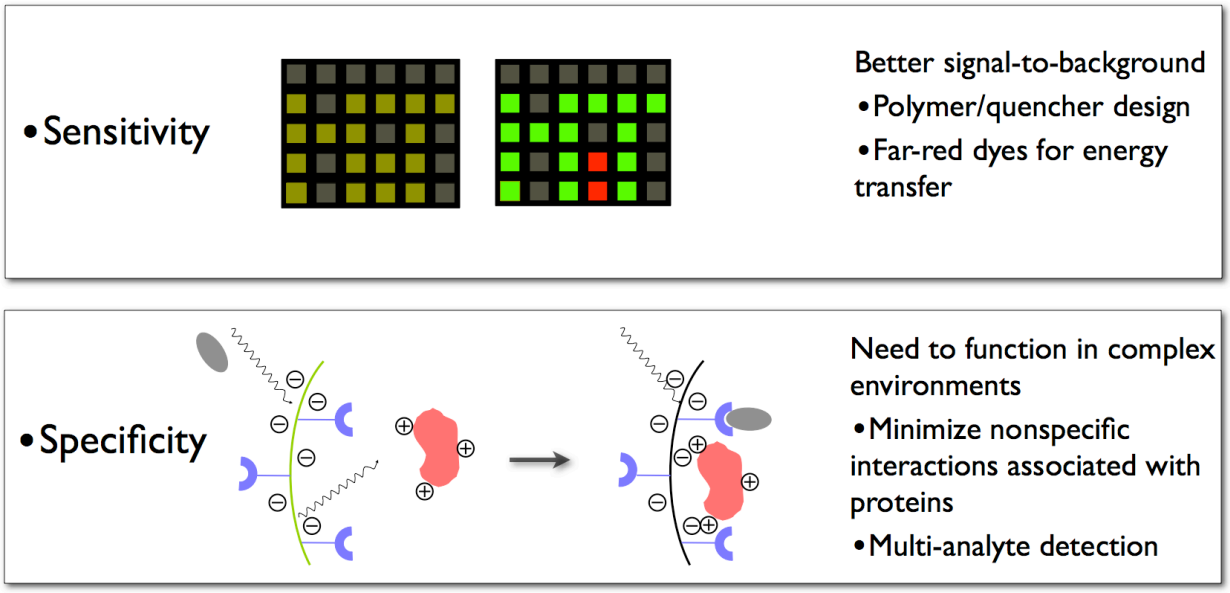

Figure 1.2. Challenges for designing robust biosensors.

1.5 Detection of protease activity with particle sensors

We are interested in creating activatable polymeric particle platforms as highly sensitive and specific biosensors. To demonstrate our goals, we have designed a particle sensor for the detection of protease activity. Proteases are enzymes responsible for the protein turnover process implemented in many regulatory systems in the body. The ability to localize and quantify the activity of these proteases *in vitro* and *in vivo* with a rapid assay that has high-throughput capabilities would prove beneficial for the development of inhibitors for protease-linked diseases as therapies.

The proposed sensory scheme for protease detection is shown in Figure 1.3 as a core-shell particle. The increase in surface area afforded from micro- and nano-sized particles versus planar surfaces offers opportunity for improving sensor-analyte interactions. In addition, particles can be readily dispersed in various assay media. The core is composed of the fluorophore, in our case a conjugated polymer (CP). The shell, which encapsulates the core, is a crosslinked hydrophilic polymer network, or hydrogel, that shields nonspecific interactions, but permits the transport of the modulating species, either a quencher or a dye, to the core. The hydrogel shell is designed such that the outer functionality links the modulator with the target. When activation of the target occurs, the modulator diffuses to the CP, resulting in a detectable and quantifiable signal.

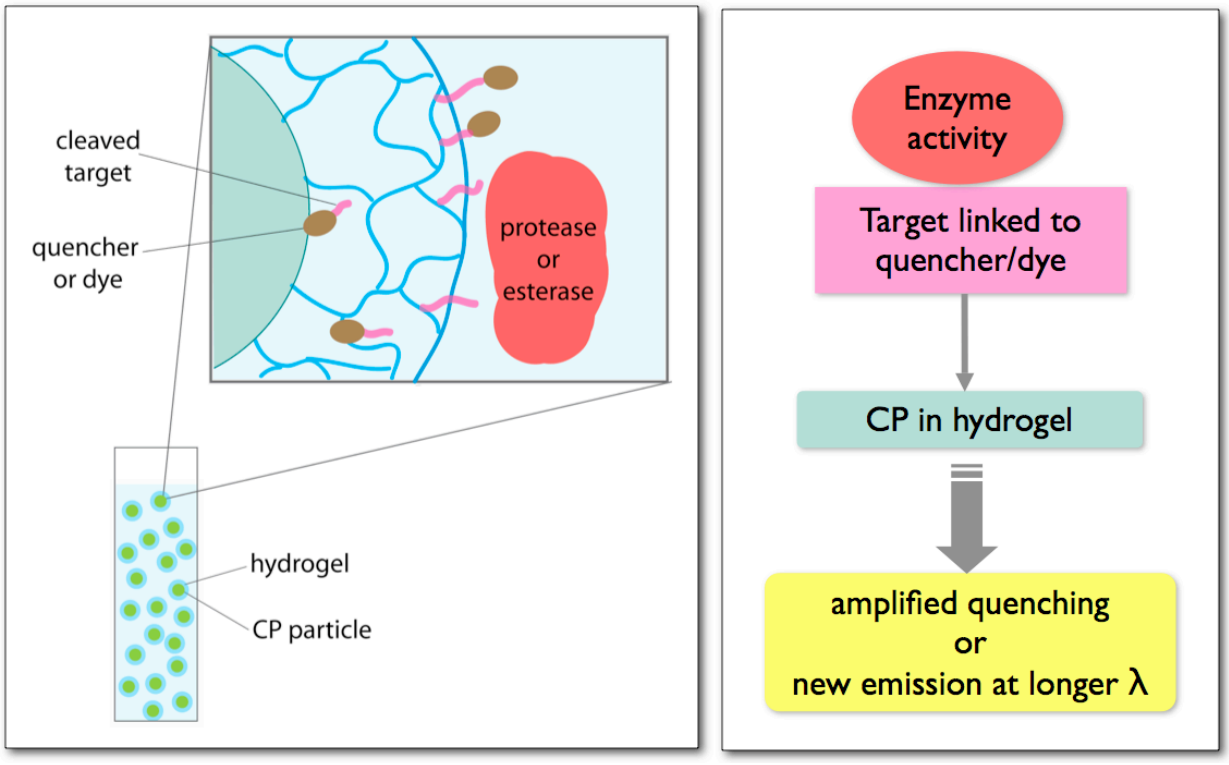

Figure 1.3. Detection of protease activity with particle sensors.

1.5.1 A brief introduction of conjugated polymers

The discovery of conjugated polymers transformed the polymer community and captivated the scientific world with their unique properties, which led to the Nobel Prize in Chemistry in 2000 awarded to Heeger, Shirikawa, and MacDiarmid. The unsaturated π-bonded macromolecules have created a number of opportunities in chemistry and physics, and offer engineering possibilities due to their remarkable optical, electronic, and mechanical properties. Several monographs have been published regarding their fundamental characteristics and innovations.[22-25] The research of these organic polymers as active semiconductors has advanced rapidly since the early discoveries of doped conjugated polymers, and a review by Friend et al.[26] summarized the pioneering work in this field to create next-generation devices. Some classes of conjugated polymers can also undergo molecular actuation, and are currently under investigation for artificial muscle applications.[27] Figure 1.4 depicts the most common and thoroughly studied classes of conjugated polymers.

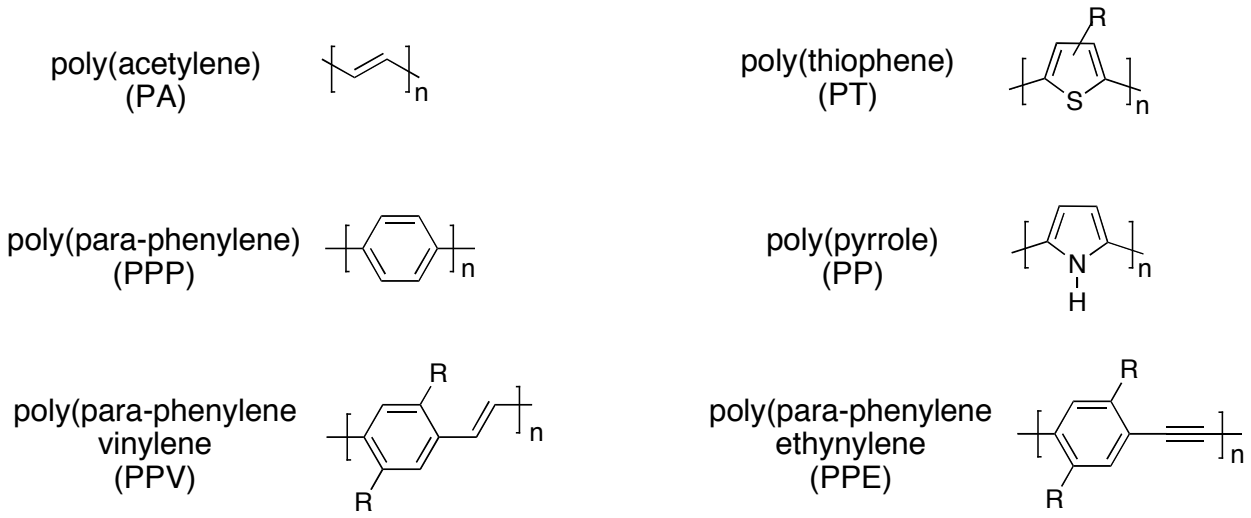

Figure 1.4. Chemical structures of commonly encountered classes of conjugated polymers.

1.5.2 Poly(phenylene ethynylene)s (PPE)s

This thesis focuses on the class of conjugated polymers known as poly(phenylene ethynylene)s (PPE)s. A review by Bunz[28] summarizes the synthetic strategies that have been developed, as well as some applications of the materials. Generally, the preparation is via Sonogashira-Hagihara Pd-catalyzed cross-coupling reaction conditions,[29] with the stoichiometric reaction of terminal aryl alkynes and aryl dihalides in amine solvents. Aryl diiodides react much faster than the corresponding dibromides, and are the preferred substrate. The versatility in monomers that can undergo polymerization allow for tunable properties, in terms of processibility, functionality, and photophysical characteristics in PPEs.

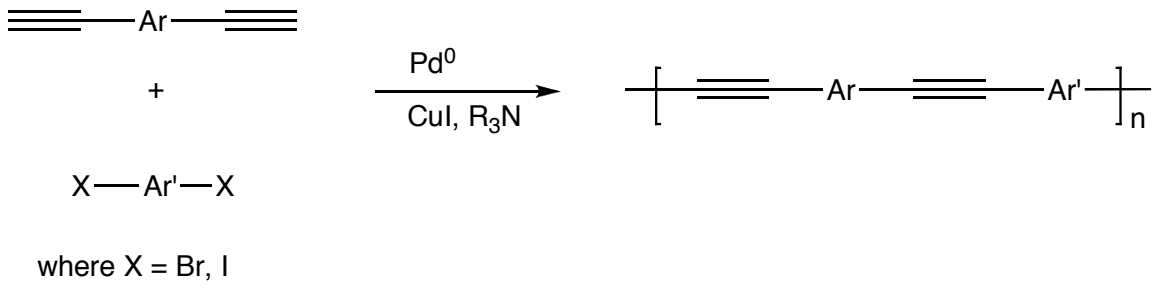

Figure 1.5. Pd-catalyzed cross-coupling polymerization for PPE formation.

1.5.3 Conjugated polymers as chemical and biological sensors

The development of conjugated polymers as sensor materials was led by the pioneering work of Swager, in which the "molecular wire" approach to sensing[30-32] was demonstrated. The molecular wire, or polyreceptor, consisted of receptor-incorporated PPEs, which were able to outperform the analogous monomeric receptors, indicating the amplification effect afforded from the connectivity of receptor units.[30] The schematic is shown in Figure 1.6, comparing the

traditional single molecule sensor, in which the sensitivity is determined by the equilibrium constant of binding to the receptors, to the receptors "wired in series" which form a collective response.

Understanding exciton transport in intrachain as well as interchain interactions led to the development of a rigid pentiptycene moiety for incorporation into PPEs. This molecular scaffold reduces deleterious self-quenching effects and also creates a nanoporous material for specific analytes to percolate and "quench" the polymer emission.[33,34] The highly sensitive polymeric system was applied for the detection of TNT and other explosives,[34] since licensed to ICx Nomadics, Inc., and used by the U.S. Army for deployment of landmines. Several reviews have highlighted the progress of conjugated polymers[35,36] and specifically PPEs[37] as sensor materials, for both chemical and biological detection.

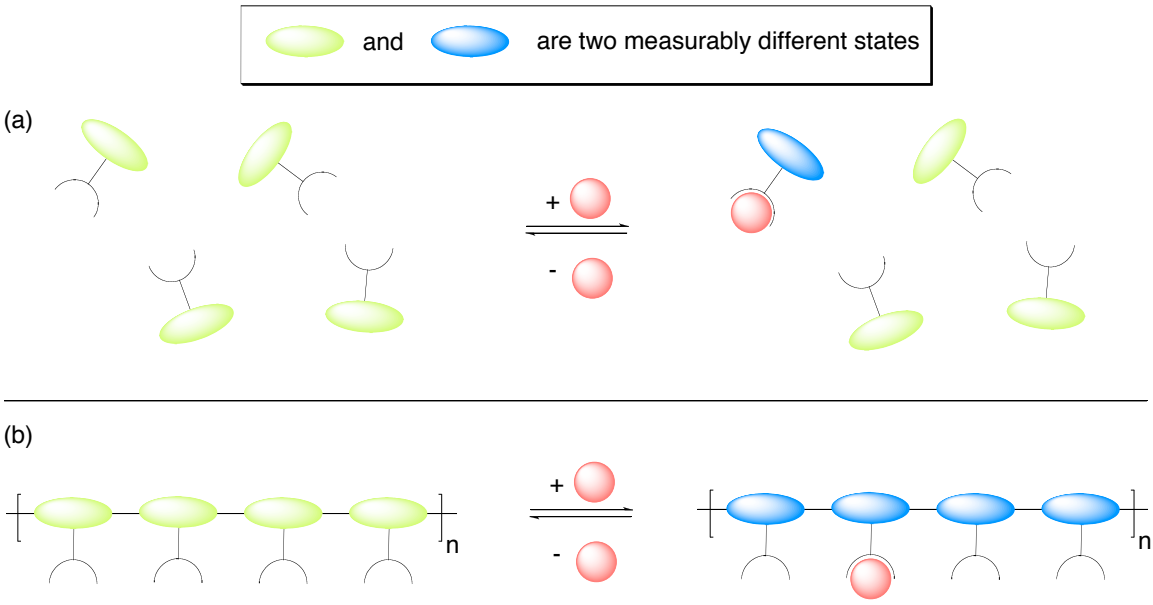

Figure 1.6. The "molecular wire" approach for sensing, comparing (a) traditional sensors and (b) receptors wired in series. Adapted from ref.[38]

Conjugated polymers as biosensors, based on the molecular wire principle,[38] have the potential to be much more sensitive than the conventional small molecule fluorophore assays. In addition, since it is a polymeric material, it can be processed and integrated into sensory schemes not achievable with small molecules. There are challenges, however, in designing robust biosensors, as mentioned in section 1.4. With conjugated polymers, molecular design is required to maintain the inherent luminescent properties in biologically relevant environments as well as material engineering to devise a selective transduction scheme for monitoring biological activity.[36]

1.5.4 Synthesis of conjugated polymers for biosensor applications

Conjugated polymers, due to their rigid nature, are particularly hydrophobic and insoluble materials. Solubility is imparted by the side chain functionality, and in the case of organic-soluble materials, alkyl chains are incorporated. For biosensors, an aqueous environment is generally required, and strategies such as hydrophilic ionic or nonionic side chains have been employed to synthesize water-soluble derivatives. Ionic conjugated polymers have been synthesized and have proven useful for developing homogeneous DNA assays.[39-42] The work of Bazan[39] and LeClerc[41,42] show examples of utilizing aggregation and conformational changes in the conjugated polymer for detection of DNA. Various applications of conjugated polyelectrolytes as biosensors have been reviewed recently.[43] The polyelectrolytes, however, have notoriously been recognized to have nonspecific interactions with proteins in solution.[44,45] Transduction schemes that rely on charge interaction also may be affected in environments with higher ionic content that screen the net effective charges of the system and reduce the transduction efficiency.[45] The synthesis of nonionic water-soluble derivatives also have been of interest, since these polymers may be less susceptible to nonspecific interactions with charged

species.[36,45-47] These polymers, while having no effective charge, have respectable quantum yields in solution,[46] but most likely will suffer from self-aggregation in the solid state. Challenges still remain to synthesize a water-soluble derivative that can perform as well as the organic counterpart.

1.5.5 Conjugated polymers as protease sensors

Whitten and coworkers[48] have developed protease sensors with PPE-coated microspheres, utilizing a quencher-tether-ligand approach (QTL) for associating PPE with the quencher. The approach is a "turn-on" sensor, in which the activity of the protease removes the quencher from the PPE microspheres, resulting in enhanced fluorescence emission. The assays developed, however, require rather controlled environments to attain the desired sensitivity and avoid any nonspecific interactions.

Our initial work in developing protease sensors was pursued by Wosnick et al.,[49] in which a substrate specific to trypsin was covalently linked between a nitroaromatic quencher and a PPE, in a quenched state. Similarly, the sensor developed was a "turn-on" approach, in which addition of trypsin cleaved the substrate, liberating the quencher from the PPE and resulting in an increase in fluorescence. The solution assay was limited to only a 10-fold increase in signal in aqueous environments due to the strong hydrophobic interactions between the PPE and quencher to dominate the response.

To improve detection limits for protease sensors, we focus on creating an analog to our chemical "turn-off" sensors, which upon analyte binding provide an amplified quenching response.[34] The "turn-off" mechanism is capable of producing a highly sensitive sensor due to the multiplicity of analyte binding sites available to attenuate the emission of the polymer.[30] For example, in the case of paraquat and trinitrotoluene (TNT), the formation of the charge-transfer

complex yields efficiencies greater than any energy transfer scheme.[30] Sensors of this second type have been made utilizing by electrostatics to associate the fluorophore and the quencher in solution.[50] The reliance on electrostatic effects may produce nonspecific polymer-analyte interactions, reducing the sensitivity or fidelity of the system.[49] In general, the "turn-off" sensor has a faster response time than the "turn-on" due to dominant hydrophobic interactions between the quencher and the conjugated polymer backbone.[36] In this thesis, we utilize this scheme to develop a particle-based sensory platform that will be effective in achieving greater sensitivity by several orders of magnitude and address selectivity in biologically relevant environments.

1.6 Introduction to fluorescence[a]

Fluorescence is a luminescent optical phenomenon, in which the molecular absorption of a photon triggers the emission of another photon with a longer wavelength. The shift in wavelength is known as the Stokes' shift. The energy loss between the excitation and emission can be represented in an energy plot known as the Jablonski diagram, as shown in Figure 1.7. The singlet ground, first, and second electronic states are depicted as S_0, S_1, and S_2, respectively. Each electronic state can exist in a number of vibrational energy levels, which give rise to the observed band structure in the emission spectrum.[51] Upon absorption of a photon, the fluorophore is excited to a higher electronic state, either S_1 or S_2. The molecules rapidly relax to the lowest vibrational level of S_1 by the internal conversion process, to reach a thermally equilibrated excited state. Return to the ground state occurs to a higher excited vibrational ground-state level, then quickly reaching thermal equilibrium, for fluorescence emission. Molecules in the S_1 state can also undergo a spin conversion to the first triplet state, T_1, known

[a] A brief primer to fluorescence is provided here; for more in-depth discussion of relevant topics, see refs. 51 and 52.

as intersystem crossing. Transitions to the singlet ground state are forbidden, and the emission rates are slow, resulting in a longer lifetime emission as phosphorescence.

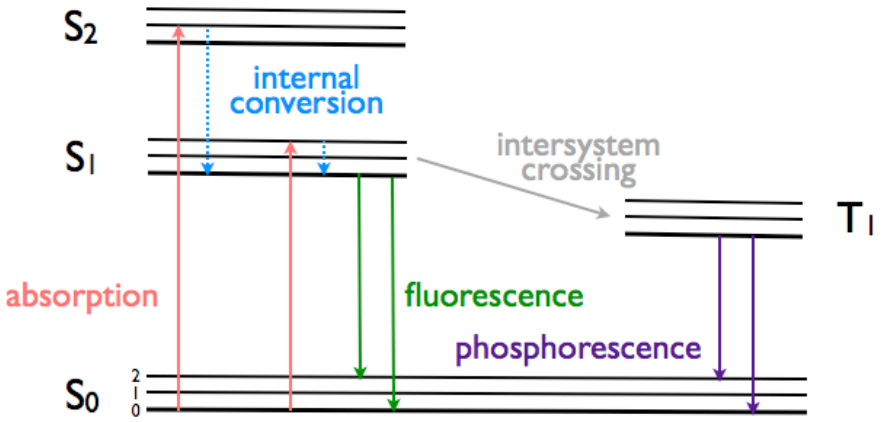

Figure 1.7. Typical Jablonski diagram. Adapted from ref.[52]

1.6.1 Characteristics of fluorescence

Fluorophores are characterized by their fluorescence lifetime and quantum yield. Quantum yield is the number of emitted photons relative to the number of absorbed photons, and thus represents the "efficiency" of the fluorophore. The energy yield of fluorescence is always less than unity because of Stokes' losses, but there are also possible non-radiative decay processes. The quantum yield (Φ) depends on the emissive rate of the fluorophore (k_r) and the rate of non-radiative decay processes grouped as (k_{nr}), and given by[52]

$$\Phi = \frac{k_r}{k_r + k_{nr}}$$

The lifetime (τ) of the excited state is defined by the average time the molecule spends in the excited state prior to emitting a photon, and is defined by

$$\tau = \frac{1}{k_r + / k_{nr}}$$

1.6.2 Fluorescence quenching

Fluorescence quenching, referring to any process that decreases the fluorescence intensity of a sample,[52] can be caused by a variety of molecular interactions.

Collisional or dynamic quenching occurs when the excited state fluorophore, through diffusion-controlled processes, encounters another molecule, known as a quencher, and returns to the ground state. The rate of quenching is dependent on the temperature and viscosity of the solution. The decrease in intensity is described by the Stern-Volmer equation:

$$\frac{F_0}{F} = 1 + K_{SV}[Q] = 1 + k_q \tau_0 [Q]$$

Here K_{SV} is the dynamic Stern-Volmer quenching constant, k_q is the biomolecular quenching constant, and τ_0 is the unquenched lifetime, and *[Q]* is the quencher concentration. It should be noted that dynamic quenching of fluorescence is usually negligible for quencher concentrations less than 1 mM.[51]

Another type of quenching known as static quenching can occur via the formation of nonfluorescent complexes with quenchers. This process occurs in the ground state and does not rely on molecular diffusion or collisional processes, and thus is not a time-dependent process. The linear relationship is identical to the one derived for diffusive interactions, except here the constant is based on association complexes. The Stern-Volmer constant for static quenching is defined as the ratio of the complex concentration to the concentrations of the uncomplexed species:

$$K_{SV} = \frac{[F - Q]}{[F][Q]}$$

The magnitude of K_{SV}, observed from quenching experiments, can give an indication whether quenching is dynamic or static, since dynamic quenching cannot account for such large

decreases in intensity. Lifetime measurements can also be performed, since the lifetime is not affected in the case of static quenching.

Analysis of the observed quenching provides insight into the involved interactions. Plotting the ratio of initial fluorescence to the fluorescence (F_0/F) at varying $[Q]$ versus $[Q]$ gives an indication of the mechanism of quenching. For linear quenching, the slope of the plot can be extrapolated as K_{SV}, and is interpreted as either dynamic or static quenching depending on the magnitude. Any observed curvature is ascribed to a more complex quenching mechanism, and generally equations can be written to describe these situational quenching behaviors. Typically, upward curvature accounts for both dynamic and static quenching processes being observed, or if there is a cooperativity associated with fluorophore-quencher complex formation.[52] In some cases, as the quencher concentration increases, an overlap of "quenching spheres" can occur due to fractional accessibility, resulting in a downward curvature.

1.7 Outline of thesis

Chapter 2 describes early explorations into multilayered polymer films on colloidal substrates that utilize layer-by-layer assembly to create core-shell and hollow-shell particles, and will introduce some of the issues discussed in later chapters. As identified in Chapter 2, there is a need for precisely quantifying the sensory response from particles, especially in the assessment of various components for their performance. The quantification method is described in Chapter 3 and applied in Chapter 4 for assessing various quencher libraries. Addressing specificity is presented in Chapter 5 with the incorporation of particles in hydrogel materials. The last two chapters show prospects of grafting polymers either from particle surfaces (Chapter 6) or from conjugated polymers in solution (Chapter 7) to produce nanostructured materials that have potential for integration into biological sensing.

1.8 References

(1) Goodman, L. *J. Clin. Invest.* **2004**, *114*, 448.

(2) World Biosensors Markets, Frost and Sullivan, 2005.

(3) Bogue, R. W. *Sensor Review* **2004**, *24*, 253-260.

(4) Jianrong, C.; Yuqing, M.; Nongyue, H.; Xiaohua, W.; Sijiao, L. *Biotechnol. Adv.* **2004**, *22*, 505-518.

(5) Ferrari, M. *Nature Reviews Cancer* **2005**, *5*, 161-175.

(6) Roco, M. C. *Curr. Opin. Biotechnol.* **2003**, *14*, 337-346.

(7) Rosi, N. L.; Mirkin, C. A. *Chem. Rev.* **2005**, *105*, 1547-1562.

(8) He, L.; Musick, M. D.; Nicewarner, S. R.; Salinas, F. G.; Benkovic, S. J.; Natan, M. J.; Keating, C. D. *J. Am. Chem. Soc.* **2000**, *122*, 9071-9077.

(9) Walt, D. *Science* **2000**, *287*, 451-452.

(10) Elghanian, R.; Storhoff, J. J.; Mucic, R. C.; Letsinger, R. L.; Mirkin, C. A. *Science* **1997**, *277*, 1078-1081.

(11) Zhao, X.; Tan, W. *J. Am. Chem. Soc.* **2003**, *125*, 11474-11475.

(12) Taylor, J. R.; Fang, M. M.; Nie, S. *Anal. Chem.* **2000**, *72*, 1979-1986.

(13) Perez, J. M.; Josephson, L.; O'Loughlin, T.; Högemann, D.; Weissleder, R. *Nat. Biotechnol.* **2002**, *20*, 816-820.

(14) Cui, Y.; Wei, Q.; Park, H.; Lieber, C. M. *Science* **2001**, *293*, 1289-1292.

(15) Chen, R. J.; Bangsaruntip, S.; Drouvalakis, K. A.; Kam, N. W. S.; Shim, M.; Li, Y. M.; Kim, W.; Utz, P. J.; Dai, H. J. *Proc. Natl. Acad. Sci.* **2003**, *100*, 4984-4989.

(16) Weizmann, Y.; Patolsky, F.; Willner, I. *Analyst* **2001**, *126*, 1502-1504.

(17) Wang, J.; Xu, D.; Kawde, A.-N.; Polsky, R. *Anal. Chem.* **2001**, *73*, 5576-5581.

(18) Wang, J.; Liu, G.; Merkoci, A. *J. Am. Chem. Soc.* **2003**, *125*, 3214-3215.

(19) Ilic, B.; Yang, Y.; Craighead, H. G. *Appl. Phys. Lett.* **2004**, *85*, 2604-2606.

(20) Adams, M. L.; Enzelberger, M.; Quake, S.; Scherer, A. *Sens. Actuators, A* **2003**, *104*, 25-31.

(21) Byfield, M. P.; Abuknesha, R. A. *Biosens. Bioelectron.* **1994**, *9*, 373-400.

(22) Salaneck, W. R.; Lündstrom, I.; Rånby, B. *Conjugated Polymers and Related Materials: The Interconnection of Chemical and Electronic Structure*; Oxford University Press: Oxford, 1993.

(23) Barford, W. *Electronic and Optical Properties of Conjugated Polymers*; Clarendon Press: Oxford, 2005.

(24) Brėdas, J.-L.; Silbey, R. J. *Conjugated Polymers: The Novel Science and Technology of Highly Conducting and Nonlinear Optically Active Materials*; Kluwer Academic: Netherlands, 1991.

(25) Elsenbaumer, R. L.; Reynolds, J. R.; Skotheim, T. A. *Handbook of Conducting Polymers*; 2nd ed.; Marcel Dekker: New York, 1998.

(26) Friend, R. H.; Gymer, R. W.; Holmes, A. B.; Burroughes, J. H.; Marks, R. N.; Taliani, C.; Bradley, D. D. C.; Dos Santos, D. A.; Brédas, J. L.; Lögdlund, M.; Salaneck, W. R. *Nature* **1999**, *397*, 121-128.

(27) Smela, E. *Adv. Mater.* **2003**, *15*, 481-494.

(28) Bunz, U. H. F. *Chem. Rev.* **200**, *100*, 1605-1644.

(29) Sonogashira, K.; Tohda, Y.; Hagihara, N. *Tetrahedron Lett.* **1975**, *16*, 4467.

(30) Zhou, Q.; Swager, T. M. *J. Am. Chem. Soc.* **1995**, *117*, 12593-12602.

(31) Swager, T. M. *Acc. Chem. Res.* **1998**, *31*, 201-207.

(32) Swager, T. M.; Wosnick, J. H. *MRS Bulletin* **2002**, 446-450.

(33) Yang, J.-S.; Swager, T. M. *J. Am. Chem. Soc.* **1998**, *120*, 5321-5322.

(34) Yang, J.-S.; Swager, T. M. *J. Am. Chem. Soc.* **1998**, *120*, 11864-11873.

(35) McQuade, D. T.; Pullen, A. E.; Swager, T. M. *Chem. Rev.* **2000**, *100*, 2537-2574.

(36) Thomas, S. W., III; Joly, G. D.; Swager, T. M. *Chem. Rev.* **2007**, *107*, 1339-1386.

(37) Zheng, J.; Swager, T. M. *Adv. Poly. Sci.* **2005**, *177*, 151-179.

(38) Wosnick, J. H.; Swager, T. M. *Curr. Opin. Chem. Bio.* **2000**, *4*, 715-720.

(39) Liu, B.; Bazan, G. C. *Chem. Mater.* **2004**, *16*, 4467-4476.

(40) Gaylord, B. S.; Heeger, A. J.; Bazan, G. C. *Proc. Natl. Acad. Sci.* **2002**, *99*, 10954-10957.

(41) Ho, H.-A.; Doré, K.; Boissinot, M.; Bergeron, M. G.; Tanguay, R. M.; Boudreau, D.; Leclerc, M. *J. Am. Chem. Soc.* **2005**, *127*, 12673-12676.

(42) Doré, K.; Dubus, S.; Ho, H.-A.; Lévesque, I.; Brunette, M.; Corbell, G.; Boissinot, M.; Bolvin, G.; Bergeron, M. G.; Boudreau, D.; Leclerc, M. *J. Am. Chem. Soc.* **2004**, *126*, 4240-4244.

(43) Achyuthan, K.; Bergstedt, T.; Chen, L.; Jones, R. M.; Kumaraswamy, S.; Kushon, S. A.; Ley, K. D.; Lu, L.; McBranch, D.; Mukundan, H.; Rininsland, F.; Shi, X.; Xia, W.; Whitten, D. G. *J. Mater. Chem.* **2005**, *15*, 2648-2656.

(44) Kim, I.-B.; Dunkhorst, A.; Bunz, U. H. F. *Langmuir* **2005**, *21*, 7985-7989.

(45) Dwight, S. J.; Gaylord, B. S.; Hong, J. W.; Bazan, G. C. *J. Am. Chem. Soc.* **2004**, *126*, 16850-16859.

(46) Khan, A.; Müller, S.; Hecht, S. *Chem. Comm.* **2005**, 584-586.

(47) Kuroda, K.; Swager, T. M. *Chem. Comm.* **2003**, 26-27.

(48) Kumaraswamy, S.; Bergstedt, T.; Shi, X.; Rininsland, F.; Kushon, S.; Xia, W.; Ley, K.; Achyuthan, K.; McBranch, D.; Whitten, D. *Proc. Natl. Acad. Sci.* **2004**, *101*, 7511-7515.

(49) Wosnick, J. H.; Mello, C. M.; Swager, T. M. *J. Am. Chem. Soc.* **2005**, *127*, 3400-3405.

(50) Pinto, M. R.; Schanze, K. S. *Proc. Natl. Acad. Sci.* **2004**, *101*, 7505-7510.

(51) Ingle, J. D., Jr.; Crouch, S. R. *Spectrochemical Analysis*; Prentice Hall: Englewood Cliffs, 1988.

(52) Lakowicz, J. R. *Principles of Fluorescence Spectroscopy*; 2nd ed.; Kluwer Academic/Plenum Publishers: New York, 1999.

Chapter 2:

Layer-by-Layer Assembly of PPE Polyelectrolytes on Colloidal Particles

2.1 Introduction

The photophysical properties of conjugated polymers require robustness in aqueous environments in order for implementation as high performance biosensors. Specifically, with poly(phenylene ethynylene)s (PPE)s, aggregation due to interchain interactions often limits the overall sensitivity of the system, especially in the solid state. The pentiptycene moiety has proven to minimize these interactions,[1] resulting in higher quantum yields and higher sensitivity achievable. By synthesizing a pentiptycene-incorporated anionic PPE,[2] we can form films on various charged substrates via layer-by-layer assembly, alternately depositing with a cationic species. Colloidal substrates are particularly interesting to us, since we can capitalize on the surface area gained versus planar substrates to immobilize PPE films, and perform solution-quenching experiments in aqueous environments as a heterogenous assay. The three-dimensionality afforded from the immobilized films allows for greater sensitivity gains to be achieved due to increased exciton transport.[3] We have observed that films supported on particles show a greater response towards electron-transfer quenching versus the native polymers in solution.[4] Layer-by-layer assembly is a powerful and relatively simple technique to prepare PPE-coated particles, providing opportunities to develop particle-based sensors with core-shell and hollow-shell structure with added functionality and versatility.

2.1.1 Layer-by-layer assembly

In the early 1990s, Decher introduced the use of non-covalent interactions for forming polymer thin films with the sequential adsorption of polyelectrolytes.[5,6] The method, known as layer-by-layer assembly, is illustrated in Figure 2.1. A charged substrate is immersed in a solution of an oppositely charged polyelectrolyte, forming a thin polymer layer on the substrate. The adsorption leads to overcompensation of charge and a reversal in the net charge of the support,[7] thus allowing subsequent sequential deposition of polycations and polyanions for multilayer film formation. Layer-by-layer assembly has the capacity to create films and heterostructured assemblies on a wide variety of substrates using relatively simple processing techniques. The versatility in tuning the functionality and the morphology is evidenced in the amount of research conducted with this method for creating materials with unique properties.[8] A recent review highlights the use of layer-by-layer assembly for biological applications.[9]

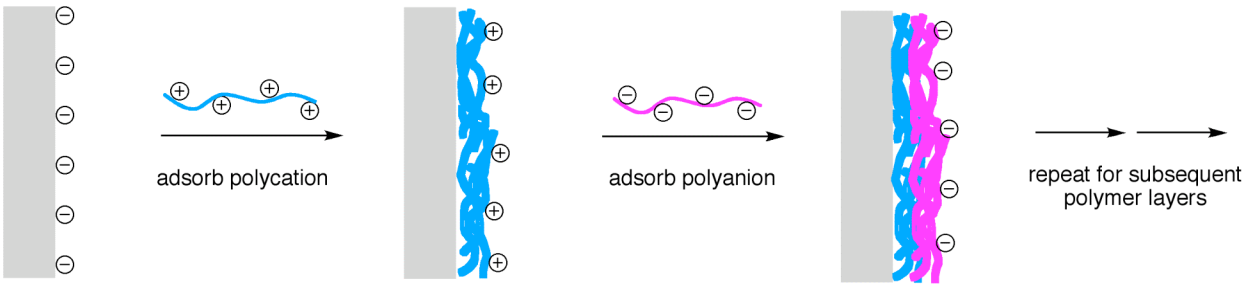

Figure 2.1. Layer-by-layer assembly of polyelectrolytes onto a charged substrate.

Advances in the field since Decher's pioneering work have resulted in a greater physical understanding in multilayer buildup. Initial work was based on the behavior of highly charged polyelectrolyte systems, but Rubner and coworkers[10-12] discovered that by using weak polyelectrolytes one could control surface charge, layer interpenetration, and layer thicknesses

with pH.[13] In addition, hydrophobic interactions,[14] as well as the effect of counterions,[15] have been found to contribute to the adsorption behavior of polyions of surfaces. Layered assemblies can also be constructed using hydrogen-bonding forces,[16] further expanding the palette of materials to nonionic polymers.

2.1.2 Layer-by-layer assembly on colloidal particles for core-shell and hollow materials

Multilayer films on micro- and nanoscale particles can create opportunities for different applications due to the inherent increase in surface area and dimensionality created from the spherical format. The capability for layer-by-layer assembly onto colloidal substrates was first demonstrated by Caruso, Donath, and coworkers,[18,19] in which the particle and polyelectrolyte solution concentrations were properly adjusted such that uniform adsorption could occur without flocculation. Since then, colloidal particles have been utilized as the substrates for electrostatic layer-by-layer assembly as well as hydrogen-bonded self assembly[20,21] for a variety of applications. Particles have been modified with adsorbed polyelectrolytes for colloidal stability in the case of gold nanoparticles.[22,23] Metal oxide and semiconductor nanoparticles have been incorporated into the multilayers via direct deposition[24-26] or *in situ* transformation.[27] Enzyme multilayers composed of glucose oxidase and horseradish peroxidase were immobilized on particle surfaces for enzyme catalysis reactors, for their potential to yield higher enzymatic reaction efficiencies versus planar films.[28]

Hollow spheres provide an opportunity to carry a payload or act as a membrane. Möhwald and coworkers introduced the use of a sacrificial core in layer-by-layer assembly to create a diverse array of hollow spheres,[29] in which dissolution of the template, depending on the material, can be accomplished with solvent or acidic treatment. The mechanically stable shell can be implemented as a “nanoreactor”, which has been used for *in situ* polymerization of

polystyrene,[30] thereby trapping the large molecular weight species within the capsule. Encapsulation and release has been explored, utilizing pH[31] and other factors such as ionic strength and solvent[32] to control the permeability of multilayer capsules, for applications in drug delivery and membrane technology.

2.1.3 Layer-by-layer assembly with conjugated polymers

Conjugated polymer multilayer films have been primarily applied in optoelectronic research. Rubner and coworkers conducted early work with the layer-by-layer assembly of charged poly(thiophene),[33] p-type doped conducting polymers with *in situ* polymerized poly(pyrrole) and poly(aniline),[34] and poly(phenylene) and poly(phenylene vinylene) derivatives.[35-37] Water-soluble poly(phenylene ethynylene)s (PPE)s, shown in Figure 2.2, have also been synthesized for layer-by-layer assembly for signal harvesting[38] and the fabrication of electroluminescent devices.[39] Once deposited as films, however, these materials are self-aggregated due to strong hydrophobic and π-π interactions. Attempts to resolve this reduction in the quantum yield include adjusting the deposition pH[39] and introducing spacer layers between the conjugated polymer layers.[38]

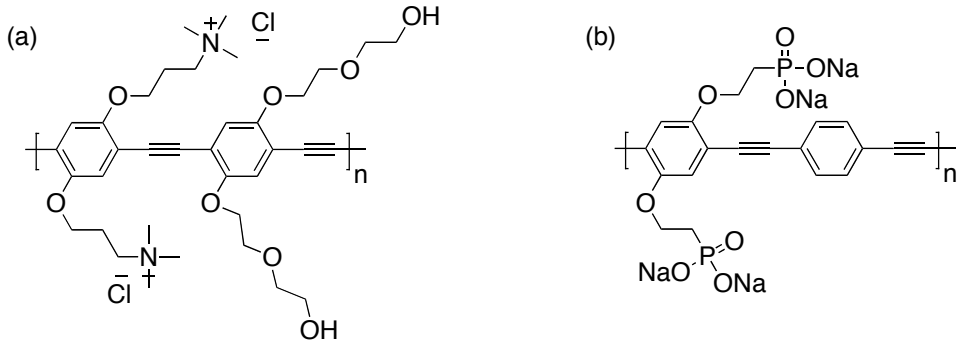

Figure 2.2. PPEs (a)[38] and (b)[39] used for layer-by-layer assembled films.

While other approaches for producing core-shell and hollow structures exist with self-assembly methods such as block or graft copolymers, layer-by-layer assembly is by far the most versatile in terms of material synthesis and assembly since it allows for fine control over shell thickness and composition.[40] This chapter will utilize the layer-by-layer assembly method for initial explorations in creating PPE-immobilized films on inorganic and organic colloidal substrates. The remainder of this thesis will also use this method for assembling the core of our particle sensors.

2.2 Results and Discussion

2.2.1 Synthesis of anionic PPE

Most of the conjugated polyelectrolytes that have been prepared have ionic functional groups such as sulphonate (SO_3^-), carboxylate (CO_2^-), phosphonate (PO_3^{2-}) and ammonium (NR_3^+).[41] For the synthesis of anionic PPEs, there have been strategies to polymerize with the protected form of the monomer, followed by post-polymerization deprotection. This strategy was attempted for the synthesis of a carboxylate-containing PPE, but purification of the polymers from the starting monomers was difficult even with vigorous solvent treatment with Soxhlet extraction. In addition, although the post-polymerization method of deprotection is generally quantitative, there are usually a number of protecting groups that remain and thus may not be fully ionized. These hindrances led us to utilize the synthesis developed by Wosnick[2] to prepare the anionic PPE. The scheme is shown in Figure 2.3, and utilizes a non-protected form of the carboxylic acid as the diiodo monomer. The carboxylic acid groups provide a versatile handle for further conjugation to alcohols or amines in either the monomer or polymer form to synthesize various derivatives. An ester-protected carboxylic acid precursor monomer, prepared using Williamson ether synthesis procedures, was treated with neat trifluoroacetic acid

to furnish the diiodo monomer. The dialkyne pentiptycene monomer, now commercially available from ICx Nomadics, Inc., has been utilized for minimizing aggregation effects in the solid state,[1] and thus was incorporated for the preparation of a non-aggregating anionic copolymer to ensure high quantum yields in the resulting films. Previous studies conducted by Wosnick showed that non-pentiptycene containing anionic PPEs had very poor fluorescent properties when assembled into multilayer films.[2] Pd-catalyzed conditions for Sonogashira cross-coupling in 5 : 4 : 1 (v/v) *N*-methylpyrrolidine : toluene : diisopropylamine yielded the anionic PPE, **P1**, in quantitative yield. This solvent mixture was the optimized ratio in order for the polymerization to proceed, and is attributed to the ability to satisfy the solubility requirements of the two different monomers and the growing polymer chain for the reaction.[2]

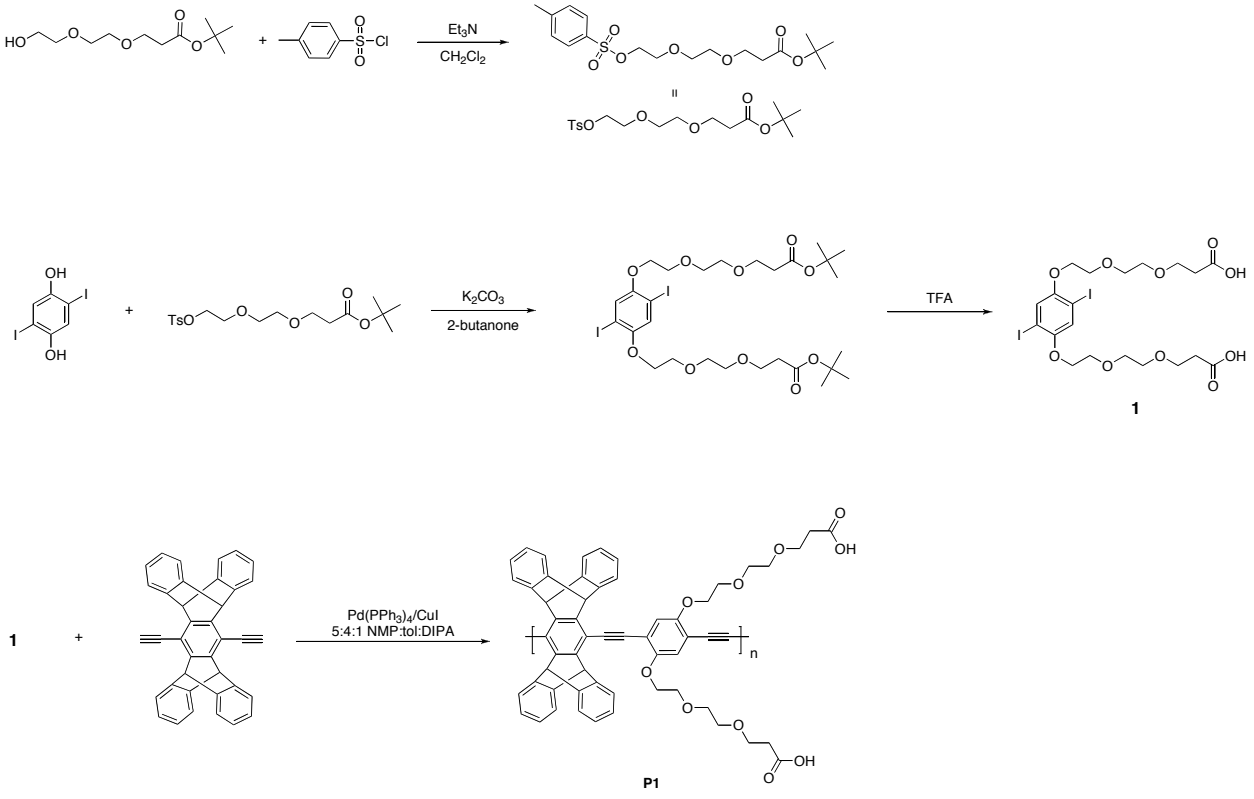

Figure 2.3. Synthesis of monomer **1** and polymer **P1**.

2.2.2 Layer-by-layer assembly of anionic PPE

Although the introduction of the rigid and bulky group for **P1** limits the solubility to DMF and mixtures of DMF/water, layer-by-layer assembled films can be readily achieved. Initial films were made by alternately depositing **P1** at pH 7 conditions with poly(diallyl diammonium chloride) (PDAC), a commonly used strong cationic polyelectrolyte.

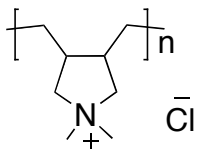

Figure 2.4. Structure of PDAC.

Deposition on glass slides was first performed to monitor the assembly process. UV/Vis absorbance spectroscopy in Figure 2.5 shows consistent buildup of the alternating polyelectrolytes. There is a noticeable blue shift in the absorbance maximum after 10 bilayer depositions, from 410 nm to 405 nm, suggesting that there is reorganization in the multilayer film causing changes in the delocalization behavior of the PPE. The absorption behavior with increasing number of bilayers is curvilinear, with less material being deposited after the initial 5 bilayers. This deviation could be due to depletion or contamination of the solutions over time changing the kinetics of the absorption process. The critical number of bilayers were identified as the maximum amount of PPE deposited while maintaining an optical density of less than 0.1, and found to be 4 bilayers of PDAC/**P1**. The optical density requirement is necessary to avoid any inner filter effects within the sample and distortion in emission spectra.[42]

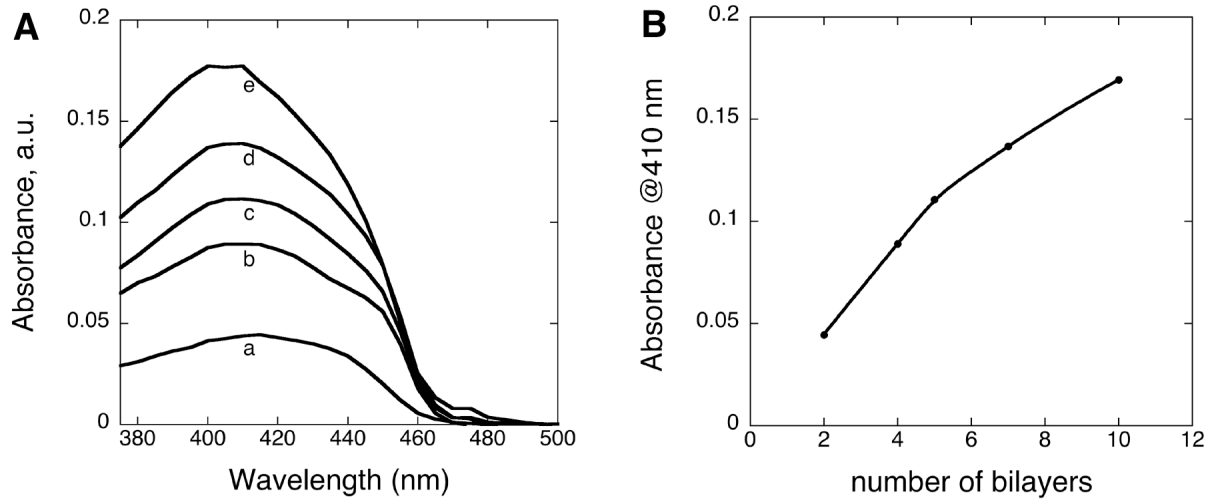

Figure 2.5. (A) UV/Vis absorbance spectra with increasing bilayers of PDAC/**P1** deposited on glass slides. (B) Absorbance at 410 nm versus number of bilayers.

2.2.3 Layer-by-layer assembled films on colloidal particles

We proceeded with adsorbing the polymers onto silica microspheres. Layers of PDAC and **P1** were adsorbed on silica particles (d = 5.0 μm) in solution, similar to the procedure developed by Caruso et al.[18,19] The particles were suspended in the corresponding polymer solution and vortexed for a 15-minute adsorption time, followed by a centrifugation and washing process to remove excess polymer. Microspheres coated with **P1** were bright yellow in color by visual inspection and could be readily dispersed in aqueous and organic solvents to provide a bright blue-green fluorescent turbid suspension.

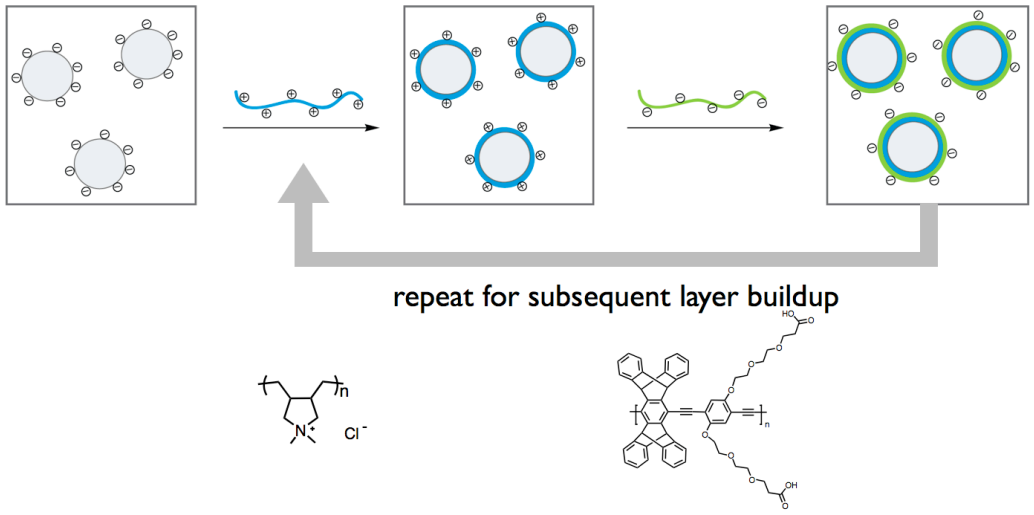

Figure 2.6. Schematic of layer-by-layer assembly on negatively charged colloidal particles with PDAC/ **P1**.

2.2.4 Characterization of PPE-coated particles

The zeta potential of the particles was measured in Milli-Q water to monitor the deposition of PDAC and **P1**. As shown in Figure 2.7, there is a reversal of effective charge, illustrating the overcompensation of the surface charge of adsorbing polyelectrolyte with each layer. The difference in surface charging between positive and negative values can be attributed to the weakly ionizing carboxylate groups of **P1** compared with the cationic PDAC.

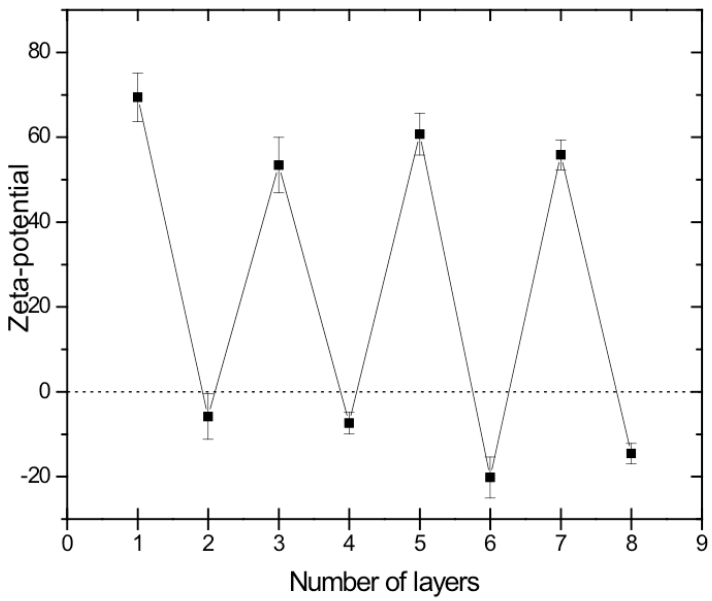

Figure 2.7. Zeta potential (in mV) of PDAC/**P1** silica particles in Milli-Q water. Error bars indicate standard error (n = 3). Odd and even numbers refer to respective PDAC and **P1** adsorption steps.

Figure 2.8 shows the microscopy images of the **P1**-coated particles. The scanning electron microscopy (SEM) microscopy image shows the uniform and relatively smooth coating with the deposition process. Confocal laser scanning microscopy confirms the surface-confined nature of the polymer film on the silica particles. The PPE-coated particles appear as bright "rings", indicating that the fluorescent material is located only at the outer surface of the particle. In addition, the images show the resultant particles are well-dispersed after the deposition process.

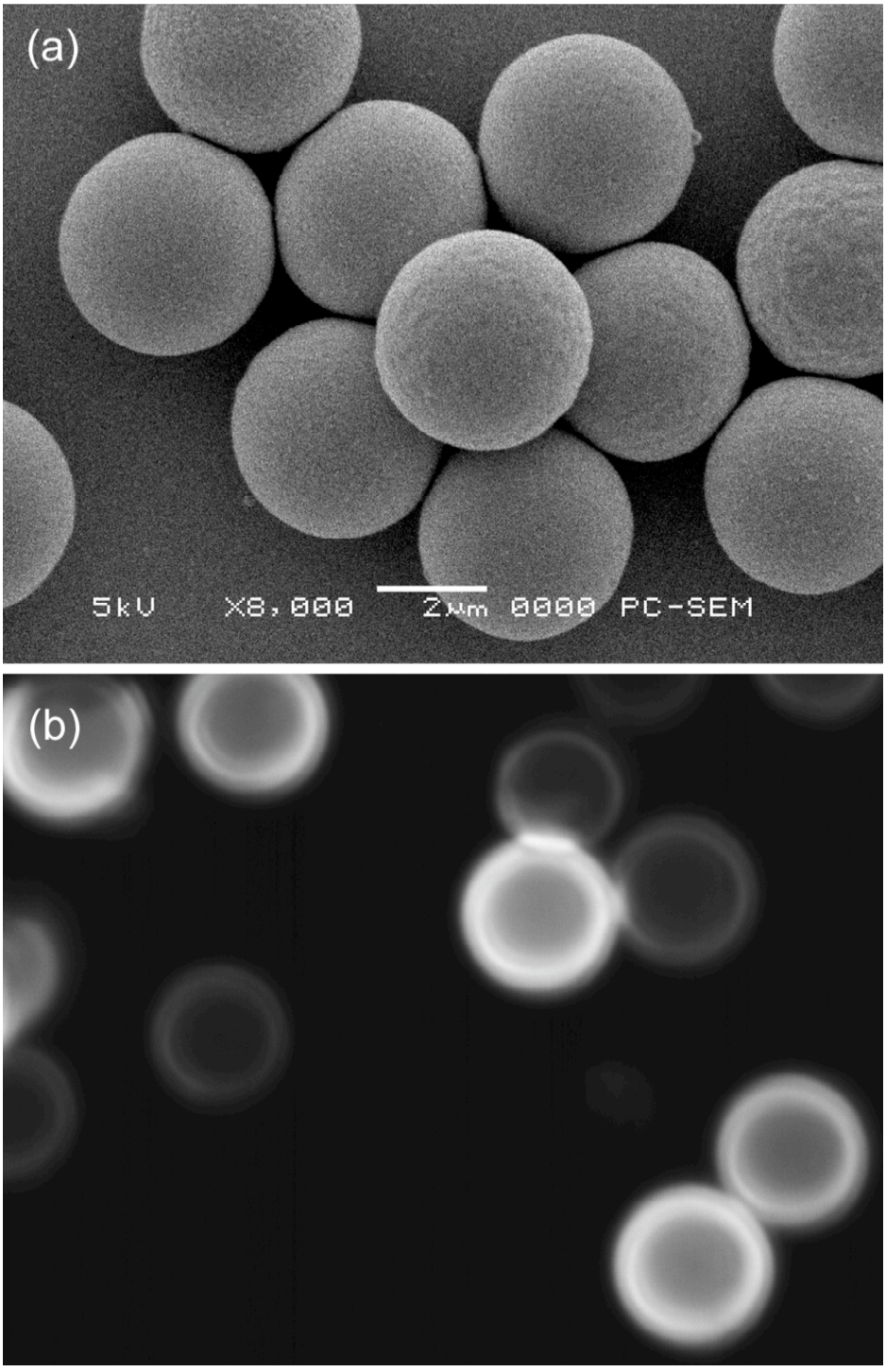

Figure 2.8. (a) Scanning electron microscopy and (b) confocal laser scanning microscropy images of **P1**-coated silica particles (d = 5.0 μm). Reproduced with permission.[4] Copyright 2007 American Chemical Society.

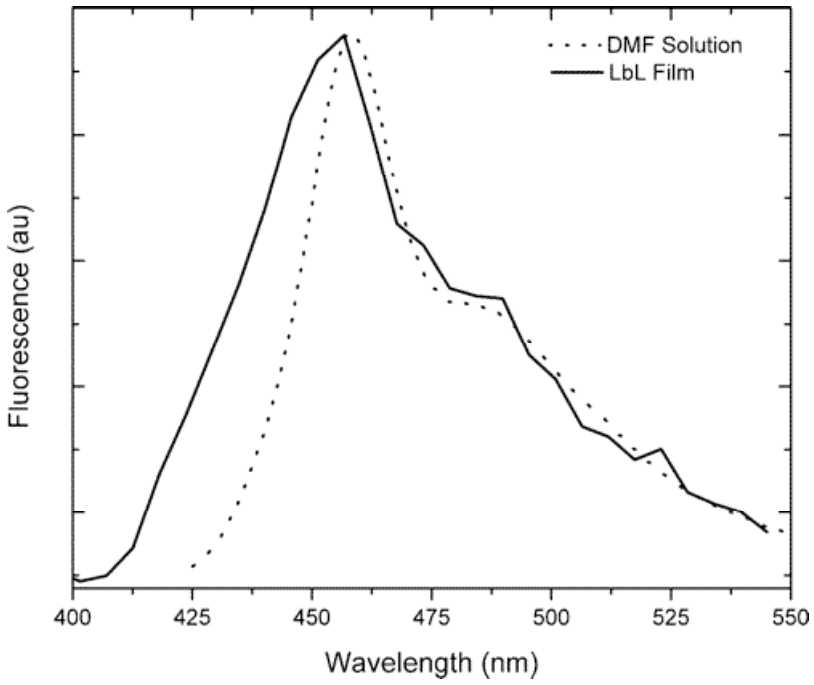

Figure 2.9. Fluorescence spectra of **P1** coated onto a single microsphere (solid line, ex = 364 nm) and in DMF solution (dotted line, ex = 405 nm). Reproduced with permission.[4] Copyright 2007 American Chemical Society.

The coated PPE particles display comparable photophysical behavior as the PPE in solution, indicating the ability of the pentiptycene unit to prevent interchain aggregation,[1] as shown in Figure 2.9 (spectra taken by Dr. Jordan H. Wosnick). The non-aggregating behavior of **P1** eliminates the need to incorporate spacer layers, as was proposed by McQuade et al.[38] for improving quantum yields. The fluorescence spectra of the **P1**-coated particle (Figure 2.9 – solid line) was taken from an individual particle in suspension using the confocal laser scanning microscope in a xyλ scan, and therefore shows much more scattering in the spectrum as compared to that in DMF solution (Figure 2.9 – dotted line) due to background noise in the confocal image.

2.2.5 Preliminary quenching studies of PPE-coated particles

Similar to Wosnick's work with silica-coated microspheres,[2,4] quenching experiments were conducted with 2,4-dinitrophenyl-l-lysine (LysDNP) for polystyrene-coated (PDAC/**P1**)$_4$ particles to explore its possibility as a quencher in our assays. The dinitrophenyl groups have proven to associate strongly with pentiptycene-incorporated PPEs having alkoxy side chains for thin film chemical sensors.[1] LysDNP was utilized as a test quencher since it is commercially available in Fmoc-protected form and can be readily installed on the N- or C-terminus of a peptide substrate in solid-phase peptide synthesis for implementation into the particle sensor as described in Chapter 1. Polystyrene was utilized as the core, since it can be dissolved with solvent to subsequently form hollow capsules.[30] The layer-by-layer assembly procedure for the polystyrene particles is the same as for the silica particles.

The excitation and emission spectra of PS-(PDAC/**P1**)$_4$ particles are shown in Figure 2.10. The excitation spectrum was measured, since the absorption spectrum of PS-(PDAC/**P1**)$_4$ cannot be obtained due to the turbidity of the solution. Scattering is greatly reduced when setting the fluorescence spectrometer to front-face illumination, a configuration useful for highly scattered solutions.[42] The solution spectra were measured under constant stirring with magnetic stirbar in the quartz cuvette. Both the excitation and emission spectra are characteristic of pentiptycene-incorporated PPEs, with a peak emission wavelength at 468 nm and the lower 0–1 band at 500 nm. The lack of broad, weak red-shifted bands indicate the influence of the rigid pentiptycene groups to prevent significant interchain aggregation in the solid state.[1]

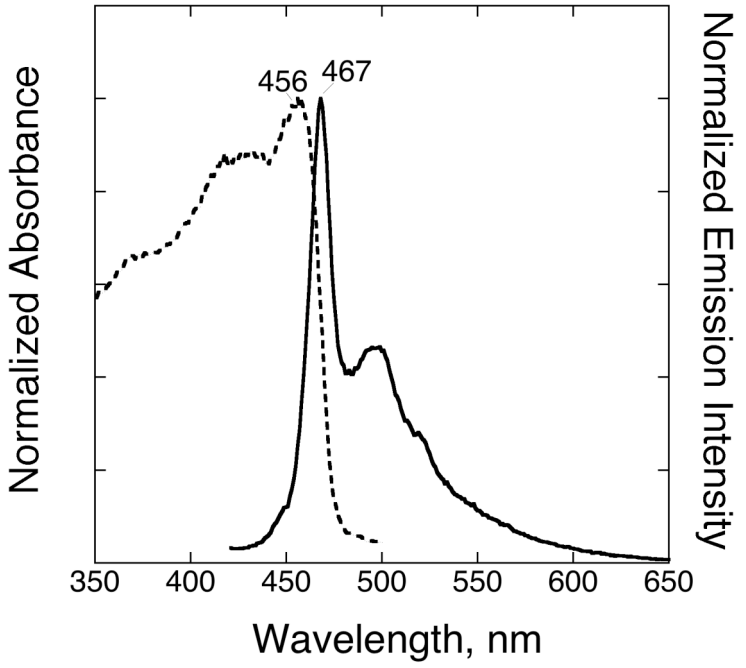

Figure 2.10. Normalized excitation (left axis) and emission (right axis) spectra of PS-(PDAC/**P1**)$_4$ particles in water.

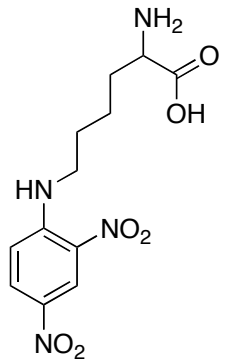

LysDNP

Figure 2.11. Structure of 2,4-dinitrophenyl-l-lysine (LysDNP).

For the quenching experiments with LysDNP in unbuffered water, fluorescence intensity was monitored initially with an excitation wavelength set near the absorbance maximum of **P1**

and at absorbance minimum of LysDNP ($\lambda_{max,abs}$ = 365 nm). Excitation at 410 nm allows for the majority of photons to be absorbed by **P1** and not by LysDNP, to carefully delineate the quenching process from any inner filter effects. At increasing concentrations of LysDNP, the fluorescence is monitored. The ratio of initial fluorescence to concentration-dependent fluorescence is then plotted against quencher concentration. The slope of this linear plot is known as the Stern-Volmer constant (K_{SV}) and is a quantitative measure of the efficiency of quenching, as described in Chapter 1.

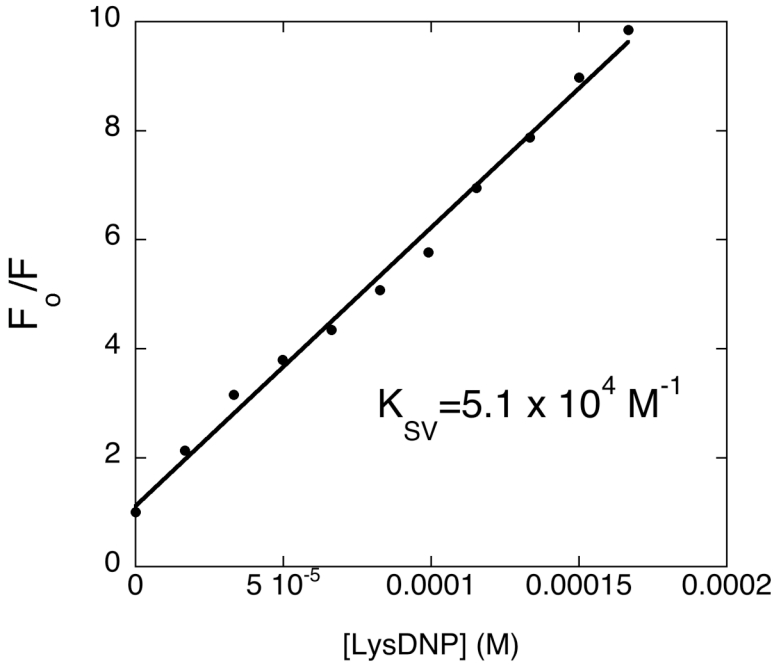

Figure 2.12. F_o/F versus [LysDNP] for PS-(PDAC/**P1**)$_4$ particles in unbuffered water, with fit based on Stern-Volmer equation.

From the Stern-Volmer constant, the concentration needed to quench the polymer to 50% of its initial fluorescence is the reciprocal, and quantified as 19.5 μM of LysDNP. This is a fairly considerable amount of quencher necessary and insufficient for attaining desirable sensitivity for protease assays. Whitten and coworkers have reported nanomolar

concentrations as the limit of detection of protease activity with their conjugated polymer-coated microspheres.[43] This system, however, utilizes streptavidin-biotin interactions to activate the quenching response, and is not a true comparison to our particle quenching system.

We tried to improve the quenching response by looking at several parameters, such as film thickness and quencher type. For nonionic pentiptycene polymers, it was found that for nitro- containing analytes, thicker films (100 Å vs. 25 Å) displayed much lower quenching due to strong surface interactions and slower diffusion through the film.[3] Data from ellipsometry indicates a film thickness of ~200 Å for $(PDAC/PPE)_4$ multilayers, and thus decreasing the number of deposited layers may improve quenching. In all subsequent chapters of this thesis, only one layer of PPE was deposited on the particle surface to minimize this thickness effect. Other molecules can also be assayed for their role as quenchers in improving the overall sensitivity of the amplified quenching response. The assessment of newly designed quenchers is shown in Chapters 3 and 4.

Another aspect of the particle-based quenching is the stability and precision of the measurements. With the previous experiments conducted by Whitten and coworkers,[43] the reproducibility of the measurements was not reported, suggesting there is some error from experiment to experiment. Upon repeating similar conditions to Wosnick's experiments,[2] the response towards the quenchers could not be reproduced. Examining the dynamic nature of the dispersion, there is an associated settling time with the particle suspension due to the size of the particles, and even with stirring it is difficult to keep the particles dispersed. Quencher addition also dilutes the particle concentration to some extent, and methods typically employed for correcting for the dilution cannot be used in this case. These heterogeneities cause problems with reproducibility and the ability to conduct assessments in different conditions. A more reliable method is required for quantification of fluorescence quenching for PPE-coated particles, and this is addressed specifically in Chapter 3.

2.2.6 Incorporating a passive layer "shell" via layer-by-layer assembly: Implications for quenching

A passive layer is required to prevent nonspecific interactions in our sensor design, as described in Chapter 1. Poly(allylamine) hydrochloride (PAH) and poly(acrylic acid) (PAA) were sequentially adsorbed onto the PS-(PDAC/**P1**)$_4$ particles to investigate the use of polymeric multilayers. The Rubner group has shown the ability of these weak polyelectrolytes to form controlled micro- and nano-porous structures with pH treatment.[13,44,45] This type of architecture is preferred in the passive layer, for favorable diffusion of the quencher to the PPE but still providing sufficient distance to eliminate interactions between the quencher and the PPE.

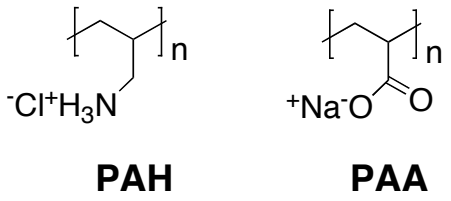

Figure 2.13. Structures of PAH and PAA.

Figure 2.14 and Table 2.1 summarizes the quenching response in unbuffered water when bilayers of PAH/PAA are adsorbed from pH 7 solutions onto PS-(PDAC/**P1**)$_4$ particles. With inclusion of 1 bilayer of PAH/PAA on PS-(PDAC/**P1**)$_4$ the quenching response significantly decreases to half of that of the original particles. The inability of the quenchers to penetrate and come into contact with the PPE coating may be due to the charged environment associated with the additional polyelectrolyte layers. Upon encountering the carboxylate groups of PAA, the positively charged amine groups of LysDNP may associate near the top of the film, giving rise to the much lower quenching response with one bilayer of PAH/PAA. An additional bilayer

decreases the quenching further, indicating the thickness of the multilayer also may have some effect, as described in the previous section.

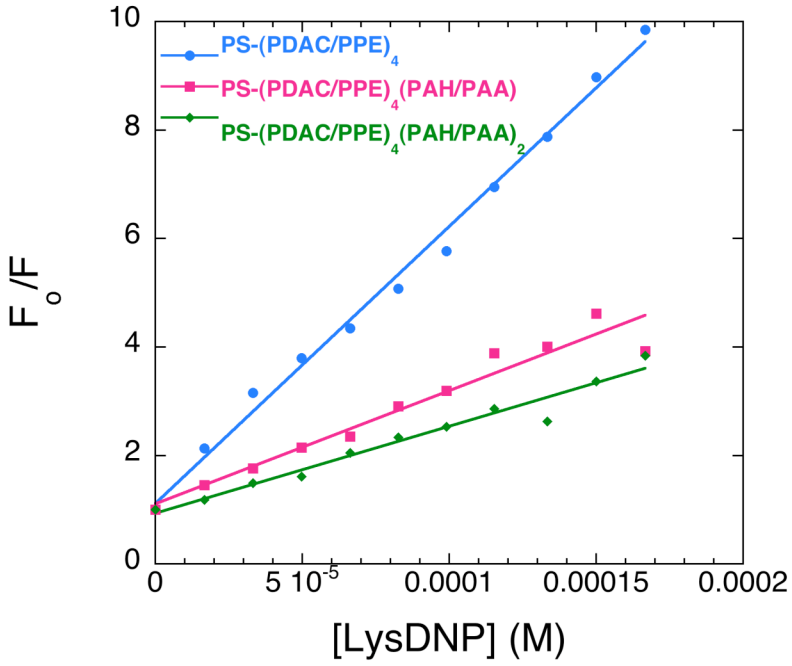

Figure 2.14. Effect of the number of PAH/PAA bilayers on quenching response towards LysDNP. Linear fits based on Stern-Volmer equation.

Number of PAH/PAA bilayers	K_{sv} (M^{-1})
0	5.1×10^4
1	2.1×10^4
2	1.6×10^4

Table 2.1. Quenching constant data for PS-(PDAC/**P1**)$_4$ in response to LysDNP with inclusion of PAH/PAA bilayers.

The pH of the assembling solutions also has an effect on the film porosity.[11] To investigate the pH effect for quenching implications, two bilayers of PAH/PAA were assembled on PS-(PDAC/**P1**)$_4$ particles from solutions of pH 6.5/6.5, 4.5/4.5 and 7.5/3.5 for the respective polycation and polyanion. The solution pK_a values of PAH and PAA are about 9.0 and 5.0

respectively.[10] When the weak polyelectrolytes are assembled at pH 6.5/6.5, both polymers are completely ionized and a highly ionically crosslinked multilayer film is created.[10] Reducing the pH of the dipping solutions to 4.5/4.5 deposits fully ionized PAH and a low ionized PAA on the surface, resulting in a non-stoichiometric pairing of repeat units for a relatively low ionic crosslink density within the film. The result is a readily swellable film that is thicker than that deposited at pH 6.5/6.5.[10] The swelling may allow for the quencher to reach the PPE more readily, resulting in a higher observed K_{SV}. Assembling PAH/PAA at pH 7.5/3.5 creates a "loopy" conformation[10] resulting from the PAA chains adsorbing at a low pH onto fully charged chains of PAH, and subsequent charge neutralization due to the differing pH conditions. The data shown in Figure 2.15 and Table 2.2 suggest this effect of polymer conformation on quenching, i.e. the "loopiness" of the 7.5/3.5 system[11] contributes to the observed increase in quenching.

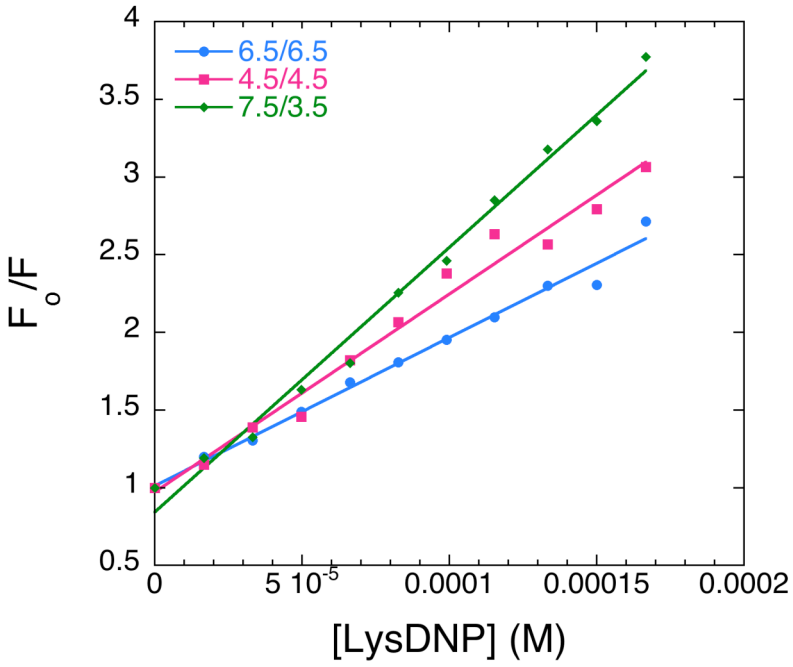

Figure 2.15. Effect of the pH of PAH/PAA dipping solutions (pH denoted as "*x/x*") on quenching response towards LysDNP. Linear fits based on Stern-Volmer equation.

pH of PAH/PAA	K_{SV} (M^{-1})
6.5/6.5	9.5×10^3
4.5/4.5	1.3×10^4
7.5/3.5	1.7×10^4

Table 2.2. Quenching constant data for PS-(PDAC/**P1**)$_4$(PAH/PAA)$_2$ in response to LysDNP, with PAH/PAA deposited at different pH conditions.

The use of the weak polyelectrolyte system, PAH/PAA, proved to be problematic in constructing the passive layer since the quencher-PPE interaction was severely affected, even with two deposited bilayers. Multilayers assembled using hydrogen bonding interactions on the particles[20,21] would provide a nonionic environment, and reduce the charge interactions that may be limiting the observed quenching in this study.

2.2.7 Hollow capsules of PPE formed using layer-by-layer assembly

Hollow capsules can be formed from layer-by-layer assembled films deposited on a sacrificial core such as polystyrene. The polyelectrolytes for assembling the multilayer films are generally soluble in polar solvents and insoluble in solvents such as toluene or chloroform. Depositing multilayer films onto a template core, followed by preferential solvent treatment of the core, can produce hollow capsules.[30] We can introduce nonionic PPEs with this method by encapsulating the macromolecules in a matrix suitable for layer-by-layer as a template, followed by removal of the matrix. The implementation of nonionic conjugated polymers allow for a greater diversity of synthesized materials to be used for biosensing applications. The hollow capsule introduces permeability with the structure, which may prove beneficial for rapid transport of the quencher to the PPE. The localization of the hydrophobic PPE in the interior of

the capsule may increase the uptake of the hydrophobic quencher through the multilayer wall due to solute-solvent partitioning.

In collaboration with Dr. Saif Khan of Professor Klavs Jensen's group at MIT, a nonionic analog to **P1** was encapsulated in polystyrene (PS) particles of controlled size using their developed microfluidic reactors[46] and traditional free-radical emulsion polymerization techniques. The PPE is mixed with the precursor styrene solution to create fluorescent particles of discrete size.

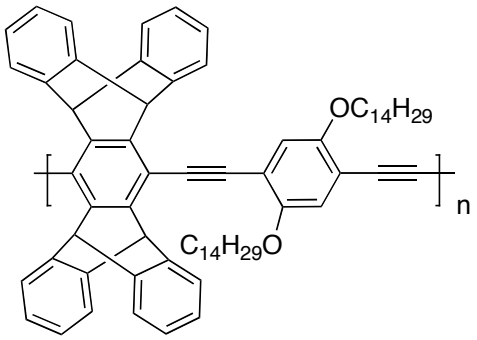

P1a

Figure 2.16. Structure of nonionic PPE (**P1a**) used for encapsulating in polystyrene particles.

Depositing 4 bilayers of PAH/PAA at pH 7 conditions onto PS-**P1a** particles, followed by toluene treatment, results in dissolution of the PS to form hollow capsules. The spatial profile from confocal microscopy in Figure 2.17 indicates the diameter of the PS-**P1a** particles to be ~2 μm. The capsules are only fluorescent along the wall, while the solid core particles are fluorescent throughout the structure. The multilayer film swells in toluene to allow the dissolved PS to diffuse out and maintain a shell in which the PPE is entangled. The spectra obtained from the confocal xyλ scan of individual particles show that both the solid and hollow structures display emission maximum wavelengths identical to the PPE in chloroform solution (~450 nm),

indicating no major alterations in the photophysical properties upon incorporation into a PS material and subsequent core removal. While this method provided for nonionic PPEs to be incorporated into particles, we had hoped to encapsulate a greater amount of fluorescent material in the interior of the capsule rather than only being localized at the capsule wall. Toluene treatment partially dissolved the PPE as well as the PS core, leading to less encapsulated PPE material. In addition, the capsules assembled from PAH/PAA multilayers do not have the structural integrity we desired, as they are rather flexible and are prone to collapsing. The SEM images in Figure 2.18 show after solvent treatment the dried particles have collapsed, further confirming capsule formation. While we will not utilize the capsules for constructing particle sensors in this thesis, the ability to form fluorescent hollow structures that are not prone to leakage with changes in the environmental pH, in contrast to the conventionally small molecule dyes that are generally used,[32] may aid other researchers in measuring the membrane transport properties of these multilayer films utilizing fluorescence and energy or electron transfer interactions.

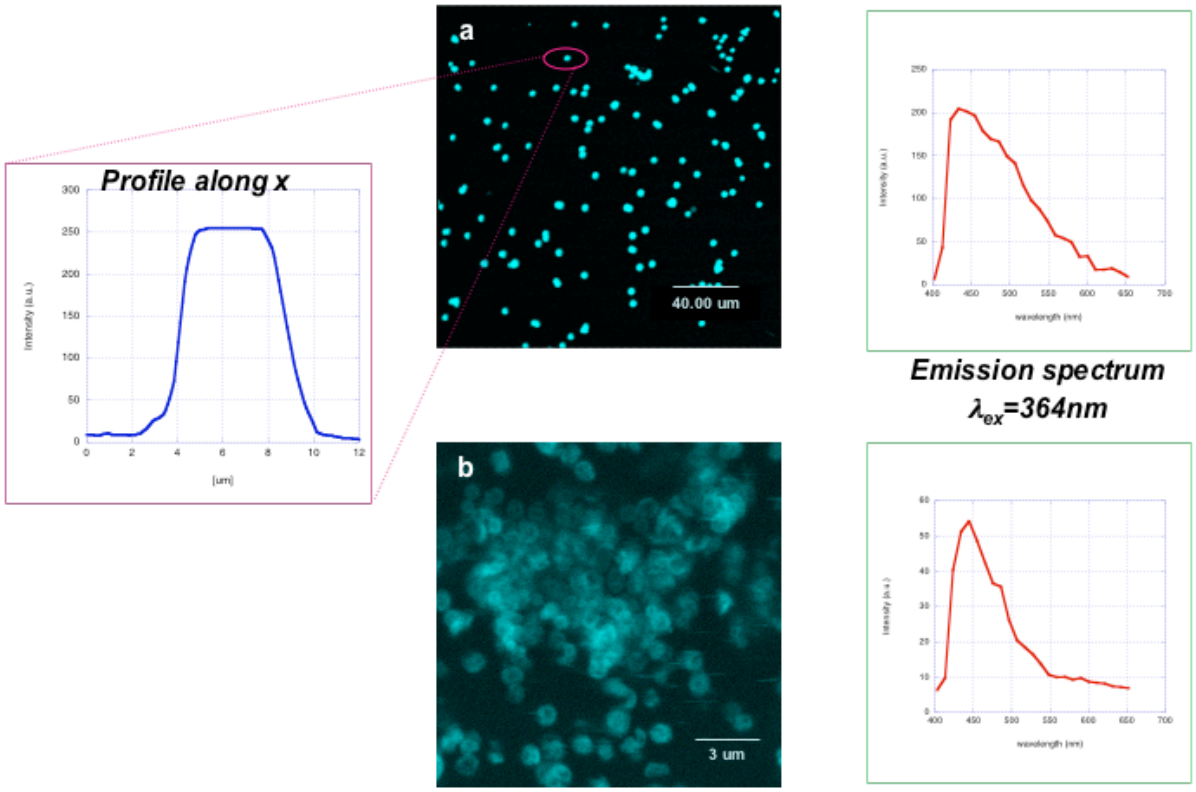

Figure 2.17. Confocal microscopy images and spectra for **P1a**-PS-(PAH/PAA)$_4$ (a) before and (b) after toluene treatment. Spatial profile is shown for particles before solvent treatment.

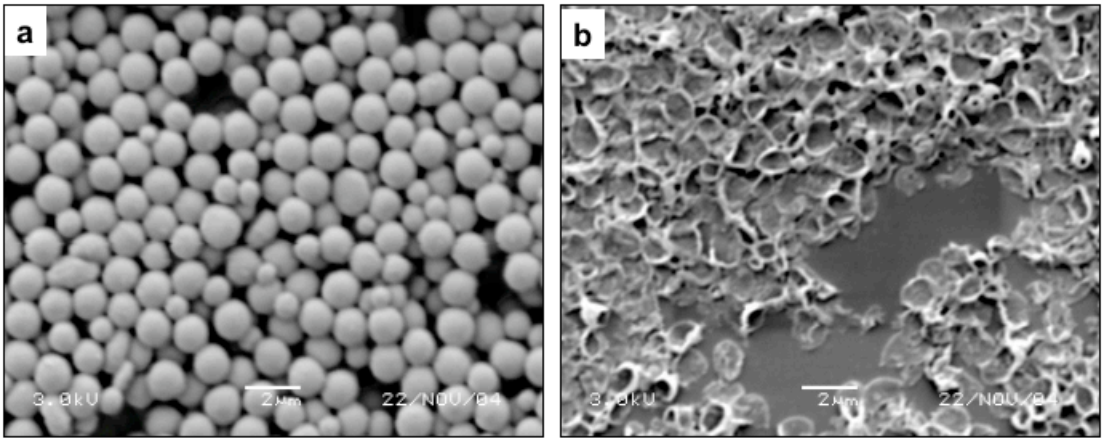

Figure 2.18. SEM images of **P1a**-PS-$(PAH/PAA)_4$ particles (a) before and (b) after toluene treatment.

2.3 Conclusion

Layer-by-layer assembly has been used to create PPE multilayer films with a synthesized pentiptycene-incorporated anionic PPE. Characterization has been performed for both planar and colloidal substrates to show the layer buildup is consistent, and the films are smooth and uniform. Solution-based quenching studies can be performed with the PPE-coated particles in suspension, but a need still exists for improving the assay in terms of sensitivity and reliability of measurement. Multilayer films of weak polyelectrolytes such as PAH and PAA were used as an initial "passive layer", and the effect on the quenching response was observed. Capsule formation was also pursued to encapsulate nonionic PPEs within multilayer films, providing new prospects in sensor development.

2.4 Experimental Section

Materials

Starting compounds 2,5-diiodobenzene-1,4-diol (**a**) and *tert*-butyl 3-(2-(2-(tosyloxy)ethoxy)ethoxy)propanoate (**b**) were kindly provided by Dr. Juan Zheng. Diethynylpentiptycene was purchased from ICx Nomadics Life Sciences, Inc. Copper(I) iodide (Sigma-Aldrich) and $Pd(PPh_3)_4$ (Strem) were kept in a nitrogen glovebox. Poly(diallyl ammonium chloride) (PDAC, average M_v ~300 kDa) was purchased as a 40 wt% aqueous solution from Dajac Laboratories. Poly(styrene sulfonic acid) sodium salt (PSS, M.W. 500 kDa) was obtained from Polysciences. Poly(allylamine hydrochloride) (PAH, M.W. 60 kDa) was obtained from Alfa Aesar. Poly(acrylic acid) (PAA, average M_v ~450 kDa) was obtained from Sigma-Aldrich. Unless otherwise specified, all other chemicals and solvents were purchased from Sigma-Aldrich and used as received. Glass microscope slides (VWR) and silicon [1 1 0] substrates (Wafernet, Inc.) were cleaned by sonification for 15 minutes in detergent (Lysol) solution, followed by sonification in water, and dried with nitrogen stream prior to use. Silica (d = 5.0 μm) and polystyrene (d = 1.48 μm) microspheres were purchased from Bangs Labs and stored at 0ºC. Measurements for pH were made with a Thermo-Orion pH meter, and polymer solutions were adjusted with dilute solutions of NaOH and HCl. All water used in experiments was obtained from a Millipore Milli-Q purification system.

Methods

General characterization

^{1}H and ^{13}C NMR spectra were recorded on a Varian Mercury or Inova instrument in deuterated solvents (Cambridge Isotopes Laboratories). Polymer molecular weights were determined using gel permeation chromatography using a Hewlett Packard series 1100 GPC system equipped with a diode array detector (254 nm and 450 nm) and a refractive index detector running at 1.0 mL/min. in THF. Molecular weights are reported relative to polystyrene (Polysciences) as standard. Absorbance was measured using a Cary 50 UV-Vis spectrophotometer, corrected for substrate baseline. Steady-state fluorescence was acquired for the particle suspensions using a Jobin Yvon SPEX Fluorolog-τ2 fluorometer at room temperature using a 1 cm-path length quartz cuvette in front-face detection mode, with constant magnetic stirring. Ellipsometry measurements were performed on silicon substrates, modeled with an oxide layer and a Cauchy layer for the multilayer film. Confocal microscopy images were taken on a Leica TCS-SP2 confocal laser scanning microscope using an argon 360 nm laser as the excitation source and a 63x/1.4 oil immersion lens. Confocal image from Figure 2.7(a) and spectra from Figure 2.8 were taken by Dr. Jordan H. Wosnick.[2,4]

Synthesis of monomer 1

To a 250 mL 2-neck round-bottom flask with a stirbar, 1.72 g of **a** (4.8 mmol) and 5.55 g of **b** (14.3 mmol) were added, followed by 50 mL of 2-butanone. The reaction mixture was stirred and sparged with nitrogen for 30 minutes. Potassium carbonate, anhydrous, was added (3.98 g, 28.8 mmol), and the flask was heated to reflux at 90ºC in an oil bath for 52 hours. The reaction mixture, milky white, was then cooled and subsequently filtered to remove potassium carbonate. The filtrate was washed with acetone and dried *in vacuo* to obtain the crude product

as a brown oil. Purification with silica column chromatography, running in 1 : 1 hexane : ethyl acetate, resulted in a rosy-colored oil **c** (3.1 g, 82%). ^{1}H NMR (δ in ppm, 300 MHz, $CDCl_3$) 7.22 (s, 2H), 4.09 (m, 4H), 3.88 (m, 4H), 3.75 (m, 8H), 3.65 (m, 4H), 2.52 (t, 4H), 1.44 (s, 18H). ^{13}C NMR (δ in ppm, 125 MHz, $CDCl_3$) 171.1, 153.2, 123.6, 86.6, 80.7, 71.2, 70.7, 70.4, 69.7, 67.1, 36.4, 28.3.

To a 50 mL round bottom flask, 0.9 g of **c** (1.1 mmol) was added. Neat trifluoroacetic acid (TFA) was added, and the reaction mixture was stirred at room temperature for 1 hour. TFA was then carefully pumped off by vacuum, and a white solid formed. Water was added to wash and precipitate the solid several times. The reaction mixture was centrifuged, followed by lyophilization, to collect the product (0.4 g, 44%). ^{1}H NMR (δ in ppm, 300 MHz, DMSO-d_6) 7.37 (s, 2H), 4.09 (m, 4H), 3.74 (m, 4H), 3.59 (m, 8H), 3.52 (m, 4H), 2.50 (m, 4H). ^{13}C NMR (δ in ppm, 125 MHz, DMSO-d_6) 172.7, 152.5, 122.8, 86.9, 70.1, 69.7, 69.6, 68.9, 66.3, 34.8.

Synthesis of polymer P1

To a 10 mL Schlenk tube, 17.6 mg of **1** (0.026 mmol) and 12.7mg of diethynylpentiptycene (0.027 mmol) were added, and subsequently evacuated and backfilled with argon three times. The tube was transferred to the glovebox and catalytic amounts of CuI and $Pd(PPh_3)_4$ were added. The sealed tube was transferred to air atmosphere, and 1.5 mL of the solvent mixture (5 : 4 : 1 (v/v) *N*-methylpyrrolidine : toluene : diisopropylamine, degassed for 30 minutes with nitrogen) was added under argon pressure for complete solubility of the starting materials. The tube was completely sealed and heated in an oil bath at 70ºC. The solution turned from a milky white color to a yellow solution within 1 hour of heating. The solution was further heated for 3 days, after which the solution was bright yellow and fluorescent green under UV illumination. The tube was then removed from heat and opened to the air. Ethyl acetate

was added to precipitate the reaction mixture, and centrifuged to collect a yellow solid, dried *in vacuo* (23 mg, 92% yield). ^{1}H NMR (δ in ppm, 500 MHz, DMF-d_7) 7.72 (broad s, 2H), 7.11 (broad m, 8H), 6.43 (broad s, 8H), 4.82 (broad s, 4H), 4.35 (broad s, 4H), 3.77–3.79 (broad m, 8H), 3.64–3.68 (broad m, 8H), 2.49 (broad m, 4H).

Synthesis of polymer P1a

To a 10 mL Schlenk tube, 54.6 mg of 1,4-diiodo-2,5-bis(tetradecyloxy)benzene (0.067 mmol) and 35.5 mg of diethynylpentiptycene (0.070 mmol) was added, and subsequently evacuated and backfilled with argon three times. The tube was transferred to the glovebox and catalytic amounts of CuI and $Pd(PPh_3)_4$ were added. The sealed tube was transferred to air atmosphere, and 1.5 mL of the solvent mixture (4 : 1 (v/v) toluene : diisopropylamine, degassed for 30 minutes with nitrogen) was added under argon pressure for complete solubility of the starting materials. The tube was completely sealed and heated in an oil bath at 60ºC. The solution was heated for 5 days, after which the solution was bright yellow and fluorescent green under UV illumination. The tube was then removed from heat and opened to the air. Methanol was added to precipitate the reaction mixture, and centrifuged to collect a yellow solid, dried *in vacuo* (62 mg, 92% yield). GPC in THF (UV) $M_n = 1.2 \times 10^4$ g/mol, PDI = 1.4. ^{1}H NMR (δ in ppm, 500 MHz, DMF-d_7) 7.43 (broad m, 2H), 7.32 (broad m, 8H), 4.43 (broad s, 4H), 3.70 (broad m, 4H), 1.68 (broad m, 4H), 1.41 (broad m, 4H), 1.21 (broad m, 36H), 0.84 (broad m, 6H).

Layer-by-layer assembly for film formation

Films on planar substrates were deposited using an automated slide dipper (Zeiss) by alternate immersion of glass slides (pretreated with a layer of PDAC/PSS/PDAC) for 15 minutes

into 1 mM (repeat unit) solutions of PDAC in water and **P1** in 1 : 1 mixture of DMF : water. Slides were immersed in 3 consecutive baths of water after each adsorption step for 4-minute rinse times. Films were kept wet and dried with nitrogen stream prior to characterization.

Preparation of silica (d = 5.0 μm) and polystyrene microspheres (d = 1.48μm) followed similar procedure to adsorb bilayers of PDAC/**P1**. In a 1.5 mL centrifuge tube, 100 μL of the particle solution was added with 900 μL of water. The tube was centrifuged for 4 minutes at 14,500 RPM to settle the particles. The supernatant was removed and replaced with 1 mL of the PDAC solution, sonicated with a probe sonicator (Misonix) for 10 seconds at 3.5 W (RMS) to fully disperse the particles, and vortexed at high speed for 15 minutes. The tube was then centrifuged, and the PDAC solution was removed. Water (1 mL) was added, followed by sonication and centrifugation, to wash the particles. This step was repeated twice before the next adsorption step. **P1** solution (1 mL) was adsorbed in the same manner as the previous PDAC step, with sonication and vortexing followed by the two wash steps. The procedure was repeated for the desired number of bilayers. Adsorption of PAH and PAA followed the same procedure. The coated particles were then stored in aqueous solution at 0ºC until used for subsequent experiments, resuspended with sonication.

Scanning electron microscopy (SEM)

Samples of particles and capsules were prepared by applying a drop of aqueous suspension to a glass slide and drying overnight in a vacuum oven at 25°C. The samples were sputtered with gold and measurements were conducted using a JEOL JSM-6060 Scanning Electron Microscope at an operating voltage of 3kV.

Zeta potential measurements

Electrophoretic mobilities of the PDAC/PPE-coated silica particles were measured with a Brookhaven Instruments Zeta Potential Analyzer. The mobility μ was converted into a ζ-potential by using the Smoluchowski relation $\zeta = \mu\eta/\varepsilon$, where η and ε are the viscosity and permittivity of the solution, respectively. All ζ-potential measurements were performed in resuspension of samples in Milli-Q water.

Quenching experiments

A 0.01 M LysDNP stock solution in water was prepared prior to experiments. For Stern-Volmer quenching experiments, 1–5 μL aliquots were added to the cuvette and agitated before measuring intensity. To minimize overlap of the quencher and polymer absorption, the experiments were conducted with excitation at 450 nm. Fluorescence intensity at 468 nm (λ_{max}) was recorded with each quencher addition, and plotted as the ratio of initial fluorescence to observed fluorescence (F_o/F) versus quencher concentration, in molar concentration. The Stern-Volmer constant, K_{sv}, is obtained by the linear fit of this plot.

Preparation of P1a-encapsulated polystyrene particles[47]

The procedure was conducted by Saif Khan in the Jensen group, and is provided here in brief.

P1a solutions were made in styrene monomer in two concentrations (10 mg/mL and 1 mg/mL). The following two reactant solutions were then made:

2 mL ethanol + 0.4 mL of 10 mg/mL (OR 0.4 mL of 1 mg/mL) solution of PPE.

2 mL ethanol + 4 mg azobis-isobutyronitrile (AIBN) + 80 mg polyvinylpyrrolidone (PVP, MW: 55,000)

The two reactant solutions were mixed and heated to 80ºC at 200 RPM, and kept stirring for 6–48 hours, depending on the required sizes (100 nm–2 μm).

Capsule formation from P1a-encapsulated polystyrene particles

PAH and PAA were deposited onto the PS-**P1a** particles for a total of 4 bilayers as described in the previous section. The coated particles were suspended as 0.5 wt. % solids in ethanol in a 1.5 mL centrifuge tube. The suspension was centrifuged at 14,500 RPM for 15 minutes and the supernatant was removed. Toluene (1.0 mL) was added to the pellet, and the particles were resuspended in solvent with probe ultrasonication for 5 seconds at 3.5 W (RMS). The tube was vortexed overnight at high speed, followed by centrifugation and rinsing with ethanol to remove all traces of toluene.

2.5 References

(1) Yang, J. S.; Swager, T. M. *J. Am. Chem. Soc.* **1998**, *120*, 11864-11873.

(2) Wosnick, J. H., PhD dissertation, Massachusetts Institute of Technology, 2004.

(3) Yang, J. S.; Swager, T. M. *J. Am. Chem. Soc.* **1998**, *120*, 5321-5322.

(4) Wosnick, J. H.; Liao, J. H.; Swager, T. M. *Macromolecules* **2005**, *38*, 9287-9290.

(5) Decher, G.; Hong, J.-D. *Ber. Bunsenges Phys. Chem.* **1991**, *95*, 1430-1434.

(6) Decher, G.; Hong, J.-D. *Makromol. Chem. Macromol. Symp.* **1991**, *46*, 321-327.

(7) Decher, G. *Science* **1997**, *277*, 1232-1237.

(8) Hammond, P. T. *Adv. Mater.* **2004**, *16*, 1271-1293.

(9) Tang, Z.; Wang, Y.; Podsiadlo, P.; Kotov, N. A. *Adv. Mater.* **2006**, *18*, 3203-3224.

(10) Rubner, M. F. In *Multilayer Thin Films: Sequential Assembly of Nanocomposite Materials*; Decher, G., Schlenoff, J. B., Eds.; Wiley-VCH: Weinheim, 2003; Vol. 142.

(11) Shiratori, S. S.; Rubner, M. F. *Macromolecules* **2000**, *33*, 4213-4219.

(12) Yoo, D.; Shiratori, S. S.; Rubner, M. F. *Macromolecules* **1998**, *31*, 4309-4318.

(13) Hiller, J. A.; Mendelsohn, J. D.; Rubner, M. F. *Nat. Mater.* **2002**, *1*, 59-63.

(14) Kotov, N. A. *Nanostruct. Mater.* **1999**, *12*, 789-796.

(15) Dubas, S. T.; Schlenoff, J. B. *Macromolecules* **1999**, *32*, 8153-8160.

(16) Stockton, W. B.; Rubner, M. F. *Macromolecules* **1997**, *30*, 2717-2725.

(17) Sukhorukov, G. B.; Donath, E.; Davis, S.; Lichtenfeld, H.; Caruso, F.; Popov, V. I.; Möhwald, H. *Polym. Adv. Technol.* **1998**, *9*, 759-767.

(18) Caruso, F.; Donath, E.; Möhwald, H. *J. Phys. Chem. B* **1998**, *102*, 2011-2016.

(19) Sukhorukov, G. B.; Donath, E.; Lichtenfeld, H.; Knippel, E.; Knippel, M.; Budde, A.; Möhwald, H. *Colloids Surf., A* **1998**, *137*, 235-266.

(20) Yang, S. Y.; Lee, D.; Cohen, R. E.; Rubner, M. F. *Langmuir* **2004**, *20*, 5978-5981.

(21) Yang, S.; Zhang, Y.; Yuan, G.; Zhang, X.; Xu, J. *Macromolecules* **2004**, *37*, 10059-10062.

(22) Schneider, G.; Decher, G. *Nano Lett.* **2004**, *4*, 1833-1839.

(23) Mayya, K. S.; Schoeler, B.; Caruso, F. *Adv. Funct. Mater.* **2003**, *13*, 183-188.

(24) Aliev, F. G.; Correa-Duarte, M. A.; Mamedov, A.; Ostrander, J. W.; Giersig, M.; Liz-Marzán, L. M.; Kotov, N. A. *Adv. Mater.* **1999**, *11*, 1006-1010.

(25) Caruso, F.; Schüler, C.; Kurth, D. G. *Chem. Mater.* **1999**, *11*, 3394-3399.

(26) Susha, A.; Caruso, F.; Rogach, A. L.; Sukhorukov, G. B.; Kornowski, A.; Möhwald, H.; Giersig, M.; Eychmüller, A.; Weller, H. *Colloids Surf., A* **2000**, *163*, 39-44.

(27) Caruso, F.; Shi, X.; Caruso, R. A.; Susha, A. *Adv. Mater.* **2001**, *13*, 740-744.

(28) Caruso, F.; Schüler, C. *Langmuir* **2000**, *16*, 9595-9603.

(29) Caruso, F.; Caruso, R. A.; Möhwald, H. *Science* **1998**, *282*, 1111-1114.

(30) Dahne, L.; Leporatti, S.; Donath, E.; Möhwald, H. *J. Am. Chem. Soc.* **2001**, *123*, 5431-5436.

(31) Sukhorukov, G. B.; Antipov, A. A.; Voigt, A.; Donath, E.; Möhwald, H. *Macromol. Rapid Commun.* **2001**, *22*, 44-46.

(32) Antipov, A. A.; Sukhorukov, G. B. *Adv. Colloid Interface Sci.* **2004**, *111*, 49-61.

(33) Ferreira, M.; Rubner, M. F. *Macromolecules* **1995**, *28*, 7107-7114.

(34) Fou, A. C.; Rubner, M. F. *Macromolecules* **1995**, *28*, 7115-7120.

(35) Kim, S.; Jackiw, J.; Robinson, E.; Schanze, K. S.; Reynolds, J. R.; Baur, J. W.; Rubner, M. F.; Boils, D. *Macromolecules* **1998**, *31*, 964-974.

(36) Baur, J. W.; Kim, S.; Balanda, P. B.; Reynolds, J. R.; Rubner, M. F. *Adv. Mater.* **1999**, *10*, 1452-1455.

(37) Baur, J. W.; Rubner, M. F.; Reynolds, J. R.; Kim, S. *Langmuir* **1999**, 6460-6469.

(38) McQuade, D. T.; Hegedus, A. H.; Swager, T. M. *J. Am. Chem. Soc.* **2000**, *122*.

(39) Pinto, M. R.; Kristal, B. M.; Schanze, K. S. *Langmuir* **2003**, *19*, 6523-6533.

(40) Caruso, F. *Adv. Mater.* **2001**, *13*, 11-22.

(41) Pinto, M. R.; Schanze, K. S. *Synthesis* **2002**, *9*, 1293-1309.

(42) Lakowicz, J. R. *Principles of Fluorescence Spectroscopy*; Kluwer Academic/Plenum: New York, 1999.

(43) Kumaraswamy, S.; Bergstedt, T.; Shi, X.; Rininsland, F.; Kushon, S.; Xia, W.; Ley, K.; Achyuthan, K.; McBranch, D.; Whitten, D. *Proc. Natl. Acad. Sci.* **2004**, *101*, 7511-7515.

(44) Zhai, L.; Cebeci, F. C.; Cohen, R. E.; Rubner, M. F. *Nano Lett.* **2004**, *4*, 1349-1353.

(45) Mendelsohn, J. D.; Barrett, C. J.; Chan, V. V.; Pal, A. J.; Mayes, A. M.; Rubner, M. F. *Langmuir* **2000**, *16*, 5017-5023.

(46) Khan, S. A.; Günther, A.; Schmidt, M. A.; Jensen, K. F. *Langmuir* **2004**, *20*, 8604-8611.

(47) Khan, S. A., personal communication.

Chapter 3:

Ratiometric Method for Quantification of Fluorescence Quenching of PPE-Coated Particles

3.1 Introduction

The capacity of fluorescent particles to image and monitor biological activity[1,2] has stimulated interest in the development of integrated particle platforms containing conjugated polymers (CPs).[3-8] The extended electronic structure of CPs is highly sensitive to perturbations and provides for an amplified response that has proven useful in numerous sensing applications.[9-11] Additionally, it is recognized that understanding the role of molecular structure and organization in CPs is critical for the creation of more sensitive systems for chemical detection.[12] For biosensing, the molecular design criteria are of paramount importance, and it has proved challenging to design CPs that retain their desired emissive properties while not suffering from nonspecificity in their interaction with analytes.[13,14] With these considerations in mind, we are focusing on constructing particle-based sensory systems that display high fidelity in aqueous environments and demonstrate specificity in a complex chemical/biochemical environment. To this end, we require a reliable and quantitative method for measuring the change in fluorescence upon addition of an electron-deficient quenching species. We detail herein a ratiometric method[15-17] using a noninteracting species as a reference in order to properly quantify the responses as a function of molecular structure. This approach not only allows for precise measurement by providing a standard for comparison,[18,19] but also enables direct quantification of quenching species, a beneficial output in any sensory system.

3.1.1 Internal reference for quantification of particle quenching

In this chapter, we examine a series of poly(phenylene ethynylene)s (PPE)s, **P1–P3**, as films supported on europium-incorporated polystyrene particles (d = 0.2 μm) for their fluorescence quenching response towards viologens, which are well-known electron-accepting aromatic molecules. Figure 3.1 depicts the general scheme. Methyl viologen (**MV^{2+}**) and a

naphthyl-derivative[20] (**MV^{2+}-nap**) (Figure 3.2) are compared to determine the influence of hydrophobic interactions to promote interactions with the polymer films.[21] **P1** was shown previously to display enhanced quenching on microspheres with 2,4-dinitrotoluene-*l*-lysine relative to a solution-based assay.[22] This enhancement is attributed to greater exciton diffusion lengths and the improved analyte polymer interactions in the solid state. The incorporation of pentiptycene units into the main chain of the polymer yields non-aggregating films with superior emissive properties,[23] and the carboxylic acid moiety allows for electrostatic adsorption onto charged surfaces.[24] We are also interested to interrogate the efficacy of molecular receptors[11] under different system conditions, and **P2** and **P3**, the former which contains cyclophane receptors, were synthesized to elucidate this role. Polymers **P2** and **P3** have reduced charge densities relative to **P1**, and these terpolymers to have a molar ratio of 1 : 1 pentiptycene unit : comonomer(s) to prevent unfavorable aggregation in the system.[23] This systematic comparative approach was designed to establish a better understanding of the influence of molecular structure on the polymer's performance in biosensing applications.

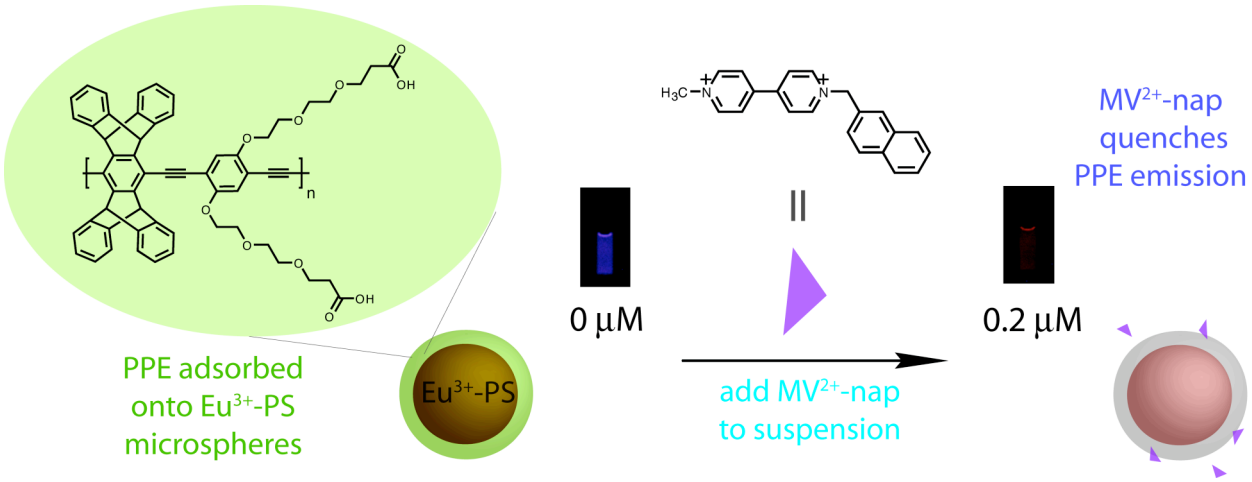

Figure 3.1. Schematic of ratiometric method for quantification of fluorescence quenching of PPE-coated particles.

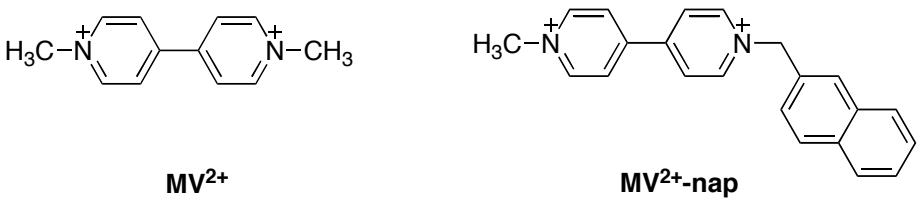

Figure 3.2. Structures of functionalized viologen quenchers.

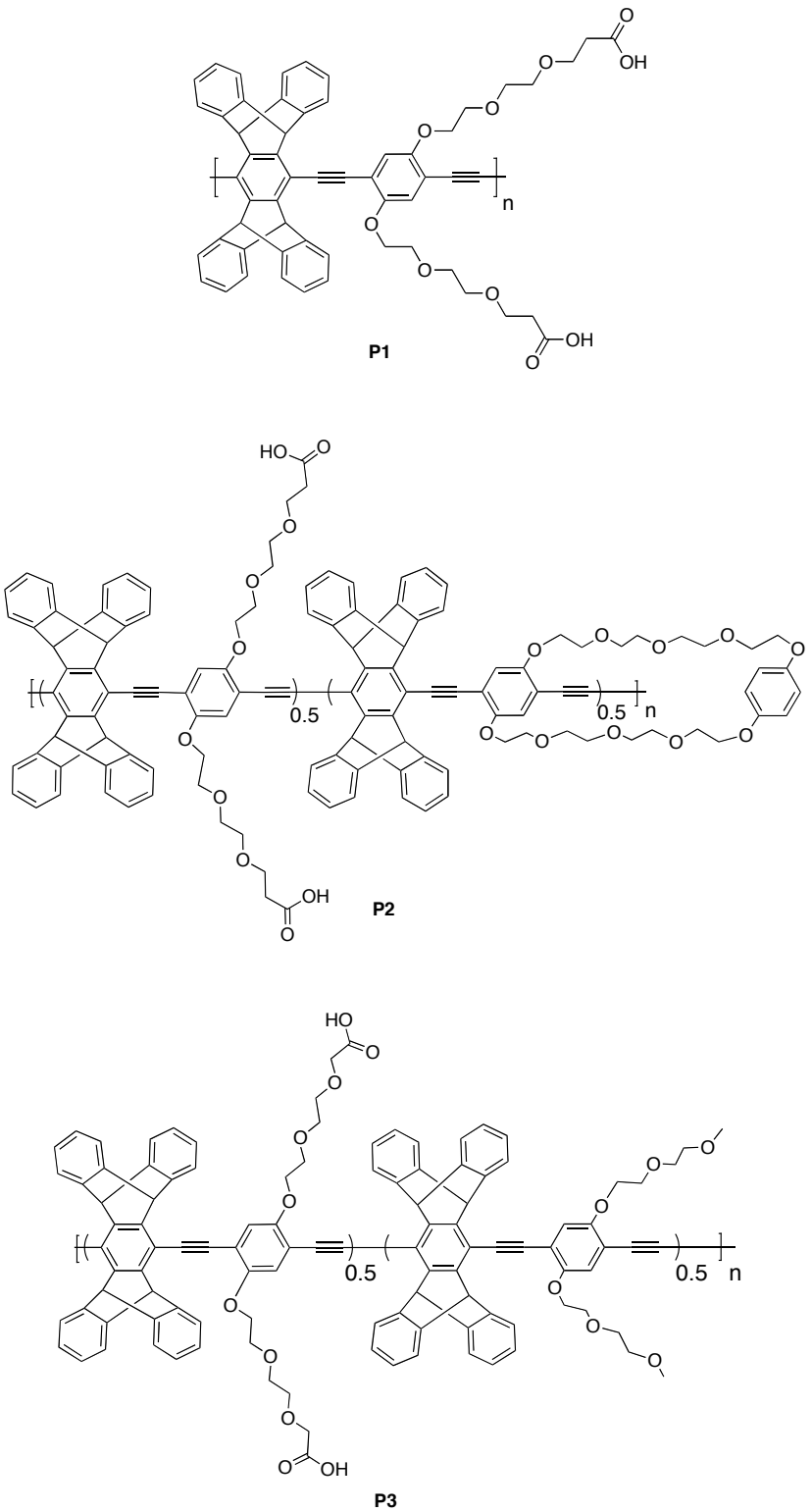

Figure 3.3. Structures of polymers **P1**, **P2**, and **P3**.

3.2 Results and Discussion

3.2.1 Polymer synthesis and characterization

The polymers were synthesized using Pd-catalyzed Sonogashira coupling reactions between respective diacetylene and diiodide monomers in quantitative yield. Initial target polymers to assess the macrocycle binding efficiency were synthesized with an equal ratio of the diiodide carboxylate monomer as **P1** in order to have similar electrostatic properties for assembling films and association with quenchers. The amount of pentiptycene monomer to incorporate was optimized for **P2** and **P3**.

To assess the target polymers, films were formed utilizing the method of layer-by-layer assembly. The rigid pentiptycene framework, prevents strong interpolymer associations and imparts solubility to the polymers in DMF and mixtures of DMF/water and insolubility in water. Films were formed by immersing glass slides (alternating with poly(ethyleneimine) (PEI)) in a 10 : 90 DMF : water PPE solution (1×10^{-3} M per repeat unit) for 15 minutes, then subjected to thorough rinsing with water and then drying in a stream of nitrogen. The slides were initially coated with a trilayer film of PEI : poly(styrene sulfonate) : PEI (PEI : PSS : PEI) to minimize defects. Figure 3.4 shows the UV/Vis absorbance and fluorescence spectra of 4-bilayer films. The incorporation of the macrocycle unit as a diacetylene monomer reduces the amount of pentiptycene units that can be incorporated in the polymer, allowing for a more flexible conformation for the resultant polymer to adopt. The broad, shapeless spectra is indicative of π-π stacking interactions and self-quenching, which is undesirable for fluorescent sensory materials and requires optimization. Synthesis of terpolymers containing an increasing amount of pentiptycene monomer resolves the fluorescence spectra, indicating reduced aggregation, as

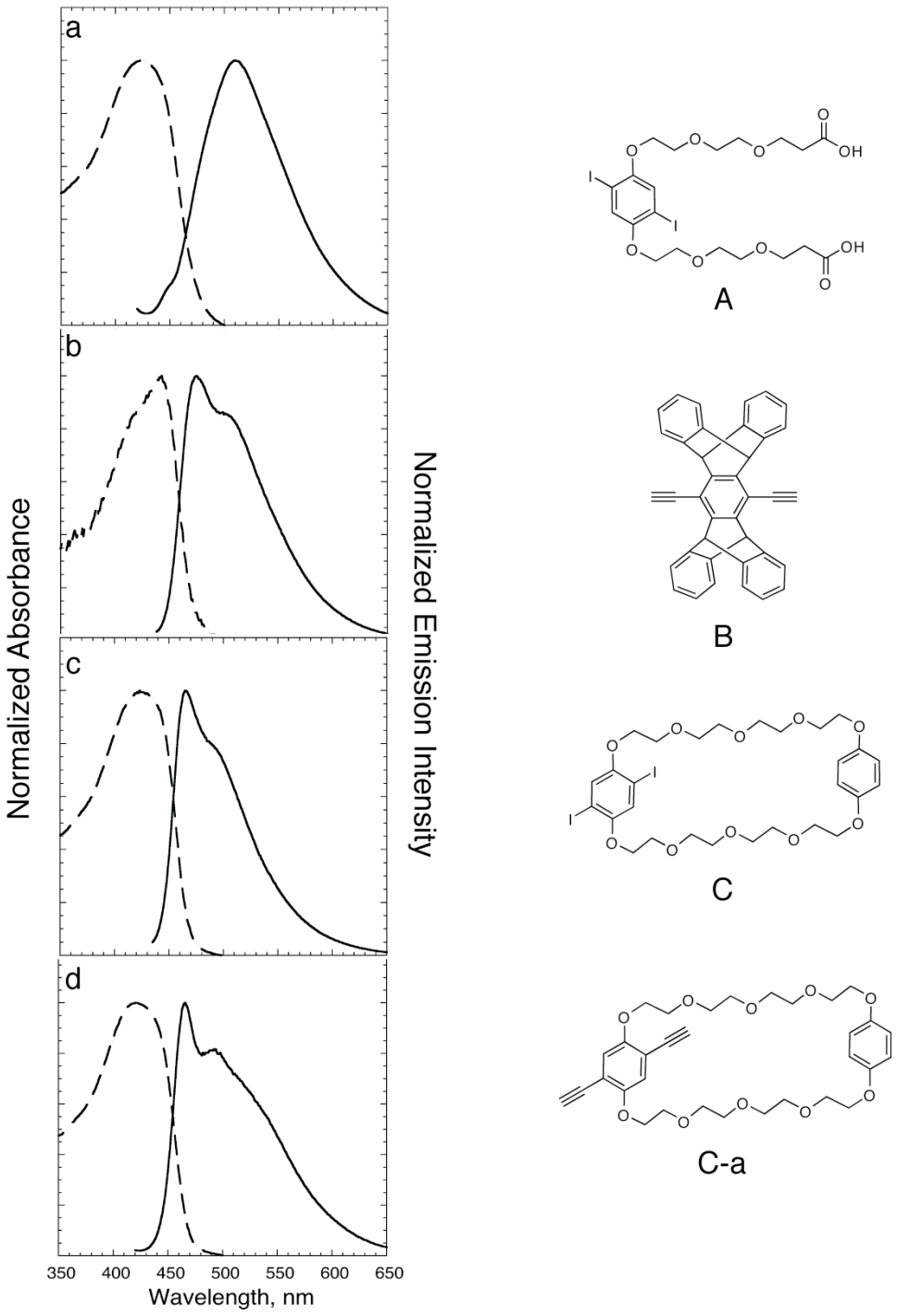

Figure 3.4. Normalized UV/Vis absorbance and fluorescence spectra of 4-bilayer films (PEI/PPE) on glass slides. PPEs (a – d) were synthesized with molar ratio of **A : B : C-a** as (a) 0.5 : 0.25 : 0.25; (b) 0.5 : 0.4 : 0.1; (c) 0.5 : 0.45 : 0.05; and **A : B : C** as (d) 0.25 : 0.5 : 0.25.

shown in Figure 3.4 (a–c), but at the same time reduces the amount of macrocycle contained in the polymer. An equal ratio of the diacetylene pentiptycene monomer (Figure 3.4(d)) was required for **P2** and **P3** to obtain similar spectroscopic properties as **P1** (shown in Chapter 2), and thus the carboxylic acid functionality was compensated for incorporation of a diiodo macrocycle-containing monomer (**C**).

The carboxylic acid groups proved problematic in molecular weight determinations and were converted using carbodiimide coupling chemistry to provide solubility characteristics that allow analysis by gel permeation chromatography (Figure 3.5). GPC analysis of the modified polymers **P1e**, **P2e**, and **P3e** in THF showed number-average molecular weights of 7 kDa (PDI = 1.4), 8 kDa (PDI = 1.5), and 17 kDa (PDI = 2.2), respectively.

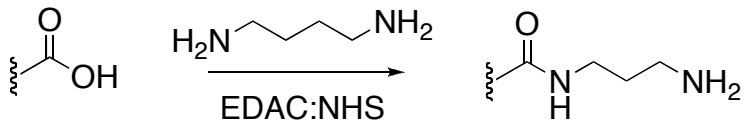

Figure 3.5. Post-polymerization conversion of carboxylic acid groups for GPC analysis.

.

Polymer	M_n (kDa)	PDI
P1e	7	1.4
P2e	8	1.5
P3e	17	2.2

Table 3.1. Molecular weight and polydispersity from GPC analysis in THF, based on PS standard.

3.2.2 Layer-by-layer assembly for film formation

Polymers **P1** – **P3** were alternately deposited with PEI onto glass slides as described in Section 3.2.2. Monitoring via UV/Vis absorbance spectroscopy indicates consistent layer buildup with subsequent layers (Figure 3.6). The synthetic molar ratio of carboxylic acid monomer in **P2** and **P3** is half of that in **P1**, and thus the optical densities of the multilayer films (Figure 3.6(b) and (c)) are smaller in comparison to **P1** (Figure 3.6 (a)).

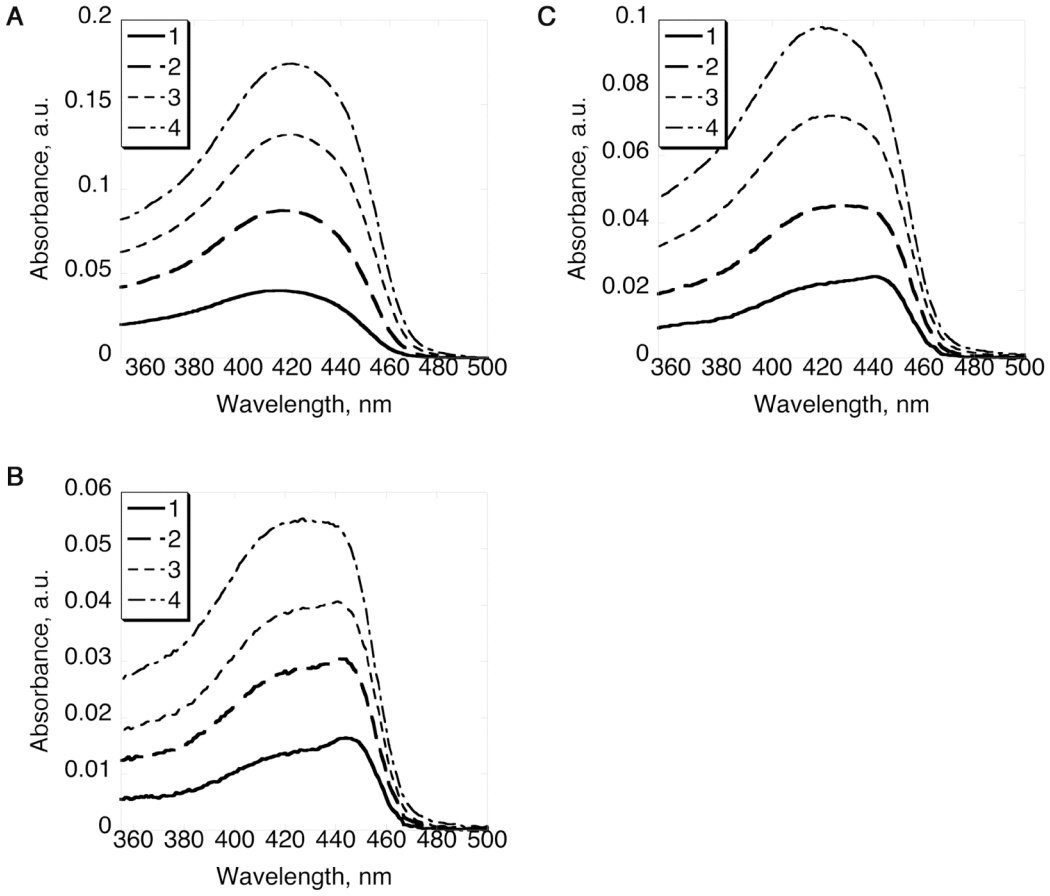

Figure 3.6. UV/Vis absorbance spectra of (a) **P1**, (b) **P2**, and (c) **P3**, alternating with PEI onto glass-PEI/PSS/PEI slide.

The absorbance and fluorescence spectra for the polymers in solution and in the immobilized films are shown in Figure 3.7. The solution and thin film spectra are nearly identical, demonstrating the capability of the bulky pentiptycene substituents to eliminate interchain aggregation when transitioning from solution to the solid state.[23] The quantum yield (Φ_F) of **P1** is greater than that of **P2** and **P3**, indicating the carboxylic acid groups of the polyelectrolyte aids in planarizing the backbone in solution and allowing for greater conjugation in the polymer. The bulky macrocycle also adds rigidity due to steric effects, giving rise to a greater quantum yield for **P2** as compared to **P3**, both having equal charge density.

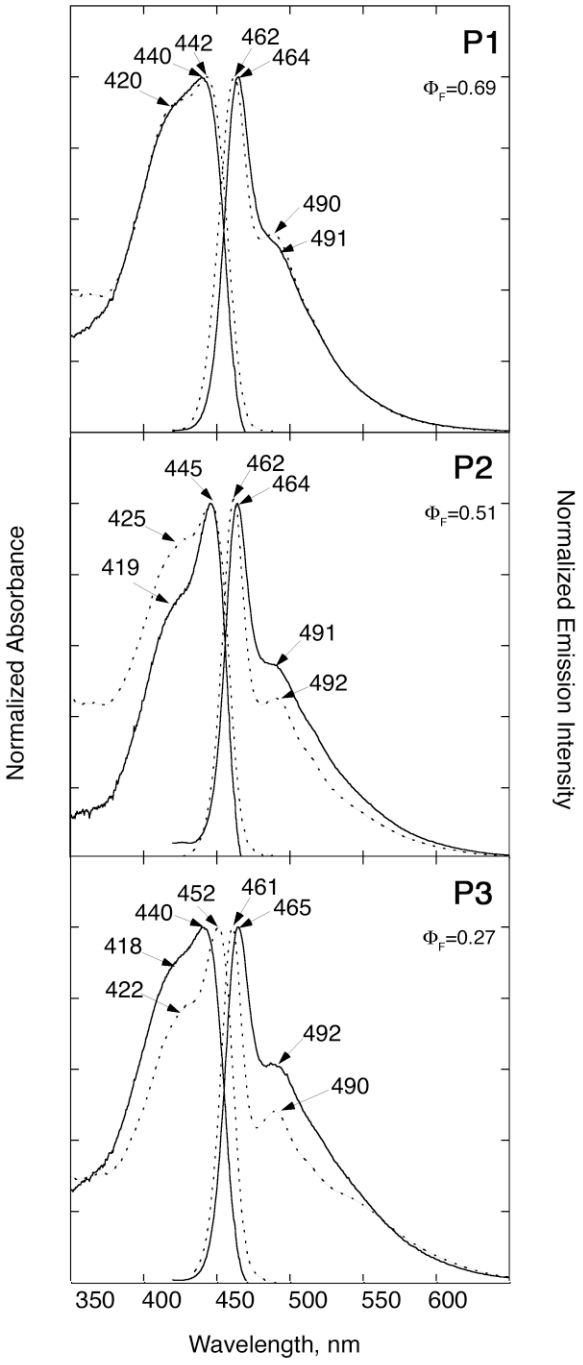

Figure 3.7. Absorption and fluorescence spectra of **P1–P3** in DMF (dotted lines) and adsorbed films on glass slides (solid lines). Quantum yields (Φ_F) are in DMF solution referenced to coumarin 6 in EtOH as standard ($\Phi_F = 0.78$).

The process to produce thin films on particles is similar to that used in Chapter 2; however, since the Eu^{3+}-PS particles are carboxylate-functionalized, a pre-layer of PEI is adsorbed before immobilization of **P1–P3**. The particles are dispersed in the polymer solution and shaken vigorously for 15 minutes, followed by centrifugation for 15 minutes at 14,500 RPM, removal of supernatant, and two rinsing steps (resuspension, centrifugation, removal of supernatant) in deionized water to ensure complete removal of the excess polymer. The polymer-coated particles are then resuspended (adjusted to a concentration 0.017% solids) in deionized water, Tris buffer (20 mM, pH 7.4), and Tris-buffered saline (20 mM, pH 7.4; 150 mM NaCl; 5 mM $CaCl_2$) for subsequent quenching experiments. Figure 3.8 shows a confocal microscopy image of the particles in deionized water, showing uniform fluorescence from the surface. The particles remain suspended for a few hours, and before each measurement a brief ultrasonication step is used to fully disperse the sample.

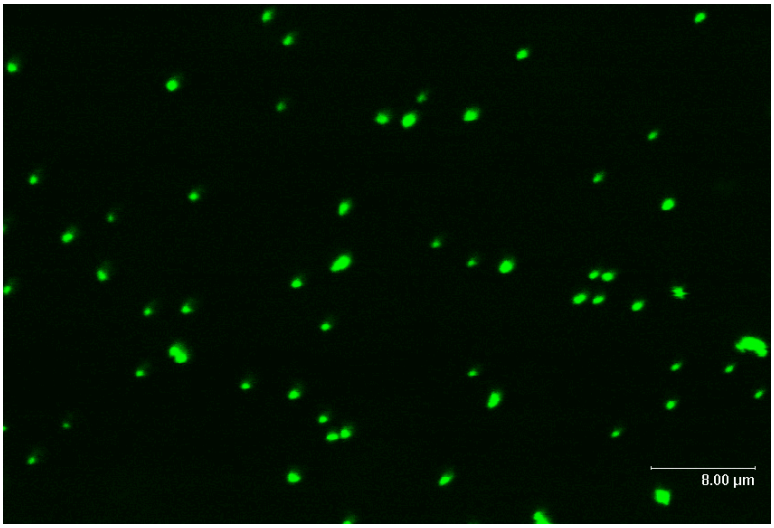

Figure 3.8. Confocal image of **P1**-coated particles in deionized water.

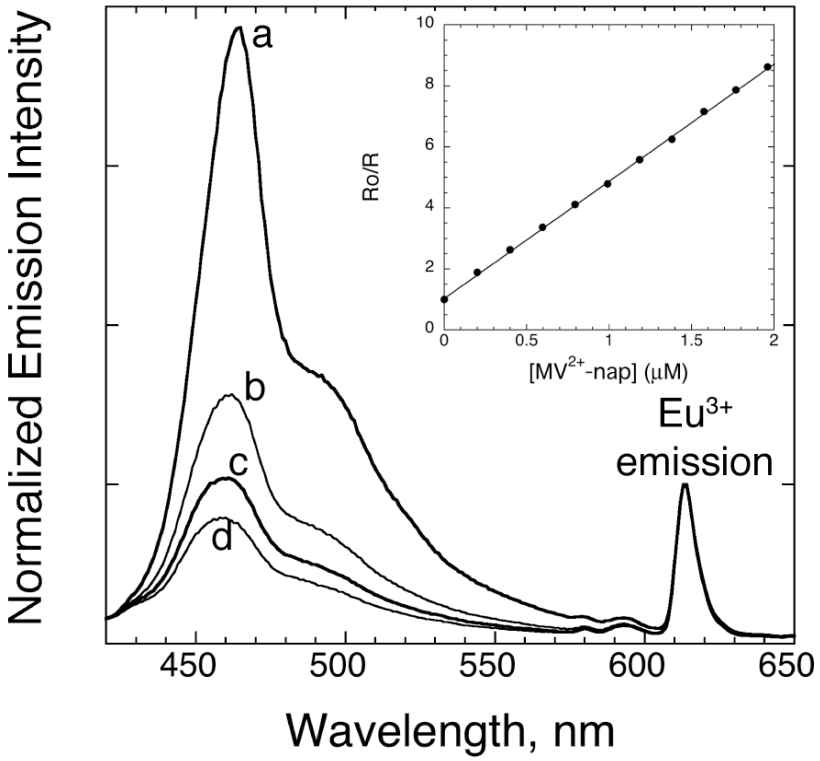

Figure 3.9. Fluorescence of **P1**-particles in Tris buffer (20 mM, pH 7.4), with Eu^{3+} as reference at 612 nm, in response to (a) 0, (b) 0.06, (c) 0.12, and (d) 0.18 μM additions of **MV^{2+}-nap**. Inset: Stern-Volmer plot of R_0/R vs. [**MV^{2+}-nap**] with linear fit.

3.2.3 Particle quenching experiments

Excitation at 390 nm allows for direct excitation of both the polymer and the Eu^{3+} incorporated in the PS particles. Figure 3.9 shows the response of **P1**-coated particles in Tris buffer (20 mM, pH 7.4) towards **MV^{2+}-nap**. Normalization of the spectra to the Eu^{3+} emission maximum at 612 nm accounts for fluctuations in the particle dispersion and for an accurate measure of the quenching response. Plotting the ratio of the polymer emission maximum to the Eu^{3+} emission maximum versus concentration yields the Stern-Volmer plot, shown in the inset of Figure 3.9. A linear best fit yields a Stern-Volmer quenching constant of $(2.9 \pm 0.3) \times 10^7$ M^{-1}. The magnitude of quenching observed exceeds the diffusion limit and therefore implies static

quenching is operative.[25] The high value for the K_{SV} is significant for the buffered conditions, since most studies with conjugated polyelectrolyte quenching are rarely reported in these ion screening conditions that generally tend to lower the polyelectrolyte-quencher association. Typically to achieve K_{SV} values on the order of what was observed in the particle quenching experiments, one requires ionic-induced and concentration-dependent aggregation to physically "collapse" the polymer to amplify the actual quenching mechanism by electron or energy transfer.[26] This aggregation effect is most likely not a contributing factor to the large quenching that we observe because the polymers are immobilized on the particle surfaces and not as flexible as other conjugated polyelectrolytes studied due to the incorporated pentiptycene groups.

Figure 3.10 presents the mean linear best-fit Stern-Volmer constants (K_{SV}) from triplicate measurements for **P1**–**P3** in response to $\mathbf{MV^{2+}}$ and $\mathbf{MV^{2+}}$**-nap** in deionized water, Tris buffer (20 mM, pH 7.4), and Tris-buffered saline (20 mM, pH 7.4; 150 mM NaCl, 5 mM $CaCl_2$). The error bars shown are the result of experiments performed in triplicate, showing the high level of reproducibility that can be realized using the ratiometric method for quantification. Tables 3.2 and 3.3 summarize the quenching constant data in each condition.

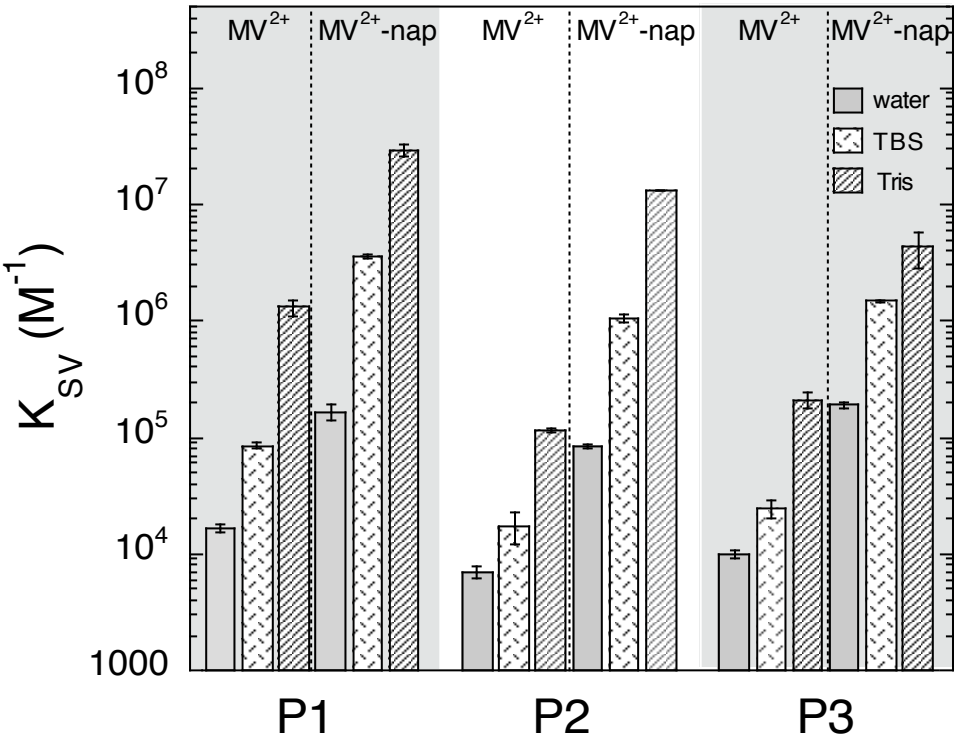

Figure 3.10. Summary of K_{SV} values for **P1–P3** in response to **MV^{2+}** and **MV^{2+}-nap** in deionized water, Tris buffer (Tris, 20 mM, pH 7.4), and Tris-buffered saline (TBS, 20 mM, pH 7.4; 150 mM NaCl, 5 mM $CaCl_2$). Error bars indicate standard errors (n = 3).

	K_{sv} (M^{-1})		
Polymer	Water	Tris 20 mM, pH 7.4	Tris-buffered saline
P1	$(1.7 \pm 0.6) \times 10^4$	$(1.3 \pm 0.2) \times 10^6$	$(8.5 \pm 0.6) \times 10^4$
P2	$(6.9 \pm 0.7) \times 10^3$	$(1.1 \pm 0.05) \times 10^5$	$(1.7 \pm 0.5) \times 10^4$
P3	$(1.0 \pm 0.7) \times 10^4$	$(2.1 \pm 0.3) \times 10^5$	$(2.4 \pm 0.4) \times 10^4$

Table 3.2. Quenching constant data for polymer-coated particles **P1–P3** in response to **MV^{2+}**.

	K_{SV} (M^{-1})		
Polymer	Water	Tris 20 mM, pH 7.4	Tris-buffered saline
P1	$(1.7 \pm 0.3) \times 10^5$	$(2.9 \pm 0.3) \times 10^7$	$(3.6 \pm 0.2) \times 10^6$
P2	$(8.4 \pm 0.4) \times 10^4$	$(1.3 \pm 0.01) \times 10^7$	$(1.1 \pm 0.08) \times 10^6$
P3	$(1.9 \pm 0.1) \times 10^5$	$(4.3 \pm 1) \times 10^6$	$(1.5 \pm 0.03) \times 10^6$

Table 3.3. Quenching constant data for polymer-coated particles **P1–P3** in response to **MV^{2+}-nap**.

From the summary plot, a few trends can be observed. Overall, **P1** shows a higher quenching response towards the quenchers. We attribute this behavior to the greater charge density of **P1** relative to **P2** and **P3**.[27,28] The response towards **MV^{2+}-nap** is greater than **MV^{2+}** for all polymers, indicating the ability of the π-π stacking interactions of the naphthyl rings and the pentiptycene backbone to provide high associative quenching in an aqueous environment. The effect produces K_{SV} values for **MV^{2+}-nap** that are more than an order of magnitude higher than **MV^{2+}**. The quenching response in the different environmental conditions, from highest to lowest, is observed as Tris > Tris-buffered saline > water. This trend cannot be understood directly from the quenching experiments. Increased ionic strength shields the electrostatic contribution and gives rise to greater hydrophobic interactions; however, Tris-buffered saline displays lower K_{SV} values compared to Tris buffer. Interestingly, our results in Tris-buffered saline also reveal a higher degree of quenching than in pure water. This behavior is in direct contrast to what has been observed for other conjugated polyelectrolytes in solution,[5,29-33] wherein buffer conditions

shield the electrostatic forces and thus reduce the amount of quenching in electrolyte versus water.

The zeta potential of the polymer-coated particles (Table 3.4) indicates the effective charge for each condition. Although water imparts the greatest net negative charge, the observed quenching is the lowest in pure water for all polymers. This result further implies that the quenching response is more complicated than the screening of electrostatic charges and the increase of the contribution of hydrophobic interactions.

Polymer	Water	Tris 20 mM, pH 7.4	Tris-buffered saline
P1	-54.6 ± 0.6	-29.1 ± 0.7	-15.2 ± 1.1
P2	-26.3 ± 0.6	-13.8 ± 1.2	-4.75 ± 1.9
P3	-31.3 ± 0.7	-26.8 ± 1.1	-11.1 ± 1.1

Table 3.4. Apparent zeta potential (mV) of polymer-coated particles.

We can examine the effect of salt on the quenching as it may yield more information to understand the trend we observe in the different environmental conditions. To first establish if there is any effect on the emission of the PPE, salt was titrated to a suspension of **P1**-coated particles and shown in Figure 3.11 as the control. The negligible effect on the fluorescence emission indicates the ionic species does not alter the conjugated polymer configuration significantly, most likely due to the rigidity of the backbone and the prevention of interchain aggregation even when the charged carboxylate groups become neutralized from the salt. This is in contrast to conjugated polyelectrolytes in solution that are able to adopt a more flexible

conformation and can self-aggregate upon addition of salt.[34] The quenchers **MV^{2+}** and **MV^{2+}-nap** were added separately for a total concentration of 20 μM to particle suspensions, and salt was titrated. With **MV^{2+}-nap** there is an increase in the quenching response when the ionic concentration is increased. The naphthyl rings may be able to stack more efficiently with the polymer when the charge is neutralized. The response with **MV^{2+}** is similar to the control and is not dependent on salt in the concentration range tested. Further studies with a greater concentration of **MV^{2+}** with the titration of salt would conclude if both quenchers are subject to increased quenching in ionic environments.

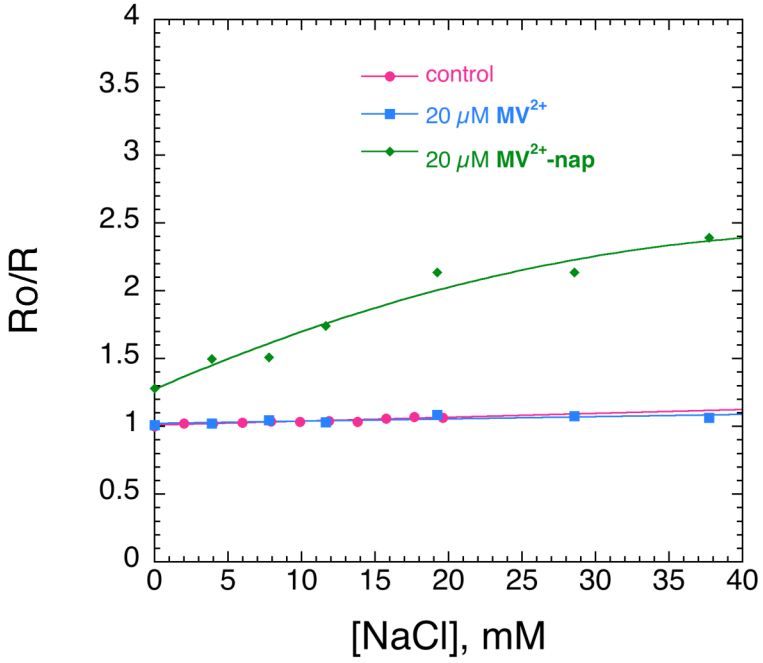

Figure 3.11. Effect of salt on **P1**-coated particle quenching. Quencher solutions were added initially for a total concentration of 20 μM and allowed to equilibrate, after which time salt was titrated.

The salt titration experiments do not completely explain the reason for higher quenching in Tris buffer versus Tris-buffered saline for both quenchers, and thus it is most likely that there is a contribution of factors such as film swelling and ionic species changing the local

environmental permeability. Changing the environmental conditions with additional ionic species can cause swelling of the immobilized polyelectrolyte coating.[35] The small ions can penetrate in the film and compete with the polyion complexation, leading to a more flexible conformation of the polyions and increased water uptake.[35] In situ ellipsometry measurements was performed to measure the difference in swelling of multilayer films in these environments. A film consisting of 8-bilayers of PEI/**P1** on a silica wafer showed negligible difference among the three environments (~70 nm in water, Tris, and TBS). Ellipsometry requires the buildup of thick multilayer films (at least 5 bilayers) to measure the thickness accurately. The properties of a 1-bilayer coating on the polymer-coated particles may not be entirely modeled, since the multilayer structure of the first layers differs from that of the bulk and the last deposited layers.[36] The higher quenching observed in Tris buffered conditions could be attributed to association of the organic salt with the PPE-coated particles, however further investigation is warranted to understand the mechanism.

The responses of **P2** and **P3** are very similar for the same conditions. This is in contrast to their behavior in DMF solution, where **P2** (K_{SV} = (2.9 ± 0.2) × 10^6 M^{-1}) shows greater quenching towards $\mathbf{MV^{2+}}$ relative to **P3** (K_{SV} = (1.9 ± 0.4) × 10^4 M^{-1}). The DMF solution quenching response of **P2** is even greater than that displayed by **P1** (K_{SV} = (4.3 ± 0.1) × 10^5 M^{-1}), illustrating that the macrocycles efficiently bind $\mathbf{MV^{2+}}$ through hydrogen bonding and π-π interactions[11,37] and thereby give an increase the overall sensitivity. The formation of a sandwich complex between viologen quenchers and the phenylenediether units of the polymer is a different approach than other microsphere quenching schemes that utilize biomolecular binding, such as streptavidin-biotin interactions,[5] to associate quencher and polymer. In the microsphere system, however, we do not observe any differentiation between the behavior of **P2** and **P3** towards the viologen quenchers. The disparity between solution and film behavior may be due

to the film formation process, wherein the receptors are geometrically constrained and cannot effectively enhance interactions with the quenchers. Spatially-organized films such as the Langmuir-Blodgett type, in which a single monolayer can be deposited, may prove to be a better arrangement for the activity of flexible molecular receptors in aqueous solution.[20]

3.3 Conclusions

We have synthesized a series of non-aggregating anionic PPEs for adsorption onto Eu^{3+}-polystyrene particles with a mean diameter of 0.2 μm to construct an internally referenced system for measuring the fluorescence quenching of films with high reliability in an aqueous environment. We have been able to measure the response toward quenchers and find that by introducing hydrophobicity with a naphthyl-functionalized viologen (**MV^{2+}-nap**) we can increase the interactions with these polymers, even in environments with high ionic content. The ratiometric method for detecting changes in the fluorescence emission allows for experiments to be conducted in order to gain further insight into the mechanisms of quenching with PPE-coated particles. We are also investigating how to harness these transduction schemes into even more reliable systems for biosensing in complex environments.

3.4 Experimental Section

Materials

Monomers **A**,[32] **C**,[38] **C-a**,[38] and **D**[39] were synthesized based on previous literature procedures. Diethynylpentiptycene (**B**) was purchased from ICx Nomadics Life Sciences, Inc. $Pd(PPh_3)_4$ and CuI were purchased from Strem and kept in glovebox. All solvents for polymerization were obtained from Aldrich and degassed by rapid sparging with argon for 20 minutes before use. Bio Beads S-3 (Bio-Rad Laboratories) used for size exclusion chromatography were pre-swelled in DMF overnight before use. *N,N*-dimethylformamide (DMF, HPLC grade), Tris (hydroxymethyl) aminomethane buffer, sodium chloride, calcium chloride, and methyl viologen dichloride (**MV^{2+}**) were purchased from Aldrich and used as received. 1-methyl-1'-naphthalen-2-yl methyl-[4,4'] bipyridinyl dication dichloride (**MV^{2+}-nap**) was synthesized and provided by Dr. Guy D. Joly.[20] Carboxylate-modified europium microspheres (d = 0.2 μm) were purchased from Invitrogen and used after rinsing with deionized water. Amine-modified polystyrene microspheres (d = 0.52 μm) for zeta potential measurements were purchased from Bangs Laboratories and used after rinsing with deionized water. Poly(ethyleneimine) (PEI, branched, MW 10 kDa) and poly(styrene sulfonic acid) sodium salt (PSS, MW 500 kDa) were obtained from Polysciences. Deionized water purified through a 0.2 μm syringe filter was used for all aqueous measurements and preparation of solutions. All solutions for electrostatic adsorption were prepared in 1×10^{-3} M per repeat unit in water for PEI and PSS, or a 10 : 90 mixture of DMF : water for **P1–P3** due to limited solubility in water. Glass slides for monitoring film adsorption were used as received from VWR and coated with a pre-layer of PEI/PSS/PEI before adsorbing **P1–P3**.

Methods

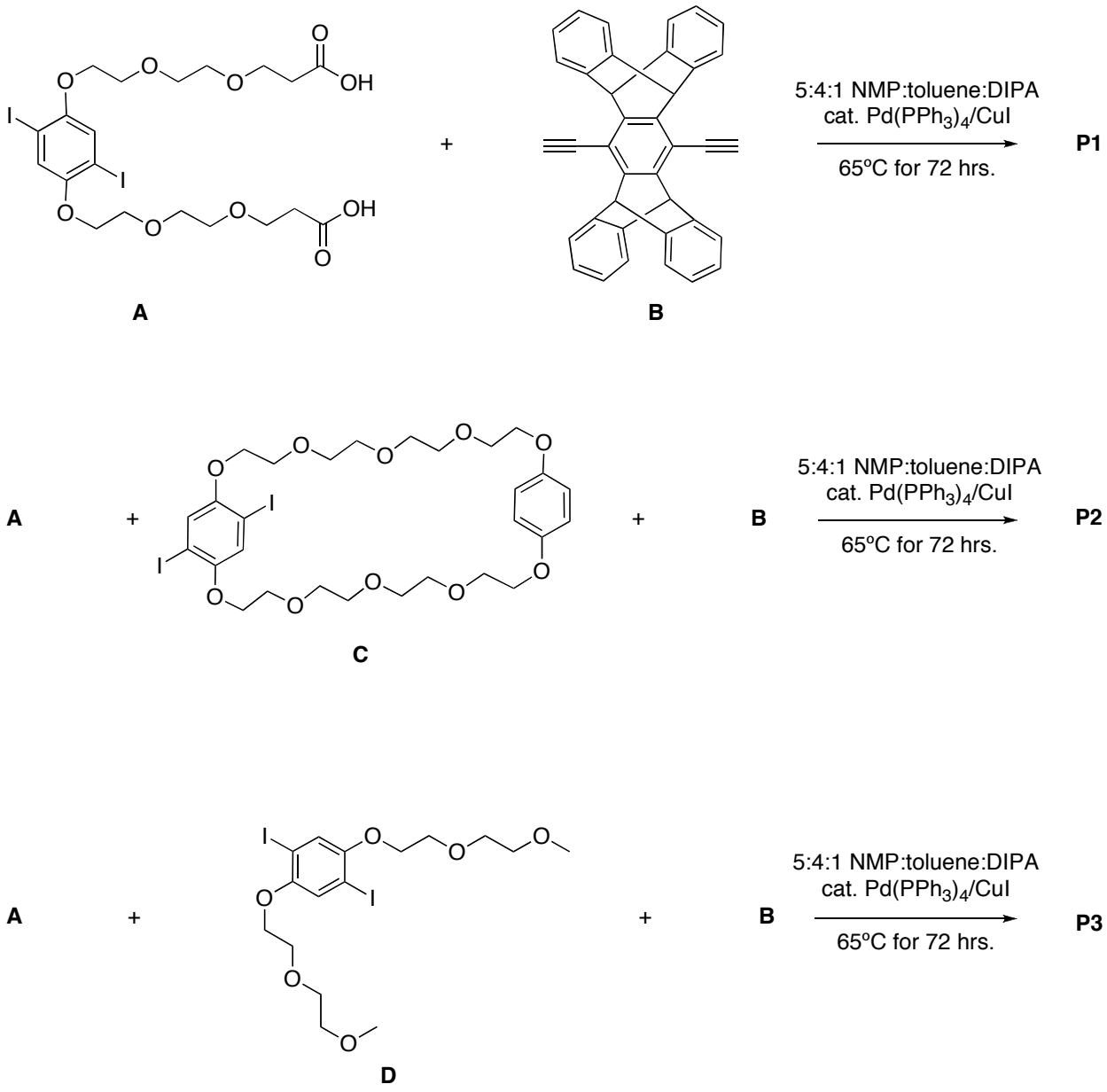

Figure 3.12. Synthesis of **P1**, **P2**, and **P3**.

General procedure for synthesis of polymers

Monomers were added to an 10 mL Schlenk tube with a stirbar and evacuated and purged with nitrogen before addition of $Pd(PPh_3)_4$ and CuI (catalytic amounts) in a glovebox.

1.5 mL of 5 : 4 : 1 (v/v) *N*-methylpyrrolidone : toluene : diisopropylamine, degassed with rapid sparging of argon, was added to the flask, for complete solubility of the starting materials. The flask was sealed and heated for 72 hours at 65°C, after which the solution turned from a milky white color to yellow with bright green fluorescence. After removing from heat, ethyl acetate was added to precipitate the reaction mixture to a yellow solid, which was subsequently purified using size exclusion chromatography with DMF as the eluent to yield the product polymers. **P1** (72%): **A** (35 mg, 0.051 mmol); **B** (25 mg, 0.053 mmol). ^{1}H NMR (δ in ppm, 500 MHz, DMF-d_7) broad peaks centered around 2.3–2.5, 3.7, 4.1–4.6, 5.0, 6.4–6.7, 7.1, 7.4, 7.7. **P2** (69%): **A** (15 mg, 0.022 mmol), **C** (17 mg, 0.022 mmol), **B** (21 mg, 0.045 mmol). ^{1}H NMR (δ in ppm, 500 MHz, DMF-d_7) broad peaks centered around 3.5–3.7, 4.1–4.8, 6.4–6.7, 7.1, 7.4, 7.7. **P3** (76%): **A** (11 mg, 0.016 mmol); **D** (9 mg, 0.016 mmol); **B** (16 mg, 0.033 mmol). ^{1}H NMR (δ in ppm, 500 MHz, DMF-d_7) broad peaks centered around 2.1–2.5, 3.6, 4.2–4.8, 5.4, 6.3–6.7, 7.1, 7.4, 7.7.

Synthesis of P1e, P2e, and P3e

Polymers **P1**–**P3** were activated with excess molar ratio of EDAC/NHS in DMF, and then subsequent addition of excess dibutylamine at room temperature for a reaction time of 12 hours, to afford a product that could be eluted from THF GPC analysis for molecular weight determination. **P1e**: GPC: M_n = 7 kDa, PDI = 1.4. **P2e**: GPC: M_n = 8 kDa, PDI = 1.5. **P3e**: GPC: M_n = 17 kDa, PDI = 2.2.

Polymer characterization

Polymer molecular weights were determined using gel permeation chromatography in THF solution vs. PS standards. ^{1}H NMR spectra were recorded on a Varian Mercury or Inova instrument (Cambridge Isotopes Laboratories). All photophysical measurements were

performed at room temperature using a 1-cm path length quartz cuvette in right-angle detection mode. Absorbance was measured using a Cary 50 or Agilent 845 UV-Vis spectrophotometer, corrected for solvent or substrate baseline. Steady-state fluorescence and lifetime spectra were acquired using a Jobin Yvon SPEX Fluorolog-τ2 or -τ3 fluorometer. Solution lifetimes were measured using the frequency domain method, with 10 frequencies ranging from 10–250MHz, fit to a single exponential. Quantum yields in solution were obtained by the reference method using coumarin 6 in ethanol as standard ($\Phi_F = 0.78$).

UV-Vis absorbance spectroscopy

To monitor the layering process of **P1**–**P3**, glass slides (pre-layered with PEI : PSS : PEI) were dipped in **P1**–**P3** solutions (1×10^{-3} M) for 15 minutes, rinsed with deionized water, and then dried with nitrogen stream before absorbance measurements. Slides were then dipped in PEI for 15 minutes, rinsed with water, and dipped with **P1**–**P3** for subsequent layers. Layer numbers indicate the number of PPE layers deposited, alternating with PEI.

Preparation of PPE-coated particles

Layer-by-layer assembly on particles followed similar procedure as described in Chapter 2. Carboxylate-functionalized europium-polystyrene particles (adjusted to a concentration of 0.025% solids) were dispersed in PEI solution for 15 minutes, followed by a washing procedure (centrifugation, removal of the supernatant, and rinsing with water), repeated twice. The **P1** solution was then added for an adsorption time of 15 minutes, removed and washed twice with water before final resuspension in medium. **P2**- and **P3**-coated particles were also prepared in the same manner for experiments.

Confocal microscopy

Confocal microscopy images were taken on a Leica TCS-SP2 confocal laser scanning microscope using an argon 360 nm laser as the excitation source and a 63x/1.4 oil immersion lens.

Zeta potential

Zeta potential of polymers adsorbed onto amine-functionalized polystyrene particles, with an adsorption time of 15 minutes, was measured using a ZetaPals Zeta Potential Analyzer (Brookhaven Instruments Corporation) in a 1-cm polystyrene cuvette with Millipore water, Tris 20 mM pH 7.4, or Tris-buffered saline (Tris 20 mM pH 7.4; 150 mM NaCl, 20 mM $CaCl_2$ as solvent. Mean zeta potential is reported based on 10 runs of 25 cycles, and converting mobility to zeta potential using the Smoluchowski equation ($\zeta = \mu\eta/\varepsilon$, where ζ is the zeta potential, μ is the electrophoretic mobility, η is the viscosity, and ε is the electric permittivity of the liquid).

Fluorescence quenching

Stock solutions of 1.0 and 0.1 mM were prepared for each quencher and condition. For solution quenching, quencher stock solutions were made from polymer stock solution (1×10^{-6} M per repeat unit) to avoid dilution effects. For each experiment, the initial fluorescence emission intensity was measured. Aliquots of the quencher stock solution were added to the cuvette and the fluorescence was measured after 5 minutes to allow for equilibration. Excitation wavelengths used for solution and particle quenching were 405 nm and 390 nm, respectively, the latter allowing for the excitation of the europium internal reference. Measurements were performed in triplicate with R-squared values of > 0.98 for each condition.

For salt titration experiments, a 1 M NaCl solution was prepared in water. **P1**-coated particles were suspended in water, and 5 μL aliquots of NaCl solution were added to either particles without quencher or with 20 μM quencher. Fluorescence was measured and recorded similarly to fluorescence quenching experiments as described previously.

In situ ellipsometry

Films consisting of 8-bilayers of PEI/**P1** were alternately deposited on a clean silica wafer (2 cm x 5 cm) with 15-minute adsorption times, followed by rinsing with deionized water, and dried with nitrogen stream before the next adsorption step. The substrate was stored in ambient conditions before the experiment.

Film thicknesses were measured on a J.A. Woollam Spectroscopic Ellipsometer using a custom quartz cell constructed by the Rubner group at MIT and modeling the film as a general oscillator. The film thickness was measured after equilibration in the solution (deionized water, Tris, TBS) for 2 minutes at room temperature.

3.5 References

(1) Medintz, I. L.; Uyeda, H. T.; Goldman, E. R.; Mattoussi, H. *Nat. Mater.* **2005**, *4*, 435-446.

(2) Ow, H.; Larson, D. R.; Srivastava, M.; Baird, B. A.; Webb, W. W.; Wiesner, U. *Nano Lett.* **2005**, *5*, 113-117.

(3) Xu, H.; Wu, H.; Huang, F.; Song, S.; Li, W.; Cao, Y.; Fan, C. *Nucleic Acids Res.* **2005**, *33*, e83.

(4) Nie, Q.; Zhang, Y.; Zhang, J.; Zhang, M. *J. Mater. Chem.* **2006**, *16*, 546-549.

(5) Kumaraswamy, S.; Bergstedt, T. S.; Shi, X. B.; Rininsland, F.; Kushon, S. A.; Xia, W. S.; Ley, K. D.; Achyuthan, K.; McBranch, D.; Whitten, D. *Proc. Natl. Acad. Sci. U.S.A.* **2004**, *101*, 7511-7515.

(6) Wu, C.; Szymanski, C.; McNeill, J. *Langmuir* **2006**, *22*, 2956-2960.

(7) Moon, J. H.; Deans, R.; Krueger, E.; Hancock, L. F. *Chem. Comm.* **2003**, 104-105.

(8) Kushon, S. A.; Ley, K. D.; Bradford, K.; Jones, R. M.; McBranch, D.; Whitten, D. *Langmuir* **2002**, *18*, 7245-7249.

(9) Huang, H.; Wang, K.; Tan, W.; An, D.; Yang, X.; Huang, S.; Zhai, Q.; Zhou, L.; Jin, Y. *Angew. Chem. Int. Ed.* **2004**, *43*, 5635-5638.

(10) McQuade, D. T.; Pullen, A. E.; Swager, T. M. *Chem. Rev.* **2000**, *100*, 2537-2574.

(11) Zhou, Q.; Swager, T. M. *J. Am. Chem. Soc.* **1995**, *117*, 12593-12602.

(12) Zhao, D.; Swager, T. M. *Macromolecules* **2005**, *38*, 9377-9384.

(13) Kim, I. B.; Dunkhorst, A.; Bunz, U. H. F. *Langmuir* **2005**, *21*, 7985-7989.

(14) Dwight, S. J.; Gaylord, B. S.; Hong, J. W.; Bazan, G. C. *J. Am. Chem. Soc.* **2004**, *126*, 16850-16859.

(15) Park, E. J.; Brasuel, M.; Behrend, C.; Philbert, M. A.; Kopelman, R. *Anal. Chem.* **2003**, *75*, 3784-3791.

(16) Brown, J. Q.; McShane, M. J. *IEEE Sens. J.* **2005**, *5*, 1197-1205.

(17) Guice, K. B.; Caldorera, M. E.; McShane, M. J. *J. Biomed. Opt.* **2005**, *10*, 064031.

(18) Wolfbeis, O. S. *J. Mater. Chem.* **2005**, *15*, 2657-2669.

(19) Demchenko, A. P. *Lab on a Chip* **2005**, *5*, 1210-1223.

(20) Joly, G. D.; Geiger, L.; Kooi, S. E.; Swager, T. M. *Macromolecules* **2006**, *39*, 7175-7177.

(21) Fan, C.; Hirasa, T.; Plaxco, K. W.; Heeger, A. J. *Langmuir* **2003**, *19*, 3554-3556.

(22) Wosnick, J. H.; Liao, J. H.; Swager, T. M. *Macromolecules* **2005**, *38*, 9287-9290.

(23) Yang, J. S.; Swager, T. M. *J. Am. Chem. Soc.* **1998**, *120*, 11864-11873.

(24) Decher, G. *Science* **1997**, *277*, 1232-1237.

(25) Lakowicz, J. R. *Principles of Fluorescence Spectroscopy*; Kluwer Academic/Plenum: New York, 1999.

(26) Thomas, S. W., III; Joly, G. D.; Swager, T. M. *Chem. Rev.* **2007**, *107*, 1339-1386

(27) Wang, D.; Wang, J.; Moses, D.; Bazan, G. C.; Heeger, A. J. *Langmuir* **2001**, *17*, 1262-1266.

(28) Liu, M.; Kaur, P.; Waldeck, D. H.; Xue, C.; Liu, H. *Langmuir* **2005**, *21*, 1687-1690.

(29) Fan, C.; Wang, S.; Hong, J. W.; Bazan, G. C.; Plaxco, K. W.; Heeger, A. J. *Proc. Natl. Acad. Sci. U.S.A.* **2003**, *100*, 6297-6301.

(30) Gaylord, B. S.; Heeger, A. J.; Bazan, G. C. *J. Am. Chem. Soc.* **2003**, *125*, 896-900.

(31) Cabarcos, E. L.; Carter, S. A. *Macromolecules* **2005**, *38*, 10537-10541.

(32) Wosnick, J. H.; Mello, C. M.; Swager, T. M. *J. Am. Chem. Soc.* **2005**, *127*, 3400-3405.

(33) Liu, B.; Gaylord, B. S.; Wang, S.; Bazan, G. C. *J. Am. Chem. Soc.* **2003**, *125*, 6705-6714.

(34) Hong, J. W.; Hemme, W. L.; Keller, G. E.; Rinke, M. T.; Bazan, G. C. *Adv. Mater.* **2006**, *18*, 878-882.

(35) Schönhoff, M. *J. Phys.: Condens. Matter.* **2003**, R1781-R1808.

(36) Ladam, G.; Schaad, P.; Voegel, J. C.; Schaaf, P.; Decher, G.; Cuisinier, F. *Langmuir* **2000**, *16*, 1249-1255.

(37) Houk, K. N.; Menzer, S.; Newton, S. P.; Raymo, F.M.; Stoddart, J.F.; Williams, D. J. *J. Am. Chem. Soc.* **1999**, *121*, 1479-1487.

(38) Anelli, P. L.; Ashton, P. R.; Ballardini, R.; Balzani, V.; Delgado, M.; Gandolfi, M. T.; Goodnow, T. T.; Kaifer, A. E.; Philp, D.; Pietraszkiewicz, M.; Prodi, L.; Reddington, M. V.; Slawin, A. M. Z.; Spencer, N.; Stoddart, J. F.; Vicent, C.; Williams, D. J. *J. Am. Chem. Soc.* **1992**, *114*, 193-218.

(39) Koishi, K.; Ikeda, T.; Kondo, K.; Sakaguchi, T.; Kamada, K.; Tawa, K.; Ohta, K. *Macromol. Chem. Phys.* **2000**, *201*, 525-532.

Appendix for Chapter 3:

Stern-Volmer Plots

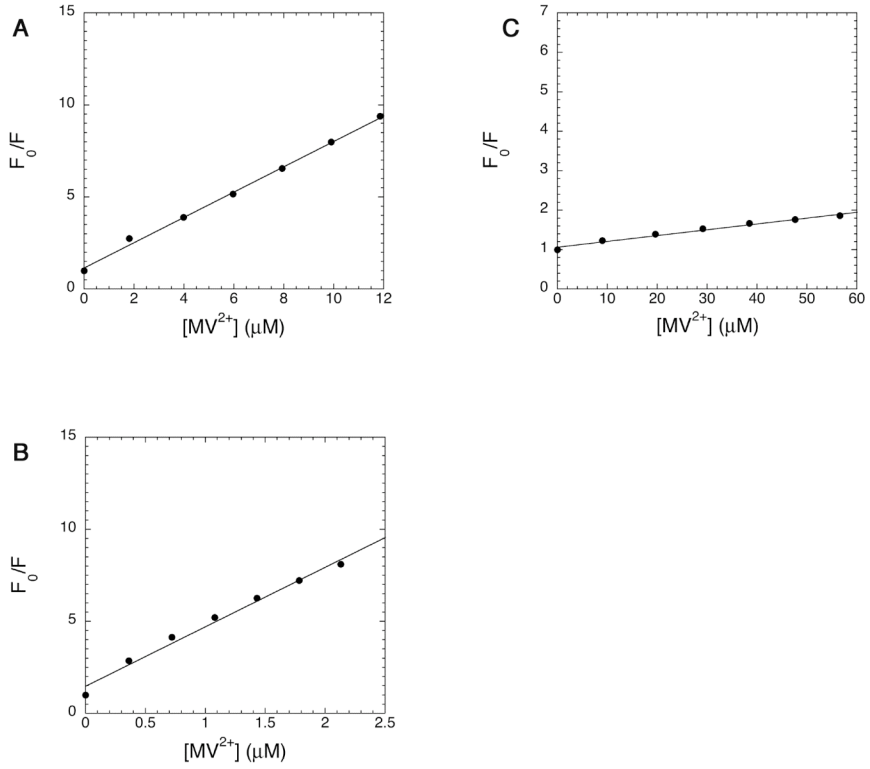

Appendix 3.1. Stern-Volmer plots of (A) **P1**, (B) **P2**, and (C) **P3** in response to $\mathbf{MV^{2+}}$ in DMF solution.

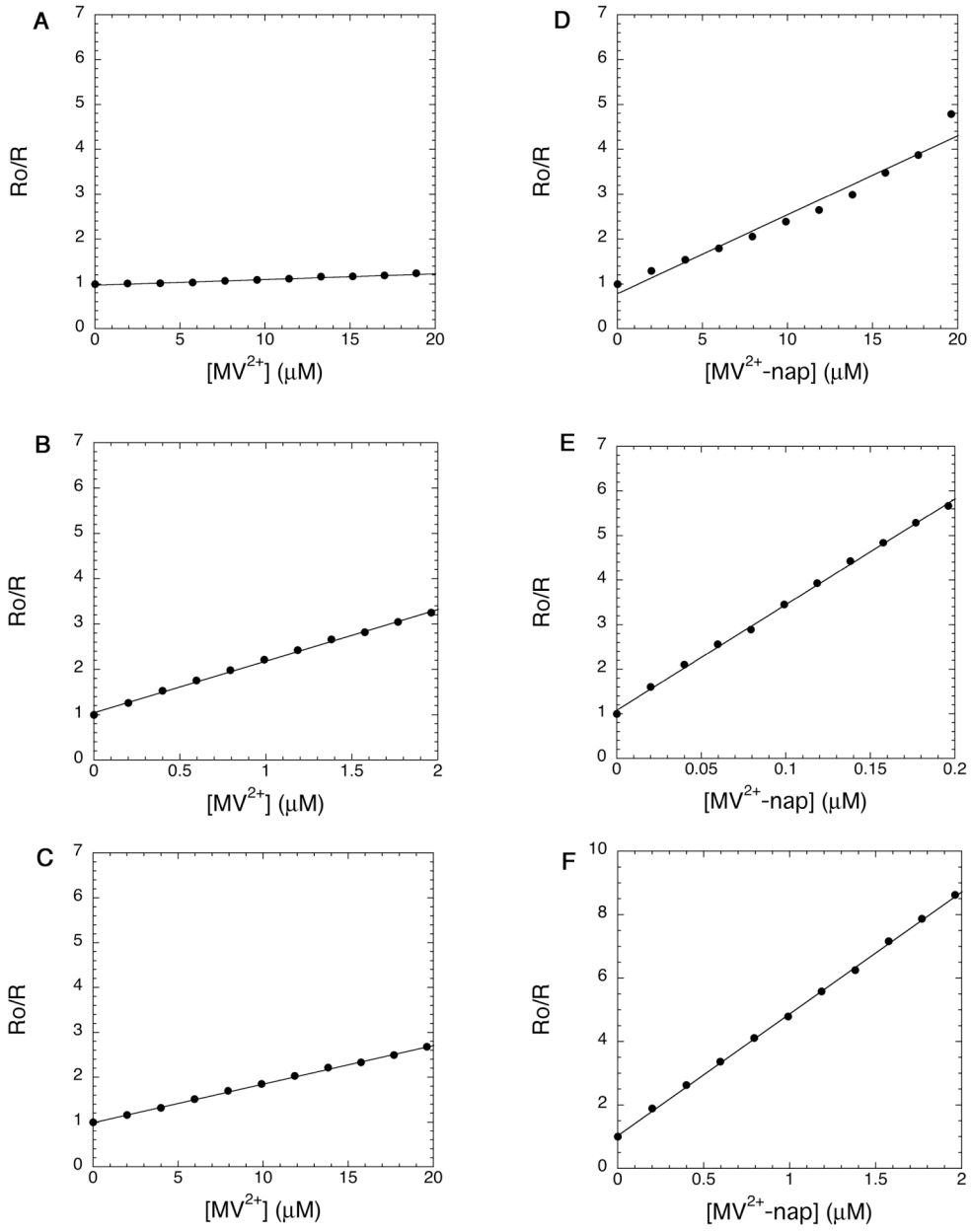

Appendix 3.2. Stern-Volmer plots of **P1**-coated particles in response to **MV^{2+}** and **MV^{2+}-nap**: (A,D) in water; (B,E) Tris buffer (20 mM, pH 7.4); (C,F) Tris-buffered saline (20 mM, pH 7.4; 150 mM NaCl, 5 mM $CaCl_2$).

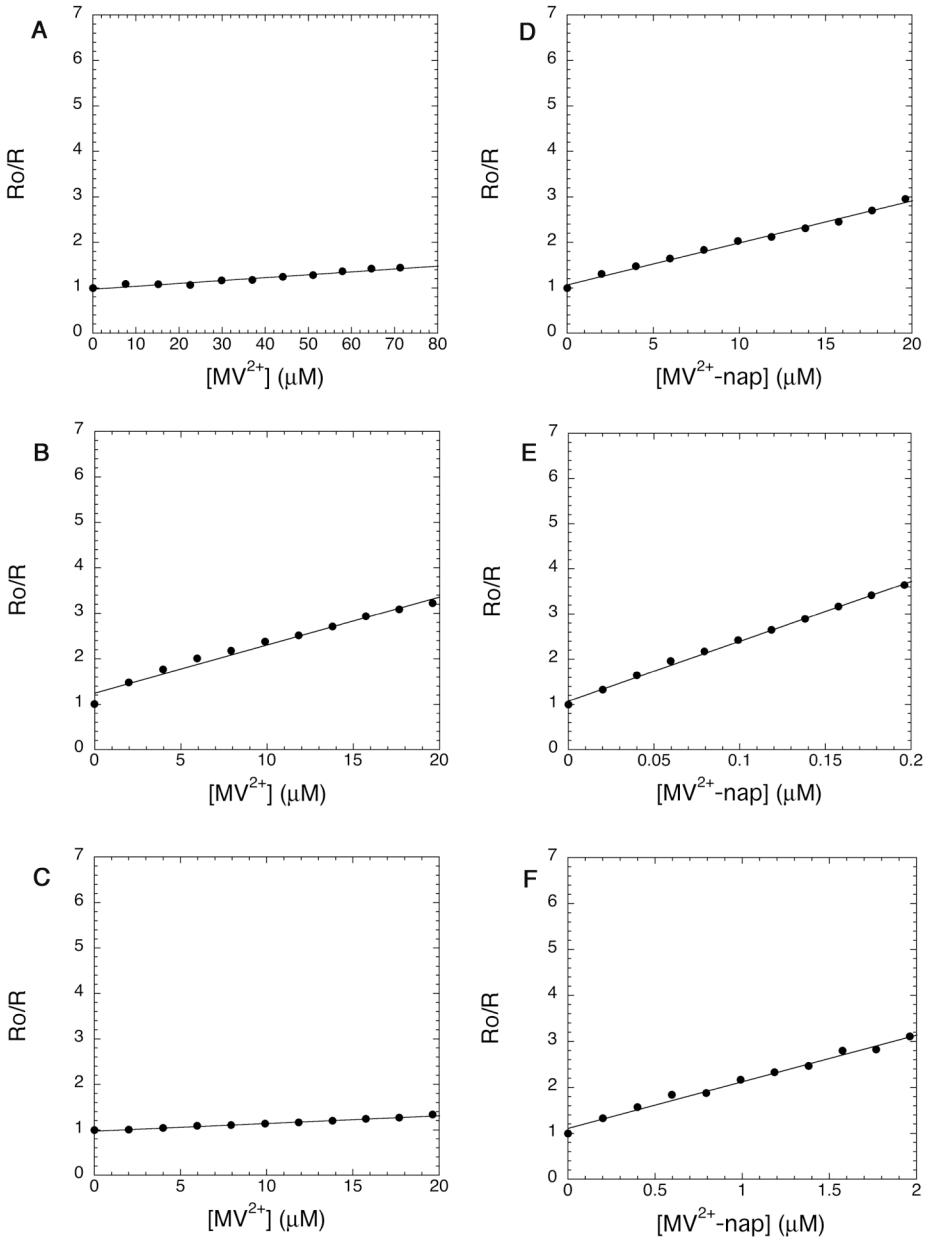

Appendix 3.3. Stern-Volmer plots of **P2**-coated particles in response to **MV^{2+}** and **MV^{2+}-nap**: (A,D) in water; (B,E) Tris buffer (20 mM, pH 7.4); (C,F) Tris-buffered saline (20 mM, pH 7.4; 150 mM NaCl, 5 mM $CaCl_2$).

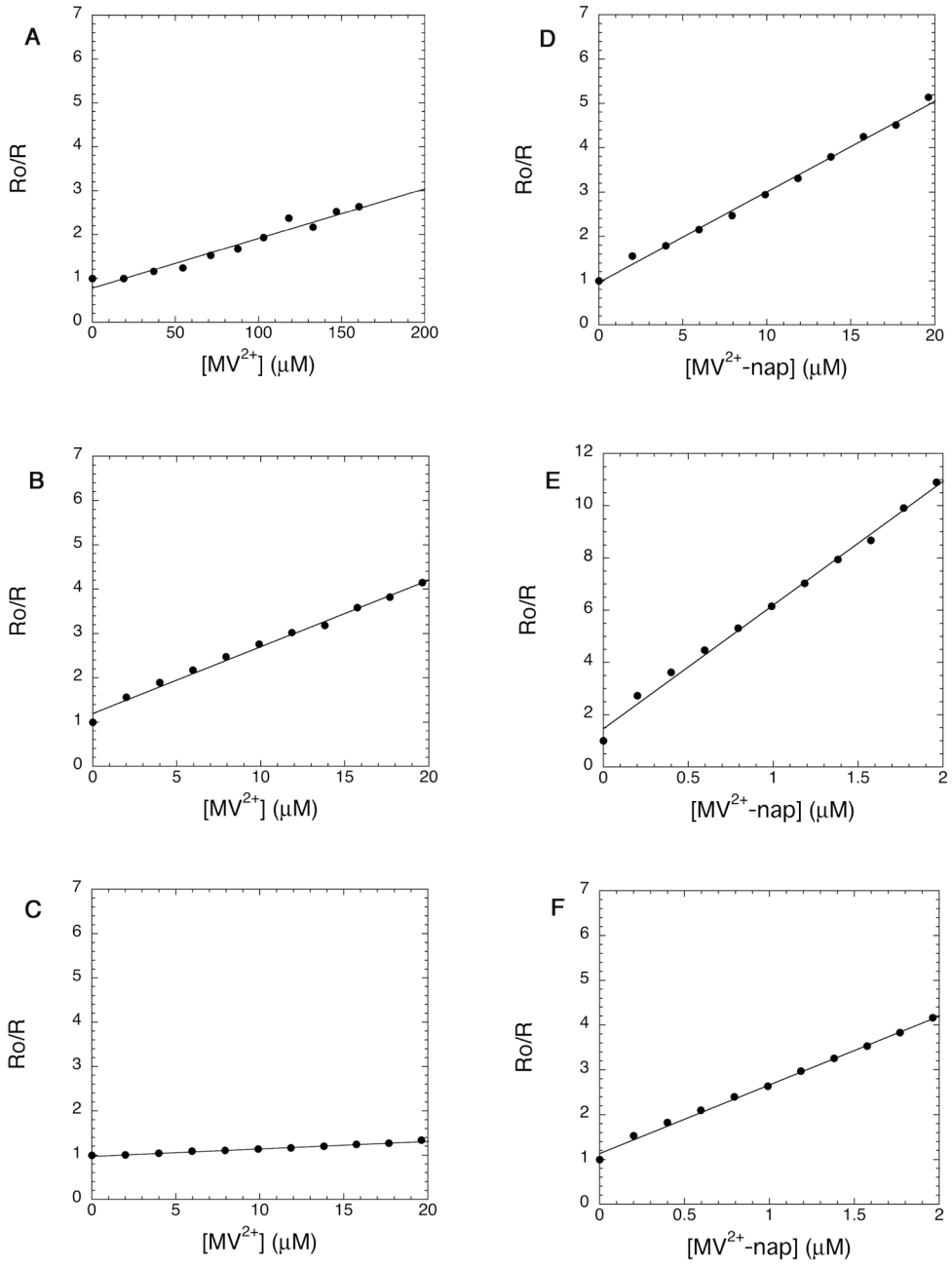

Appendix 3.4. Stern-Volmer plots of **P3**-coated particles in response to **MV^{2+}** and **MV^{2+}-nap**: (A,D) in water; (B,E) Tris buffer (20 mM, pH 7.4); (C,F) Tris-buffered saline (20 mM, pH 7.4; 150 mM NaCl, 5 mM $CaCl_2$).

Chapter 4:

Increasing Sensitivity with Dendritic Quenchers

4.1 Introduction

As shown in Chapter 3, we can increase the sensitivity of the particle-based conjugated polymer sensors with the tailoring of molecular interactions. The naphthyl-functionalized viologen was shown to increase the quenching response by several orders of magnitude due to its hydrophobic nature and its ability to π-stack with the conjugated polymer. Quenchers that are dendritic in nature may also prove to further increase our sensitivity, due to size and cooperative effects. This chapter describes the work in collaboration with Dr. Ghislaine Bailey to demonstrate and assess the use of nitroaromatic dendritic molecules as "superquenchers" towards conjugated polymer-coated particles in environments suitable for biosensing, for future implementation into our sensory schemes.

4.1.1 Dendrimers as quenchers

The flexibility afforded in the design of dendrimers[1,2] has resulted in their incorporation into diverse applications that include catalysis,[3] light harvesting,[4] and more recently drug delivery.[5,6] Herein we use the dendrimer as scaffold. The exponential growth of terminal groups with each additional generation presents an opportunity to produce a polyfunctional fluorescence quenching molecule to be used in sensor schemes. The dendrimers should provide an amplified response versus the conventional single quenching molecule.

Ternon and Bradley[7] demonstrated the concept of using multivalent interactions to increase sensitivity in a dual label protease assay and showed over a three-fold improvement utilizing a tri-DANSYL unit and the DABSYL group for their internally quenched substrate versus the monovalent substrate. A multiple antigenic peptide system was also used by the Weissleder group[8] for increasing sensitivity of protease sensors with the aggregation of the

chromophores on the multi-arm peptide substrate, and release into the environment upon enzymatic activity for a recovery of the fluorescence. The use of multiple quenchers to pair with one fluorophore has also been shown for use in molecular beacon technology for DNA hybridization, to increase the signal-to-background ratio by twenty-fold versus the conventional single quencher approach.[9] The signal amplication provided by the dendrimer has also been used where the multiple units are used as the fluorophores, resulting in an increase in interaction compared to the single molecules in a quenching scheme.[10]

Similar to these approaches, we are interested in having multiple terminal quenchers on a single molecule. The synthesis is designed with a focal point for incorporation into protease assays. The advantange of the dendritic quenchers in poly(phenylene ethynylene) (PPE)-coated particle quenching is depicted in Figure 4.1. Nitroaromatic groups have proven useful as efficient electron-accepting molecules for our conjugated polymer sensors,[11] and can easily be incorporated in dendrimer syntheses with the commercial Sanger's reagent (2,4-dinitrofluorobenzene) and other available derivatives. We hypothesize that the multiplicity of quencher units, as well as the increase in size, of the dendritic quenchers, should give rise to systems with higher sensitivity than previously accessed with monofunctional quenchers, and this will prove useful for implementation into our biosensing platform.

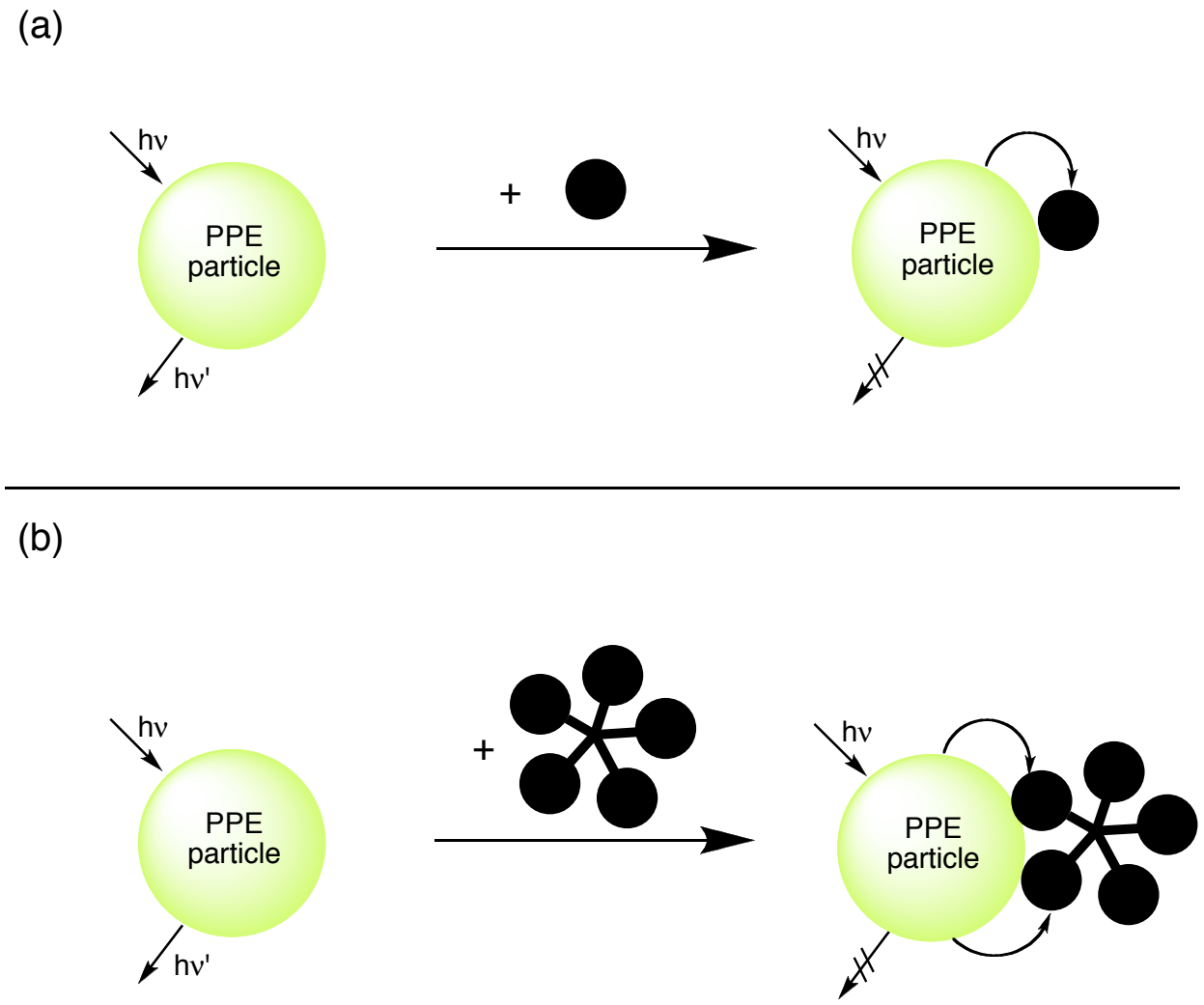

Figure 4.1. Schematic representation of the response of PPE-coated particles towards (a) a conventional molecular quencher (b) a dendritic molecular quencher with signal amplification, where the curved arrows indicate a quenching process.

4.2 Results and Discussion

4.2.1 Convergent synthesis of the dendritic quenchers[12]

The synthesis of the **G0**, **G1** (2 and 3 terminal units), and the **G2** (6 terminal units) molecules shown in Figure 4.2 was inspired by the convergent[13] synthesis of amino-acid based dendrimers.[14,15] The advantage of convergent versus divergent dendrimer growth (from the core to the periphery) is the ability to purify the products with relatively simple protocols, allowing for a greater choice of reactions.[2] Figure 4.3 illustrates the convergent synthesis approach, in which the number of branches is increased by repeated reaction and focal point activation. The higher generation quenchers (**G2**) are generated through coupling reactions with the 1st generation quenchers using HOBT/HBT and standard peptide coupling conditions to create the amide linkages. Increasing the number of branches on the higher generation quenchers was not synthetically possible due to the amount of steric crowding around the focal point, a common limit to larger structures accessible via convergent synthesis methods.[2]

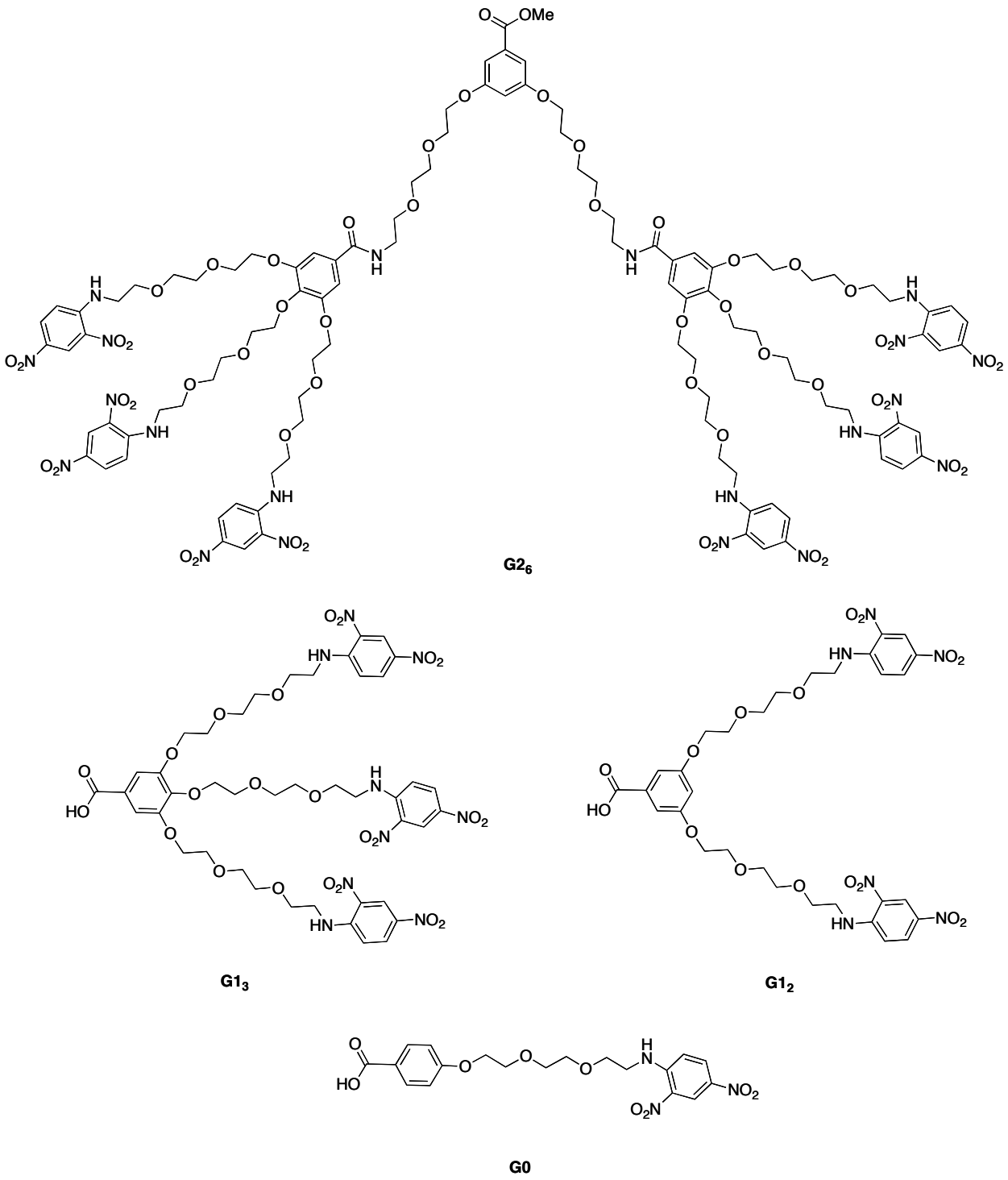

Figure 4.2. Structures of dendritic quenchers.

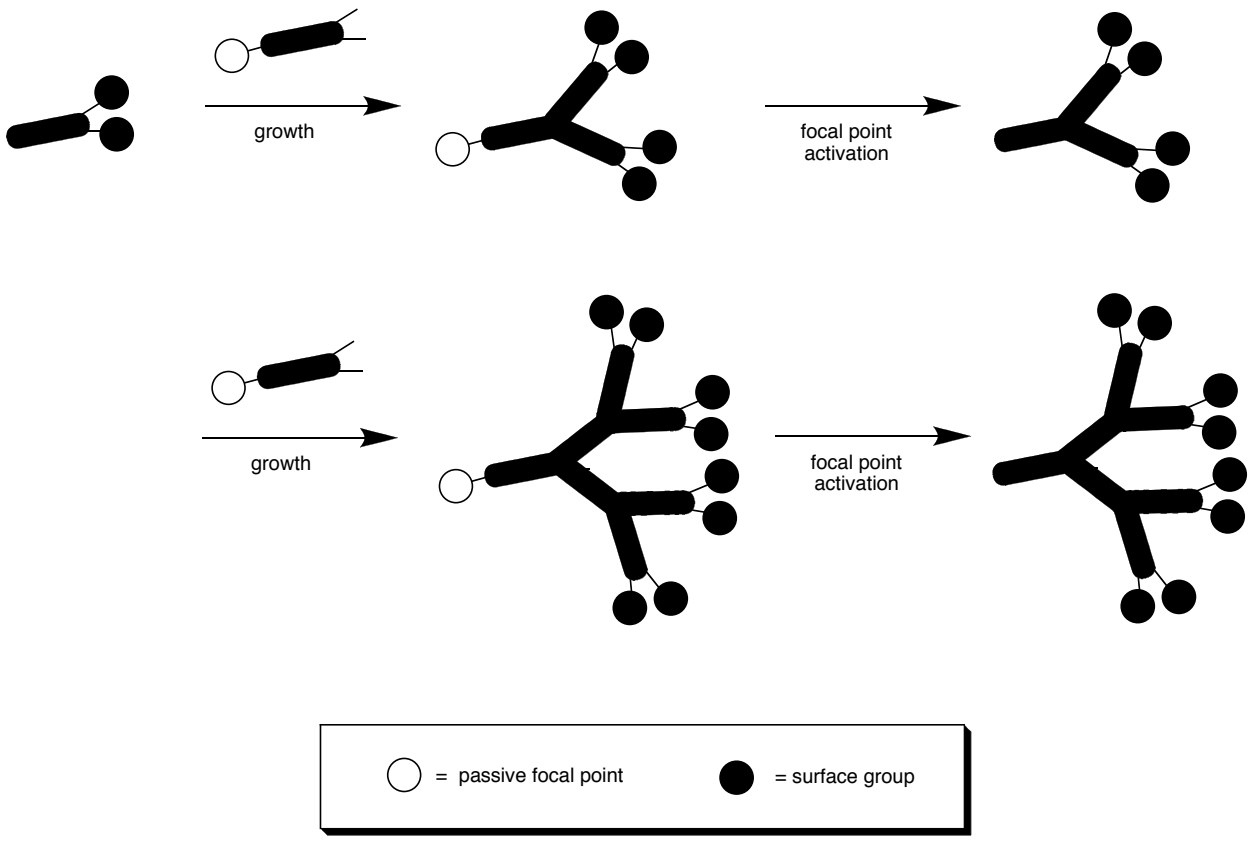

Figure 4.3. Convergent synthesis approach for dendrimer growth. Adapted from ref.[2]

4.2.2 Quenching response of PPE microspheres towards dendritic quenchers

We evaluated the response in ethanol and a common biological buffer, Tris (20 mM, pH 7.4), to assess the utility of these molecules in biosensing schemes. The internal reference system described in Chapter 3 is useful for quantifying fluorescence quenching of PPE films immobilized on particles for assessing the dendritic quencher library. The addition of these nitroaromatic dendritic molecules to PPE-coated Eu^{3+}-incorporated polystyrene microspheres (d = 0.2 μm) shows linear static fluorescence quenching behavior, indicated by the Stern-Volmer plot in the inset of Figure 4.5.

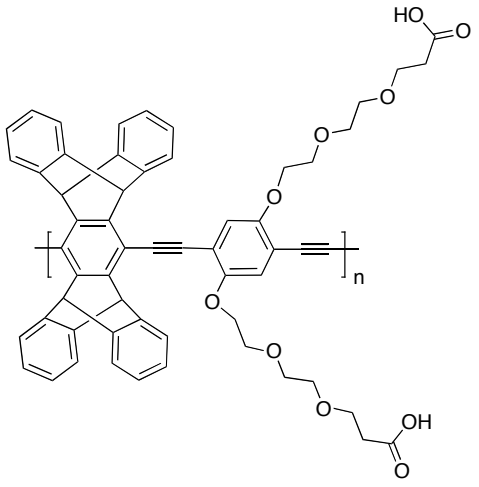

Figure 4.4. Structure of PPE used for coating Eu^{3+}-incorporated polystyrene microspheres (d = 0.2 μm).

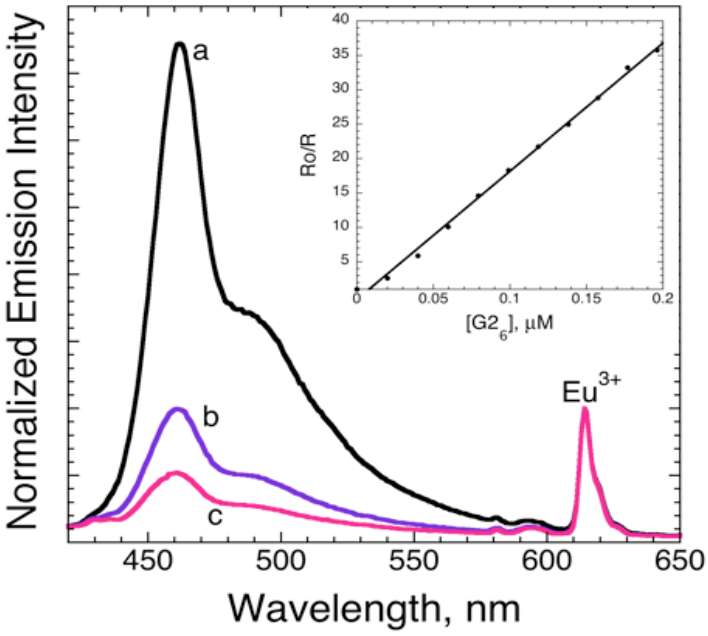

Figure 4.5. Normalized emission intensity of PPE-coated microspheres in response to (a) 0, (b) 0.02, and (c) 0.04 μM of **G2$_6$** in Tris buffer. Inset shows Stern-Volmer plot.

The effect of size on quenching is evident from the summary plot shown in Figure 4.6, particularly in Tris buffered conditions. By increasing the number of quenchers on a single molecule from one dinitrophenyl (**G0**) to six (**G2$_6$**), the quenching efficiency is seven-fold greater than what would be theoretically calculated for the concentration increase of quencher units. The cooperative quenching from the covalently linked dinitrophenyl groups improves the efficiency of associating with the PPE-coated particles versus the single quenchers by several orders of magnitude. A K_{SV} value of $(1.7 \pm 0.1) \times 10^8$ M^{-1} is the highest quenching that has been observed with PPEs in buffered conditions that are not prone to quencher-induced aggregation.[16] This is significant in improving the sensitivity of protease assays, as a smaller concentration of the dendritic quencher is needed to evoke the same response as a monofunctional quencher.

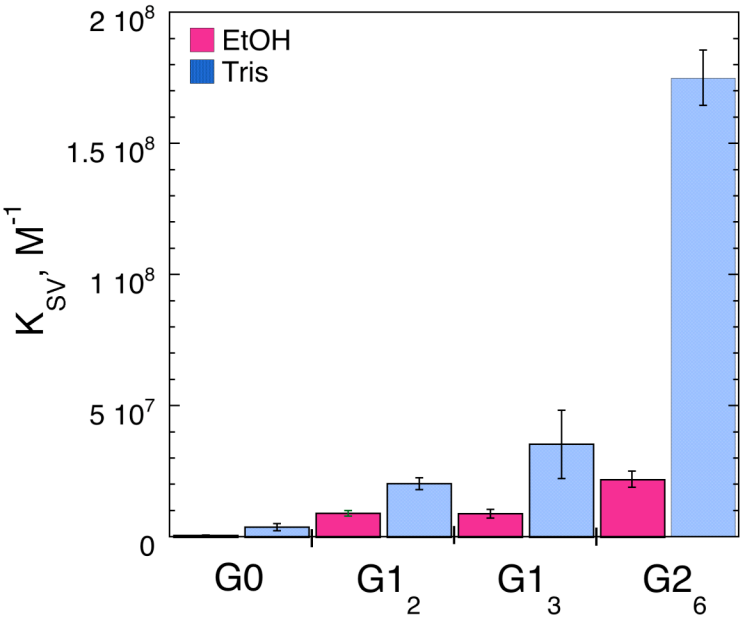

Figure 4.6. Summary plot of K_{SV} values (M^{-1}) for dendritic quenchers in ethanol and Tris buffer. Error bars indicate standard error (n = 3).

	K_{sv} (M^{-1})	
Quencher	EtOH	Tris (20 mM, pH 7.4)
G0	$(7.9 \pm 0.9) \times 10^5$	$(3.9 \pm 1.3) \times 10^6$
$G1_2$	$(1.0 \pm 0.1) \times 10^7$	$(2.1 \pm 0.2) \times 10^7$
$G1_3$	$(9.0 \pm 1.7) \times 10^6$	$(3.6 \pm 1.3) \times 10^7$
$G2_6$	$(2.2 \pm 0.3) \times 10^7$	$(1.7 \pm 0.1) \times 10^8$

Table 4.1. Summary of mean Stern-Volmer constants (n = 3) in EtOH and Tris buffer (20 mM, pH 7.4).

The quenching behavior for PPE films that are immobilized on particles is quite different than that for PPEs in solution. An anionic PPE, without pentiptycene groups to render the material water-soluble, was assessed by Ghislaine Bailey for its quenching efficiency towards the dendritic quenchers in solution,[12] and was observed to have the highest quenching response towards **$G1_3$** ($K_{SV} = 1.5 \times 10^6$). This value is most likely a combination of quenching from electron transfer as well as self-quenching from aggregation. Increasing the number of dinitrophenyl groups per molecule only decreased the amount of quenching. Since the polymer is sparingly soluble in buffer, it most likely exists in an aggregated form, especially due to the flexibility inherent to non-pentiptycene PPEs. The dendritic quenchers may be separating the PPE aggregates in solution, thereby simultaneously enhancing the fluorescence while quenching, resulting in a overall decreased quenching response observed for the higher generation. This trend is not observed in the PPE-coated particles, indicating that the immobilized films are not prone to aggregation and solubilization effects that may interfere with quencher association for polymers in solution.

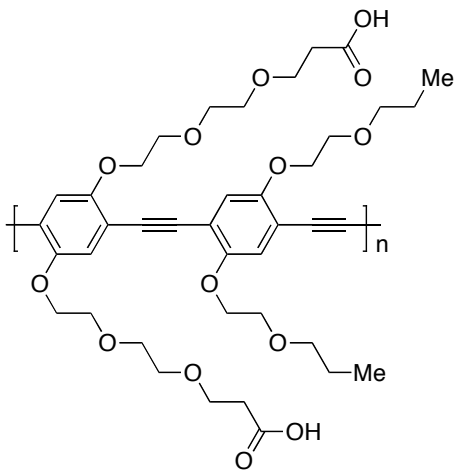

Figure 4.7. Structure of PPE used for solution quenching experiments performed by Ghislaine Bailey.[12]

4.3 Conclusions

We have utilized the ratiometric method described in Chapter 3 for assessing the quenching performance of nitroaromatic dendritic molecules with PPE-coated Eu^{3+}-incorporated polystyrene particles (d = 0.2 μm) in ethanol and Tris buffer. Fluorescence quenching follows linear static behavior according to the Stern-Volmer equation, and the response is highest in Tris buffer conditions. The quenching response varies nonlinearly with the number of nitroaromatic units per molecule, giving rise to "superquenching" behavior, and we are further investigating their incorporation into biosensors.

4.4 Experimental Section

Materials

N,*N*-dimethylformamide (Sigma-Aldrich, HPLC grade, ≥ 99.9%) and ethanol (Pharmco, 200 proof absolute, anhydrous) were used as received. Tris buffer (20 mM, pH 7.4) was freshly

prepared from tris[hydroxymethyl]aminomethane, adjusting the pH with 0.1 mM HCl or NaOH, and stored at 0ºC until use. All water used in experiments was obtained from a Millipore Milli-Q purification system.

Methods

Synthesis of dendritic molecules was performed by Dr. Ghislaine Bailey.[12] PPE-coated Eu^{3+}-polystyrene microspheres (d = 0.2 μm) were prepared as described in Chapter 3.

Fluorescence spectra were measured on Jobin Yvon SPEX Fluorolog-τ2 or -τ3 fluorometer.

Due to limited solubility of the higher generation quenchers, stock solutions of $\mathbf{G_0}$, $\mathbf{G1_2}$, $\mathbf{G1_3}$, and $\mathbf{G2_6}$ were prepared in DMF as 0.5 mM solutions. Solutions with concentrations 0.1 mM or 0.01 mM were prepared from the DMF stock solution in EtOH and Tris (20 mM, pH 7.4) for quenching studies. For each experiment, the initial fluorescence emission intensity was measured. Aliquots (5 μL additions, 50 μL total) of the quencher solutions in EtOH and Tris were added to the particles in a quartz cuvette and the fluorescence was measured after 5 minutes to allow for equilibration. The excitation wavelength for the experiments was set at 390 nm to allow for the excitation of the europium internal reference. Measurements were performed in triplicate and fitted to the Stern-Volmer equation ($F_o/F = 1 + K_{SV}$[quencher]) with R-squared values of > 0.98 for each condition.

4.5 References

(1) Vögtle, F.; Gestermann, S.; Hesse, R.; Schwierz, H.; Windisch, B. *Prog. Polym. Sci.* **2000**, *25*, 987-1041.

(2) Matthews, O. A.; Shipway, A. N.; Stoddart, J. F. *Prog. Polym. Sci.* **1998**, *23*, 1-56.

(3) Twyman, L. J.; King, A. S. H.; Martin, I. K. *Chem. Soc. Rev.* **2002**, *31*, 69-82.

(4) Adronov, A.; Fréchet, J. M. J. *Chem. Comm.* **2000**, 1701-1710.

(5) Esfand, R.; Tomalia, D. A. *Drug Discovery Today* **2001**, *6*, 427-436.

(6) Boas, U.; Heegaard, P. M. H. *Chem. Soc. Rev.* **2004**, *33*, 43-63.

(7) Ternon, M.; Bradley, M. *Chem. Comm.* **2003**, 2402-2403.

(8) Galande, A. K.; Hilderbrand, S. A..; Weissleder, R.; Tung, C. -H. *J. Med. Chem.* **2006**, *49*, 4715-4720.

(9) Yang, C. J.; Lin, H.; Tan, W. *J. Am. Chem. Soc.* **2005**, *127*, 12772-12773.

(10) Balzani, V.; Ceroni, P.; Gestermann, S.; Kauffmann, C.; Gorka, M.; Vögtle, F. *Chem. Comm.* **2000**, 853-854.

(11) Wosnick, J. H.; Mello, C. M.; Swager, T. M. *J. Am. Chem. Soc.* **2005**, *127*, 3400-3405.

(12) Bailey, G. C., PhD dissertation, Massachusetts Institute of Technology, 2007.

(13) Grayson, S. M.; Fréchet, J. M. J. *Chem. Rev.* **2001**, *101*, 3819-3868.

(14) Brouwer, A. J.; Mulders, S. J. E.; Liskamp, R. M. J. *Eur. J. Org. Chem.* **2001**, 1903-1915.

(15) Crespo, L.; Sanclimens, G.; Pons, M.; Giralt, E.; Royo, M.; Albericio, F. *Chem. Rev.* **2005**, *105*, 1663-1681.

(16) Thomas, S. W., III; Joly, G. D.; Swager, T. M. *Chem. Rev.* **2007**, *107*, 1339-1386.

Chapter 5:

Addressing Specificity with Particle-Containing Hydrogels

5.1 Introduction

The PPE-coated microspheres described in previous chapters have an effective negative charge due to the anionic groups of the polyelectrolyte coating, which may aid in the association with cationic quenchers such as the viologen derivatives (Chapter 3), but causes implications for practical biosensing due to nonspecific interactions with charged species such as proteins. While many in the field have developed systems directly with conjugated polyelectrolytes,[1] we believe a more robust system is necessary to access a larger range of environments without compromising sensitivity. In addition, opportunities for multiplexing are evident with developing more specific systems. We describe methods in this chapter for incorporating particles into hydrogel films as a proof-of-concept for achieving greater specificity.

5.1.1 Hydrogel-based sensors

Polymer gels consist of a three-dimensional network of polymer chains joined together at a number of connecting sites (Figure 5.1). These connections can be covalent crosslinks or physical interactions such as hydrogen bonds or electrostatic forces. The network is capable of absorption and swelling in good solvent, but not dissolving due to the presence of the crosslinks. Hydrogels are one type of polymer gel in which water is the dispersion medium.

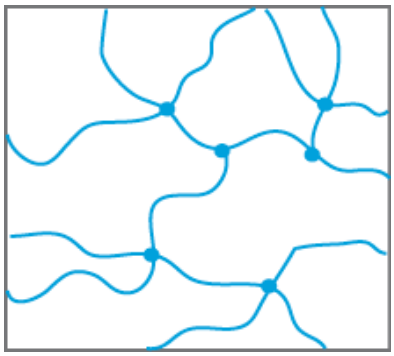

Figure 5.1. Schematic of a polymer gel.

Hydrogels were one of the first biomaterials designed for medical applications. Wichterle and Lím in the late 1950s synthesized crosslinked materials based on copolymers of 2-hydroxyethyl methacrylate with ethylene dimethacrylate and noted their specific use in biological systems.[2] Since then, hydrogels have found wide use in biomedical applications due to their hydrophilic, low fouling potential and biocompatibility properties, and have been synthesized from both natural and synthetic materials. The network of water-insoluble polymers has shown resistance to protein adsorption for implant materials such as soft contact lenses,[3] proven useful in immobilizing peptides and proteins for biochip assays,[4] and can been engineered to promote cellular adhesion for tissue engineering.[5]

Due to their physical properties, hydrogels have also been designed as sensors. The ability for polymer gels to respond to environmental stimuli and function as "smart gels" was pioneered by Toyoichi Tanaka at MIT.[6] Asher and coworkers have utilized the swelling characteristics of the hydrogel to produce different diffraction wavelengths of the photonic crystal materials[7,8] for fast responsive glucose sensors.[9] Crosslinks can also be utilized in sensing schemes, and in one example the competitive binding of antigens for antigen-antibody crosslinks changes the hydrogel swelling.[10] Triggered events are desirable for controlled release and drug delivery applications,[11] and hydrogels have been designed in which enzymatic cleavage of the crosslinks releases the payload carried by the material at the implant site.[12]

The crosslinked gel provides a protective environment for encapsulated species, and this has been used for the detection of organophosphorus neurotoxins with the incorporation of pH-sensitive dyes in poly(ethylene glycol) hydrogel materials.[13] Other hydrogel-incorporated materials have also been prepared for general pH sensors,[14,15] metal ions,[16] enzymes,[17] and glucose monitoring[7,9,18-21] for their capability to embed indicators and components without the need for covalent immobilization and the general ease of preparation of the composite sensors.

Physical crosslinks create not only a mechanically stable material, but also a barrier for large molecular species due to the entangled network of polymer chains. The molecular pores created by the polymeric network is often termed the macromolecular mesh size,[22] with the spaces between the polymer chains filled with water. Herein we utilize these hydrogels as selective membranes for the developed quenchers in our system, as shown in Figure 5.2. Molecular complexation occurs with the quenchers and the conjugated polymers due to strong π-π stacking and hydrophobic interactions, as discussed in Chapters 2 and 3. The permeability to water and solutes can be readily adjusted by varying the crosslinker concentration based on size exclusion properties. Our hypothesis assumes that most of the nonspecific quenching will occur from proteins and thus will be larger molecular weight species that will not be able to penetrate through the hydrogel due to the solute radius and the slower diffusion versus the quenchers.

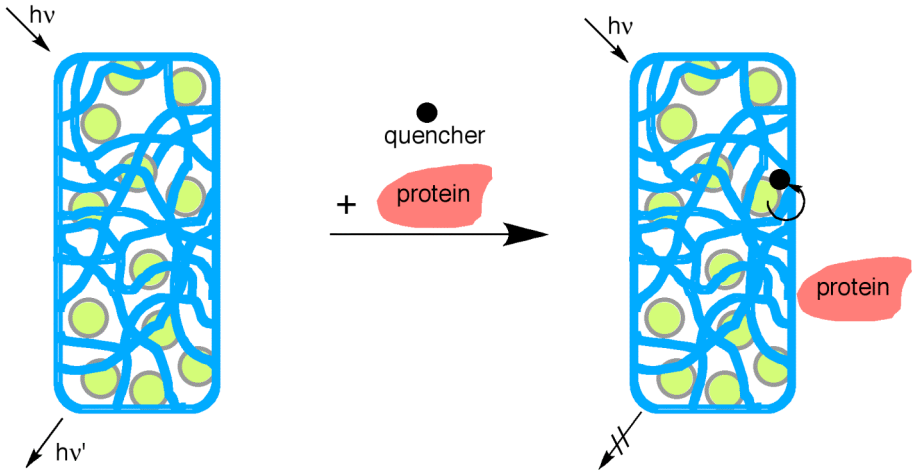

Figure 5.2. Schematic of particle-containing hydrogel to minimize nonspecific interactions with proteins due to size exclusion.

Solute transport through the hydrogel is not only controlled by the crosslink density, but also is dependent on additional factors such as thickness, ionic strength, polymer density, polymer-solvent interactions, polymer chain mobility, and the existence of charged groups on the polymer which may bind the solute.[23] It is frequently assumed that there is a direct relationship between gel swelling and solute permeability, but this only holds if the network is inert with respect to the diffusing species and is uniform. Hydrogels generally do not meet both of these conditions, and the relationship between permeability and gel swelling becomes more complex to affect the diffusivity (see Chapter 5 Appendix).[24] In this chapter, we utilize poly(acrylamide) gels to first demonstrate our size exclusion principles, and look forward to developing hydrogel materials with the desired solute transport properties with this complexity in mind.

5.2 Results and Discussion

5.2.1 Protein interactions – PPE particles in solution

Nonspecific quenching is observed between the PPE-coated particles and proteins, largely due to electrostatic interactions, even in buffered environments. In 2005, Bunz and coworkers showed the nonspecific quenching of PPEs in response to a variety of proteins as a "cautionary tale" for designing biosensors with conjugated polyelectrolytes.[25] In light of this, we decided to assay the interactions of two proteins, lysozyme and cytochrome c, with the PPE-coated Eu^{3+}-incorporated polystyrene microspheres (d = 0.2 μm). Lysozyme is an enzyme abundantly found in egg whites and serves as a model enzyme in protein crystallography.[26] Cytochrome c is a heme protein and has been utilized as a model protein to monitor adsorption onto hemodialysis membranes.[27] Both proteins are cationic at pH 7.4. Table 5.1 summarizes the protein properties.

Protein	M.W. (kDa) [28,30]	Isoelectric point (pI) [29, 31]	Number of charges/molecule at pH 7.2 [26]
Lysozyme	14.3	11.35	7
Cytochrome c	12.3	10.0 – 10.5	9

Table 5.1. Summary of the properties of lysozyme and cytochrome c.

Figure 5.3 shows the response towards lysozyme and cytochrome c in Tris buffer (20 mM, pH 7.4) in a Stern-Volmer plot. A decrease in the PPE emission upon addition of quencher is observed, arising from nonspecific quenching interactions between lysozyme and particularly cytochrome c, as we would expect from the negatively-charged PPE-coated particles. While lysozyme is positively charged at ph 7.4, there is minimal quenching observed with the titration of the protein to the PPE-coated particles. The PPE films immobilized on the particle are not conformationally affected to a large extent in the presence of lysozyme, in spite of the large concentrations added. This behavior is much different than that of PPEs in solution, which tend to aggregate upon association with charged proteins.[1] In Bunz's report, both lysozyme and cytochrome c were comparable in the fluorescence quenching of an anionic PPE in phosphate buffer (10 mM, pH 7.2).[25] The high observed quenching response towards cytochrome c with the PPE-coated particles is attributed to several inherent properties of the protein. Cytochrome c has an absorption maximum at 409 nm in water with a molar extinction coefficient (ε) of 106 $mM^{-1}cm^{-1}$.[32] An inner filter effect is most likely attributing to the large decrease in PPE fluorescence, since excitation at 390 nm will be absorbed by both the PPE and cytochrome c. The effect is often negligible in quenching studies since the concentrations of competing

absorbing species are kept low.[33] In this experiment, the final concentration of quencher added is 20 mM to evaluate high concentrations of proteins with the PPE-coated particles, and thus calculations to correct the inner filter effect are warranted. The heme protein is also is capable of electron transfer, as it physiologically forms a complex with cytochrome c peroxidase and has been utilized as a model for electron-transfer protein partners.[34]

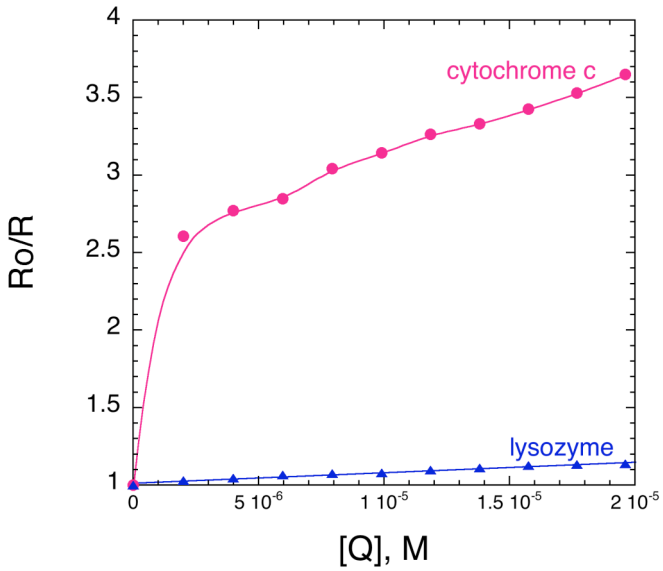

Figure 5.3. Response of PPE-coated Eu^{3+}-PS particles in Tris (20 mM, pH 7.4) towards cytochrome c and lysozyme with increasing concentration, plotted as R_o/R versus quencher concentration *[Q]*.

5.2.2 Protein interactions – PPE particles in hydrogel

To demonstrate the potential of hydrogel encapsulation to prevent nonspecific quenching, the PPE-coated particles were dispersed in a hydrogel matrix. A very well-established system using acrylamide (Aam) as the monomer and *N,N'*-methylenebisacrylamide (Bis) as the crosslinker was used for initial particle-containing hydrogels, with ammonium persulfate/*N,N,N',N'*-tetramethylethylenediamine (APS/TMEDA) as the initiating system. These polymer networks have been used extensively for electrophoresis for protein separation and

identification.[35,36] The charge-neutral gel has been shown to demonstrate enhanced selectivity based on molecular size, and is due primarily to the partitioning effect of the gel based on excluded volume.[37] The redox initiation system has a fast polymerization time as compared to other systems and is conducted at ambient temperature, and thus is desirable for the facile preparation of gels for biological analysis. Mechanisms of initiation have been proposed,[38-41] however there are some detailed aspects of kinetic behavior that remain controversial, whether or not the amine component also takes part of the initiation reaction. Empirical evidence shows TMEDA exerts a high promoting effect on the vinyl polymerization initiated by the persulfate,[39] and most likely produces a number of radical species, resulting in more network inhomogeneity[42] due to random termination. Nevertheless, the redox systems are water-soluble and have desirable kinetics to encapsulate the particle dispersion before any sedimentation occurs. Photopolymerization has also gained wide use for creating hydrogel films,[43] but since this method often uses high exposure to UV light, which may cause some photobleaching to occur with the PPE coatings, we opted for using redox initiation.

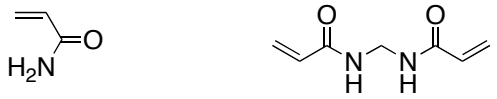

Aam **Bis**

Figure 5.4. Structures of Aam and Bis.

The PPE-coated particles were dispersed in the precursor hydrogel solution (for a total particle concentration of 0.12%), initiated with TMEDA addition and then deposited between two sandwiched slides to form a particle-containing hydrogel film, as shown in Figure 5.5. Concentrations of Aam and Bis in the precursor solution were 13% (w/v) and 0.2% (w/v), respectively, for a crosslink density of 0.015%. Fast initiation with this system allowed for the

particles to remain homogenous within the film. Removal of the top slide and spacers exposed the film to air, terminating the polymerization. The bottom slide was pretreated with glutaraldehyde to covalently attach the film to the glass surface during gelation. Thorough rinsing with water, followed by Tris buffer, was conducted with the particle-containing film to remove residual monomer/catalyst and to equilibrate the film prior to experiments.

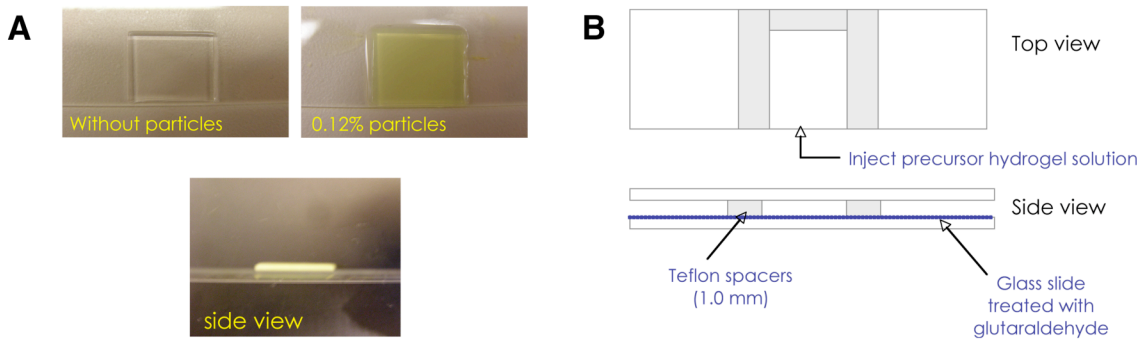

Figure 5.5. (A) Photographs of hydrogel films and (B) schematic of procedure for formation of hydrogel films.

To assess the specificity of the particle-containing hydrogel film, the fluorescence was monitored as shown in Figure 5.6. The film on the glass cover slide was affixed to one face of a 2.5 cm × 1.0 cm × 4.5 cm *(L × W × H)* rectangular quartz cuvette. Equilibrium swelling was established prior to experiments by soaking each film in Tris buffer (20 mM, pH 7.4) at room temperature. The film was kept in constant contact with the solution in the cuvette, and the fluorescence recorded at specific timepoints. Figure 5.7 shows the response of the particle-containing hydrogel films towards a 1 μM solution of **MV^{2+}-nap** in Tris buffer with time. Another film was prepared and immersed in a 1 μM solution of cytochrome c in Tris buffer and monitored with time. As a control, the fluorescence of a film was monitored versus time with Tris buffer alone.

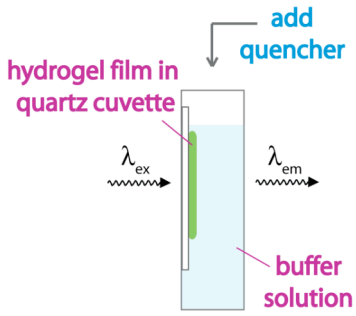

Figure 5.6. Schematic of quenching experiment with particle-containing hydrogel films.

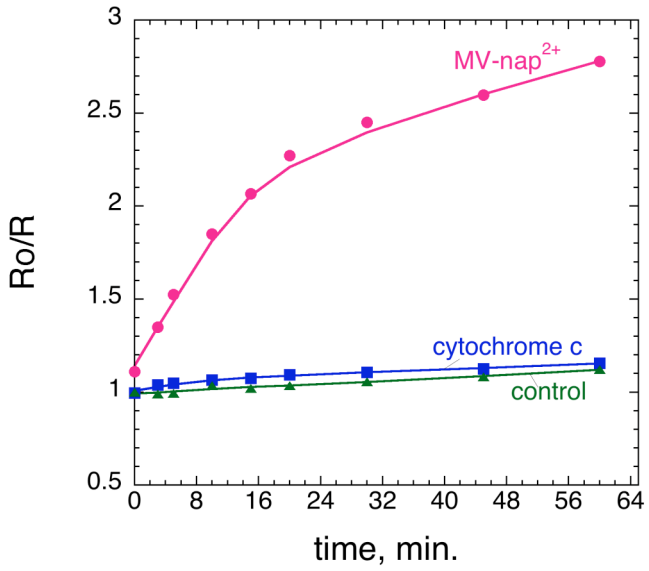

Figure 5.7. Comparison of the response of particle-containing hydrogel films to **MV^{2+}-nap** (1 μM), cytochrome c (1 μM), and control response in Tris buffer (20 mM, pH 7.4).

We observe a significant difference in the quenching response of **MV^{2+}-nap** versus the protein at equal concentrations, with the response of the protein close to that of the control. The quenching response of **MV^{2+}-nap** is highly time-dependent and nonlinear. After 1 hour, R_0/R is still increasing, and even after 2 hours of immersion in the quencher solution (data not shown) the quenching does not reach a steady-state value. A change in the swelling properties and a reorganization of the network due to the presence of **MV^{2+}-nap** may be affecting and complicating the observed quenching behavior. Although the response time of the hydrogel film

towards **MV^{2+}-nap** does not have the desired kinetics, this was our first demonstration of addressing specificity in our particle sensors.

Exposure of the hydrogel film to various concentrations of **MV^{2+}-nap** results in a quenching of the PPE emission relative to the Eu^{3+} emission, as shown in Figure 5.8. The spectra and the corresponding photographs of the films under UV lamp illumination clearly show the increase of the red Eu^{3+} emission as compared to the PPE emission with higher concentrations of **MV^{2+}-nap** (Figure 5.8 (c)).

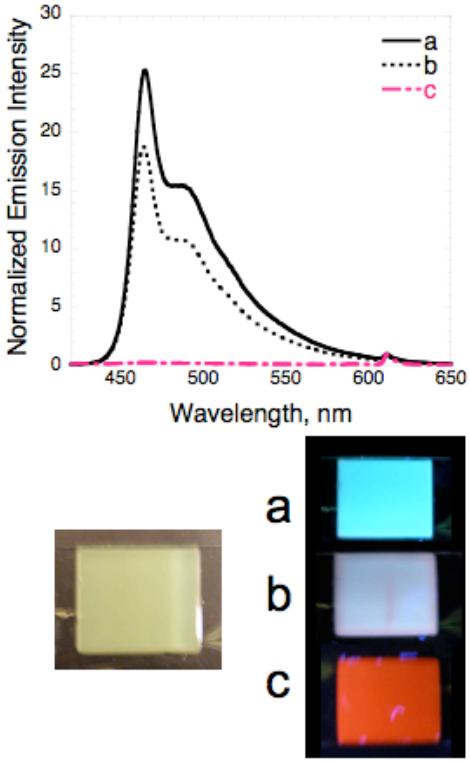

Figure 5.8. Normalized emission spectra and corresponding photographs (under UV-illumination) of particle-containing hydrogel films in response to (a) 0 μM, (b) 1 μM, and (c) 100 μM of **MV^{2+}-nap** in Tris buffer (20 mM, pH 7.4).

A similarly prepared particle-containing hydrogel film was placed in a solution of **MV^{2+}-nap** and cytochrome c, both at 1 μM concentration, in Tris buffer to assess the mobility of the quencher in the presence of the protein. As shown in Figure 5.9, minimal quenching is observed, in contrast to the previous set of experiments. The presence of cytochrome c in the solution prevents **MV^{2+}-nap** from interacting with the encapsulated PPE-coated particles, indicating the protein may be adsorbing on the surface and forming a barrier against the lower molecular weight **MV^{2+}-nap**. The hindrance with protein adsorption is not desirable for quenching in complex biological environments, and should be addressed with different hydrogel

surfaces that prevent biofouling such as poly(ethylene glycol) or fluoropolymers. Light scattering or internal reflection infrared spectroscopy studies could examine if there is surface adsorption occurring with the proteins with candidate polymers.

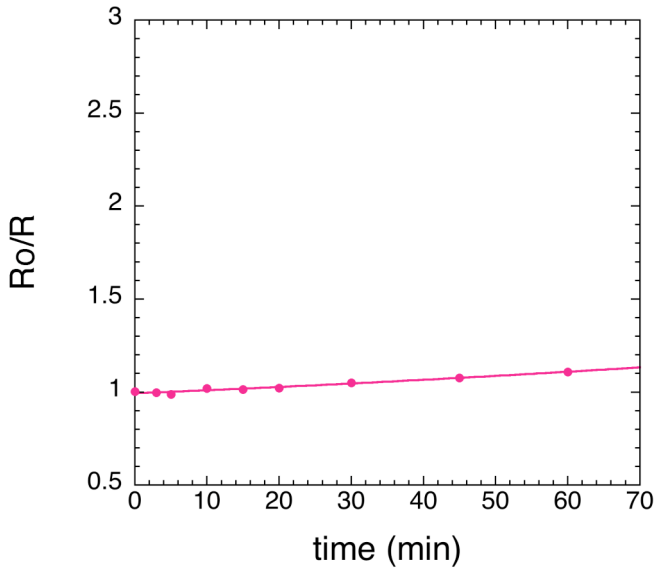

Figure 5.9. Response of a particle-containing hydrogel film to 1 μM concentrations of **MV^{2+}-nap** and cytochrome c in Tris buffer (20 mM, pH 7.4).

5.2.3 Factors that limit the quenching of particle-containing films

Several characteristics of the particle-containing film contribute to the slow response towards quenchers. The quenching kinetics is much different for the particles contained in the polymer gel versus in the particles in solution, which require less than 1 minute to reach a steady-state quenching response, even if the particles are homogeneously dispersed. The amide groups located within the gel interact with water very strongly with hydrogen bonding interactions, and the high water associated may exclude the **MV^{2+}-nap** from diffusing rapidly through the macromolecular network. The physical characteristics of the prepared film due to the geometrical constraints from the positioned glass slides and spacers are also responsible

for the decreased quenching observed. A gradient for absorption of quencher exists in the polymer gel, in which the particles at the surface are quenched at a much earlier time than the particles closest to the glass slide. The immobilization of the film on the glass slide eliminates an additional surface for active quenching. Thickness is a critical parameter, since it is inversely proportional to the diffusion coefficient. Decreasing the thickness may speed up the quenching rate significantly, since the films for these experiments were rather thick, prepared with 1 mm spacers. Furthermore, if the film dimension is closer to the particle dimension, the quencher potentially can access a larger fraction of incorporated particles. Future designs with incorporating active sensor elements within a hydrogel should keep these principles in mind for increasing the response time towards quenchers.

Reducing the crosslinker concentration can increase the macromolecular mesh size, leading to faster transport through the material. Assessing the particle-containing hydrogel films under different crosslinker concentrations was attempted to ascertain the relationship with quenching, but was unsuccessful due to lack of statistical reproducibility among samples under the same conditions. Although we had established a precise quantitative method for measuring the quenching response of PPE-coated particles (Chapter 3), the preparation of a hydrogel matrix to encapsulate the particles introduced error in the measurements. This effect is most likely attributed to the random network formed using the redox-initiated free radical polymerization method.[42] Cyclization and multiple crosslinks due to the large concentration of vinyl linkages, depicted in Figure 5.10, contributes to inhomogeneity within the material. The resultant films may vary only slightly in crosslinker density and distribution to produce significant differences in the quenching response. A more controllable method for encapsulating the particles is necessary to prepare quantitative sensors for monitoring fluorescence quenching with high specificity.

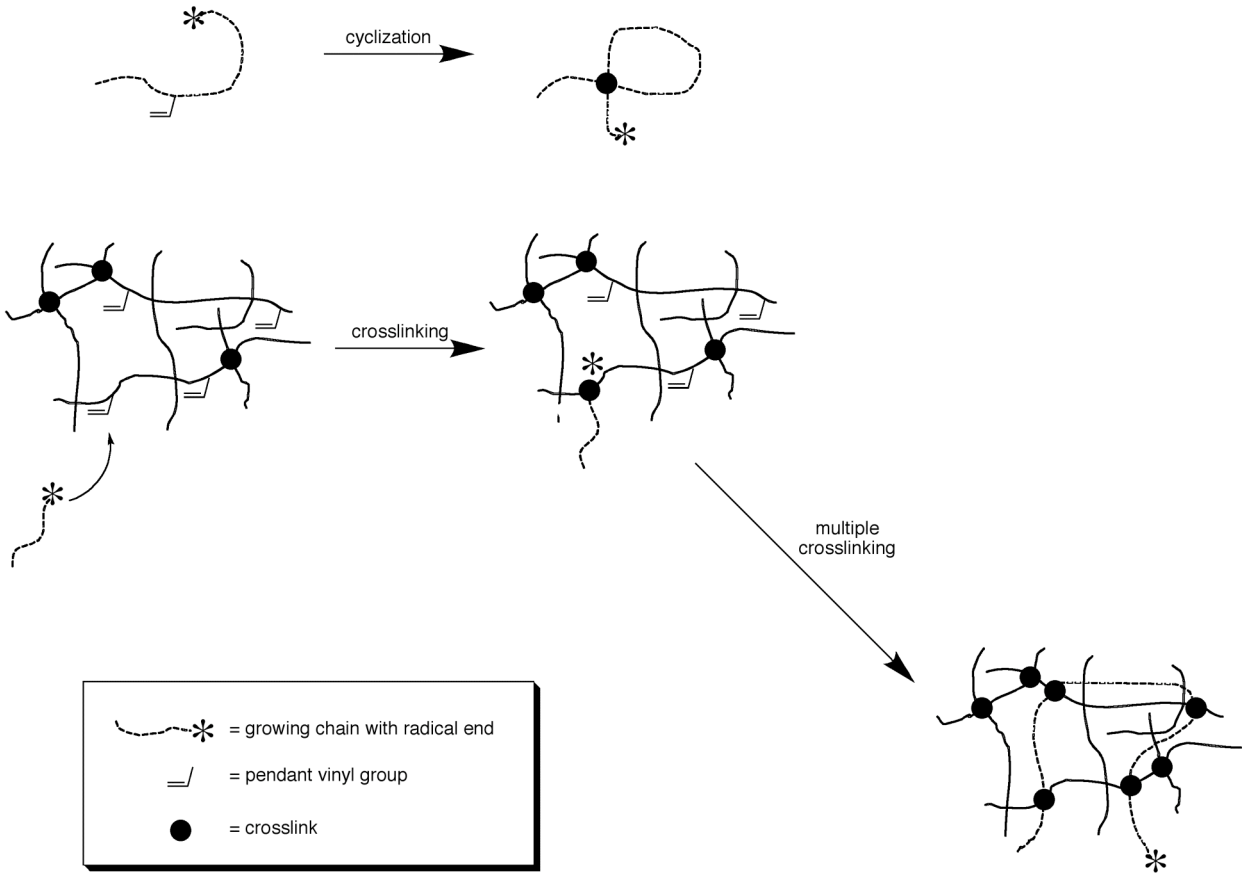

Figure 5.10. Schematic representation of cyclization and multiple crosslinking reactions in free-radical crosslinking copolymerization. Adapted from ref.[42]

5.3 Conclusions

We demonstrated that the interaction between cytochrome c and PPE-coated particles can be prevented by incorporating the particles within a crosslinked network of polyacrylamide. This principle can be extended to prevent interactions with other proteins, since cytochrome c is a relatively small protein. The prevention of surface biofouling is required to allow for the diffusion of the designed small molecule quenchers, such as **MV^{2+}-nap**, to the encapsulated PPE-coated particles. The response time of these bulk hydrogel films is not sufficient for practical biosensing applications, based on their method of preparation. We are pursuing more

controlled methods of polymerization to create encapsulated particles to address specificity, and this is shown in Chapter 6.

5.4 Experimental Section

Materials

Acrylamide (99+%, electrophoresis grade) and 3-aminopropyltrimethoxysilane (APTMS) were purchased from Alfa Aesar. *N,N'*-methylene-bisacrylamide (Bis, 99%, Sigma-Aldrich), glutaraldehyde (50 wt. % solution, Sigma-Aldrich), *N,N,N',N'*-tetramethylethylenediamine (TMEDA, Bio-Rad), cytochrome c (from bovine heart, ≥ 95%, Sigma-Aldrich), and lysozyme (from chicken egg white, ~95%, Sigma-Aldrich) were stored at 0ºC. Ammonium persulfate (APS) was purchased from EMD. Ammonia (27% in water (w/w)) was obtained from Mallinckrodt. **MV^{2+}-nap** was synthesized and generously provided by Dr. Guy D. Joly. All other chemicals were purchased from Sigma-Aldrich. Tris buffer (20 mM, pH 7.4) was freshly prepared from tris[hydroxymethyl]aminomethane (Sigma-Aldrich), adjusting the pH with 0.1 mM HCl or NaOH, and stored at 0ºC until use. All water used in experiments was obtained from a Millipore Milli-Q purification system. Glass slides and Teflon™ spacers (1.0 mm) were purchased from VWR.

Methods

Glass slide cleaning

A fresh solution of 2 : 1 (v/v) ammonia (27%) : hydrogen peroxide (30%) was prepared and added to a slide chamber loaded with glass slides for 20 minutes on a horizontal shaker (VWR) at 50 RPM. The slides were taken out of the cleaning solution, rinsed with water 3 times and transferred to a beaker with boiling water for 10 minutes. Another slide chamber with water

was loaded with the slides, and then sonicated for 20 minutes. The slides were removed, rinsed and placed in a beaker for the preparation of coating.

Glutaraldehyde-treated slides

In a plastic container, 5% (v/v) APTMS solution was prepared. The cleaned slides were sonicated in the solution for 20 minute, and then rinsed thoroughly with water to remove excess APTMS solution. The slides were then added to a freshly prepared 5% (v/v) glutaraldehyde in water, and shaken horizontally at 50 RPM. After 2 hours, the slides were rinsed with water, ethanol, and acetone before drying with nitrogen stream. All treated slides were then stored in a dry box until use.

Preparation of particle-containing hydrogel films

A 10% (w/v) solution of APS in water was freshly prepared. Acrylamide (30% (w/v) in water) and bis (2% (w/v) in water) were previously prepared and degassed with nitrogen for 30 minutes before polymerization. In a plastic centrifuge tube, solutions of acrylamide (100 μL) and bis (25 μL) were added, followed by addition of Tris buffer (5 μL) and APS (3 μL). The tube was vortexed for several seconds to mix. The PPE-coated Eu^{3+}-polystyrene microspheres (d = 0.2 μm), prepared as described in Chapter 3 and resuspended in Tris buffer, were added (100 μL) for a final particle concentration of 0.12%, and the tube was vortexed for complete mixing. TMEDA (0.5 μL) was added as the final step, before transferring quickly with syringe to two glass slides (one glutaraldehyde-treated, one untreated) separated with Teflon™ spacers and held together with binder clips. Gel formation occurred within 30 seconds, after which time the untreated slide was removed. The gel was subjected to thorough rinsing with water to remove residual monomers and catalysts before placed in a Petri dish with Tris buffer to equilibrate the film for subsequent quenching experiments.

Fluorescence quenching experiments

The equilibrated films were placed in a 2.5 cm × 1.0 cm × 4.5 cm *(L × W × H)* rectangular quartz cuvette and secured on the inside of one face with solvent-resistant tape as shown in Figure 5.6. All fluorescence measurements were made using front-face configuration on a Jobin Yvon SPEX Fluorolog-τ2 or -τ3 fluorometer. Tris buffer was added to record the initial fluorescence, and then removed and replaced with a fixed concentration (1 μM) of the specific quencher solution. Scans were then recorded at 10 timepoints, from the initial time of addition (t = 0 minutes) to 60 minutes after addition. Data was normalized according to the Eu^{3+} peak, and then plotted as the change in the ratio versus time to assess the kinetic behavior of the films.

5.5 References

(1) Thomas, S. W., III; Joly, G. D.; Swager, T. M. *Chem. Rev.* **2007**, *107*, 1339-1386.

(2) Wichterle, O.; Lím, D. *Nature* **1960**, *185*, 117-118.

(3) Nicolson, P. C.; Vogt, *J. Biomaterials* **2001**, *22*, 3273-3283.

(4) Kiyonaka, S.; Sada, K.; Yoshimura, I.; Shinkai, S.; Kato, N.; Hamachi, I. *Nat. Mater.* **2004**, *3*, 58-64.

(5) Elbert, D. L.; Hubbell, J. A. *Ann. Rev. of Mater. Sci.* **1996**, *26*, 365-394.

(6) Dagani, R. In *Chemical & Engineering News* 1997.

(7) Holtz, J. H.; Asher, S. A. *Nature* **1997**, *389*, 829-832.

(8) Weissman, J. M.; Sunkara, H. B.; Tse, A. S.; Asher, S. A. *Science* **1996**, *274*, 959-960.

(9) Ben-Moshe, M.; Alexeev, V. L.; Asher, S. A. *Anal. Chem.* **2006**, *78*, 5149-5157.

(10) Miyata, T.; Asami, N.; Uragami, T. *Nature* **1999**, *399*, 766-769.

(11) Qiu, Y.; Park, K. *Adv. Drug Deliv. Rev.* **2001**, *53*, 321-339.

(12) Miyata, T.; Uragami, T.; Nakamae, K. *Adv. Drug Deliv. Rev.* **2002**, *54*, 79-98.

(13) Russell, R. J.; Pishko, M. V.; Simonian, A. L.; Wild, J. R. *Anal. Chem.* **1999**, *71*, 4909-4912.

(14) Weidgans, B. M.; Krause, C.; Klimant, I.; Wolfbeis, O. S. *Analyst* **2004**, *129*, 645-650.

(15) Sheppard, N. F.; Lesho, M. J.; McNally, P. *Sens. Actuators, B* **1995**, *28*, 95-102.

(16) Zheng, Y.; Gattás-Asfura, K. M.; Li, C.; Andreopoulos, F. M.; Pham, S. M.; Leblanc, R. M. J. *Phys. Chem. B.* **2003**, *107*, 483-488.

(17) Kotte, H.; Grundig, B.; Vorlop, K. D.; Strehlitz, B.; Stottmeister, U. *Anal. Chem.* **1995**, *67*, 65-70.

(18) Suri, J. T.; Cordes, D. B.; Cappuccio, F. E.; Wessling, R. A.; Singaram, B. *Angew. Chem. Int. Ed.* **2003**, *42*, 5857-5859.

(19) Russell, R. J.; Pishko, M. V.; Gefrides, C. C.; McShane, M. J.; Cote, G. L. *Anal. Chem.* **1999**, *71*, 3126-3132.

(20) Brahim, S.; Narinesingh, D.; Guiseppi-Elie, A. *Biosens. Bioelectron.* **2002**, *17*, 53-59.

(21) Pishko, M. V.; Michael, A. C.; Heller, A. *Anal. Chem.* **1991**, *63*, 2268-2272.

(22) de Gennes, P. G. *Scaling Concepts in Polymer Physics;* Cornell University Press: Ithaca, NY, 1979.

(23) Amsden, B. *Macromolecules* **1998**, *31*, 8382-8395.

(24) Gehrke, S. H.; Fisher, J. P.; Palasis, M.; Lund, M. E. *Ann. N.Y. Acad. Sci.* **1997**, *831*, 179-207.

(25) Kim, I.-B.; Dunkhorst, A.; Bunz, U. H. F. *Langmuir* **2005**, *21*, 7985-7989.

(26) George, A.; Wilson, W. W.; *Acta Cryst*. **1994**, *D50*, 361-365.

(27) Valette, P.; Thomas, M.; Déjardin, P. *Biomaterials* **1999**, *20*, 1621-1634.

(28) Canfield, R. E., *J. Biol. Chem.* **1963**, *238*, 2698-2707.

(29) Wetter, L. R.; Deutsch, H. F. *J. Biol. Chem.* **1951**, *192*, 237-242.

(30) *Handbook of Biochemistry*; CRC Press, 1968.

(31) Malmgren, L.; Olsson, Y.; Olsson, T.; Kristensson, K. *Brain Research* **1978**, *153*, 477-493.

(32) Ichinose, I.; Takaki, R.; Kuroiwa, K.; Kunitake, T. *Langmuir* **2003** *19*, 3883-3888.

(33) Levine, R. L. *Clin. Chem.* **1977**, *23*, 2292-2301.

(34) Stemp, E. D. A.; Hoffman, B. M.; *Biochem.* **1993**, *32*, 10848-10865.

(35) Raymond, S.; Weintraub, L. *Science* **1959**, *139*, 711.

(36) Chrambach, A.; Rodbard, D. *Science* **1971**, *172*, 440-451.

(37) Barth, H. G.; Boyes, B. E.; Jackson, C. *Anal. Chem.* **1998**, *70*, 251R-278R.

(38) Gupta, M. K.; Bansil, R. *Polym. Prep.* **1981**, *22*, 375-376.

(39) Feng, X. D.; Guo, X. Q.; Qiu, K. Y. *Makromol. Chem.* **1988**, *189*, 77-83.

(40) Ghosh, N. N.; Gupta, G. N.; Mandal, B. M. *Makromol. Chem.* **1986**, *187*, 2097-2102.

(41) Tanaka, T. *Sci. Am.* **1981**, *224*, 124-138.

(42) Orakdogen, M.; Okay, O. J. *Appl. Polym. Sci.* **2007**, *103*, 3228-3237.

(43) Nguyen, K. T.; West, J. L. *Biomaterials* **2002**, *23*, 4307-4314.

Appendix for Chapter 5:

Hydrogel Diffusion

Appendix 5.1. Diffusion through hydrogels: A complex situation

To understand the permeability of the hydrogel, one should understand how the presence of the crosslinked network affects the transport and thermodynamic properties of the system. Diffusion of a species *"i"* can be described as a proportionality constant between the flux *"j"* and a concentration gradient *(dC_i/dz)*, for diffusion along the z-coordinate, known as Fick's First Law:

$$j_i = -D_i\left(\frac{dC_i}{dz}\right)$$

The value of D_i depends primarily on molecular weight for solutes in water, and can range from values on the order of 10^{-5} cm^2/s for simple organic compounds and dissolved gases to values on the order of 10^{-7} cm^2/s for proteins.

Permeability *(P_i)* of a solute *i* is most typically defined as the product of this transport property, the diffusion coefficient D_i, and a thermodynamic property, the partition coefficient K_i, and can be related in the following equation for steady state flux of solute across a membrane from a donor phase to a receptor phase:

$$j_i = \frac{K_i D_i}{L}\left(C_{di} - C_{ri}\right)$$

or:

$$j_i = \frac{P_i}{L}\left(C_{di} - C_{ri}\right)$$

where: j_i = flux of solute *i* (mol/cm^2s);

C_{di} = concentration of solute *i* in donor phase (mol/cm^3);

C_{ri} = concentration of solute *i* in receptor phase (mol/cm^3);

C_{gi} = concentration of solute *i* in the gel membrane (mol/cm^3);

C_{si} = concentration of solute *i* in solution (mol/cm^3);

D_i = diffusion coefficient of solute *i* (cm^2/s);

K_i = partition coefficient of solute *i* (dimensionless);

= C_{gi}/C_{ri}

P_i = permeability of solute *i* (cm^2/s);

L = membrane thickness (cm)

The diffusive motion of molecules in gels is inherently reduced versus the mobility in free solution.[1] Factors that contribute to the reduction in mobility can be chemical in nature, in which there are attractive forces between the solute and gel, or physical, which include size exclusion, hydrodynamics, and solvent structuring.[2] Size exclusion is more straightforward to understand, since it is caused by the actual crosslinks. Hydrodynamic effects can be understood by the solvation of the solute species and the frictional drag associated with the resistance of fluid flow in the proximity of the polymer-solvent interface. Water can also thought to be bound to the polymer, known as "solvent structuring,"[3] which limits the transport of solutes in the gel, versus the bulk water which is highly mobile and solvates the solutes. Careful investigation of these causes, however, is limited due to the various factors affecting diffusion that cannot be directly isolated.[2] Network inhomogeneity also needs to be considered.

Understanding how well the solute "partitions", or preferentially associates with one phase, is characterized by the partition coefficient, and here we have more control in the design of hydrogels with desired permeability. The partition coefficient is inherently dependent on the chemical properties of both the solute and the gel as well as the physical properties, and can be a combination of electrostatic, hydrophobic, biospecific, size, and conformational effects,[2] and can either increase or decrease, in contrast to the apparent decrease dictated by the diffusion coefficient. The use of hydrophobic interactions to associate the quencher with the conjugated polymer can be advantageous for faster permeability in aqueous solution, due to the tendency

of nonpolar solutes to adhere to each other in this environment.[4] Ionic contributions also need to be considered, as typically the quenchers are ionic species to provide solubility characteristics. When the solutes have the opposite charge as the polymer gel, ionic exchange can occur to yield a very high partition coefficient, or if they are of the same charge, the solutes may be excluded from the gel by Donnan ion exclusion, resulting in a partition coefficient less than one.[2]

Appendix 5.2. References

(1) Tong, J.; Anderson, J. L. *Biophys. J.* **1996**, *70*, 1505-1513.

(2) Gehrke, S. H.; Fisher, J. P.; Palasis, M.; Lund, M. E. *Ann. N.Y. Acad. Sci.* **1997**, *831*, 179-207.

(3) Brown, W.; Chitumbo, K. *J. Chem. Soc. Farad. Trans. I* **1975**, *71*, 1-11.

(4) Kauzmann, W. *Adv. Protein Chem.* **1959**, *14*, 1-63.

Chapter 6:

Particle Grafting via Atom Transfer Radical Polymerization (ATRP)

6.1 Introduction

The goal of this chapter is to demonstrate the feasibility of grafting polymers from poly(phenylene ethynylene) (PPE)-coated particles via atom transfer radical polymerization (ATRP). With ATRP to control the architecture and functionality of the grafted polymers, we can expect to obtain tunable materials for our biosensing applications. We showed in Chapter 5 that by incorporating the particles within a hydrogel matrix, a more specific response could be evoked. The grafting of polymers via ATRP can thus serve to encapsulate individual particles and prevent nonspecific quenching in a similar manner. With the choice of functional monomers, we can conjugate biomolecules or other small molecules (dyes and/or quenchers) to the particles and integrate the biosensor components. We can begin to think of other interesting sensory schemes that can be developed with varying nanostructures, such as those made with grafted (random, statistical, and block) copolymers.

6.1.1 Surface-initated atom transfer radical polymerization (ATRP)

ATRP[1,2] has developed as a widely used method of creating interesting morphologies due to the controlled nature of the polymerization to yield polymers with low polydispersity that can be further functionalized or polymerized, and its compatibility with a variety of functionalized monomers. Since the reports of Sawamoto for the controlled polymerization of methyl methacrylate[3] and Matyjaszewski for the controlled polymerization of styrene,[4] the field has exploded into the applications of ATRP to tailor the synthesis of polymers in a wide variety of environments.

The mechanism of ATRP[4] is shown in Fig. 6.1. Radical species are generated through a reversible redox process catalyzed by a transition metal complex (M_t^n–Y/Ligand, where Y may be another ligand or counterion) which undergoes a one-electron oxidation with the concomitant

abstraction of a (pseudo)halogen atom, X, from a dormant species, R–X. The process occurs with a rate constant of activation (k_{act}) and a rate constant of deactivation (k_{deact}). The polymer chain grows similarly to other radical polymerization methods, with the addition of the intermediate radical to the monomer at a rate constant of propagation (k_p). Termination (k_t) also occurs through radical coupling or disproportionation, but in a successful ATRP reaction no more than a few percent of polymer chains are terminated. This process also generates the metal complex at a higher oxidation state (X–M_t^{n+1}–Y/Ligand) as persistent radicals to reduce the stationary concentration of radicals and therefore minimize the contribution to termination.[5] Fast initiation and rapid reversible deactivation with a limited amount of termination yields uniform growing polymer chains and thus defines a successful ATRP reaction.

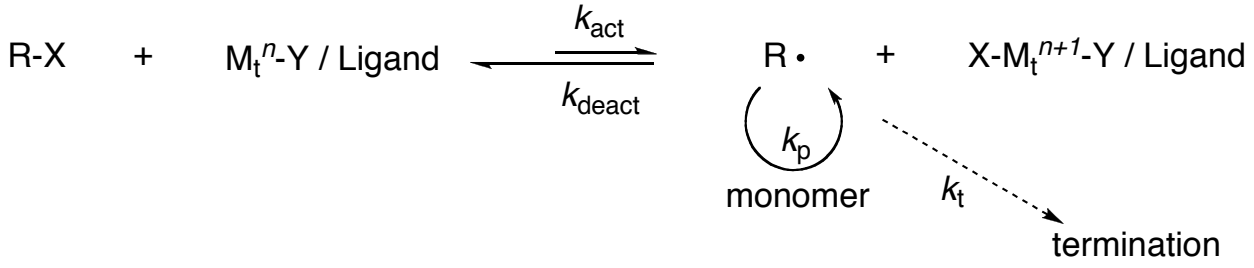

Figure 6.1. General mechanism for transition metal-catalyzed ATRP. Adapted from ref.[2]

ATRP allows for the polymer chains to be grown at a controllable rate at a surface. In principle, polymer brushes with relatively narrow molecular weight distribution can be obtained if the initiation is rapid.[6] The surface-initiated polymerization is a “grafting from” approach, generally considered to be more effective in achieving greater film thicknesses and densities versus “grafting to” methods, where preformed polymer chains are attached to a surface.[6]

One of the earliest application of surface-initiated ATRP was reported for the modification of silicon wafers with PMMA brushes.[7,8] Since then, a variety of substrates have been employed and those of particular interest in this thesis and of colloidal nature have been examples in grafting from silica particles,[9-16] polymer particles,[17-21] gold nanoparticles,[22,23] quantum dots,[24] magnetic nanoparticles,[25] carbon black,[26,27] and carbon nanotubes.[28-30] Some applications for which surface-initiated ATRP modification of colloidal substrates has been used have included chromatographic or solid-phase synthesis supports,[13,19] dispersion,[31] photochromism,[32] thermosensitivity,[10] bioconjugation,[33] and antibacterial properties.[34]

6.1.2 Layer-by-layer assembly for surface-initiated ATRP

For "grafting from" synthesis, the substrate surface must be modified with the initiator functionality for the particular synthesis employed. We propose to use the method of layer-by-layer assembly to create initiator-functionalized particles for ATRP.[35-37] Although there are numerous approaches to create initiators through self-assembled monolayers[10,32] or direct chemical modification of the surface,[11-13,21,31,34,38,39] the advantage of polyelectrolyte initiators is that uniform films can be created via electrostatic layer-by-layer assembly onto a surface that bears the opposite charge (see Chapter 2), allowing for a variety of substrates that can be modified via ATRP grafting. Various post-polymerization reactions are also possible with the functional groups on the polyelectrolyte to facilitate the synthesis of the macroinitiator. Advincula and coworkers[35] recently reported the use of a modified poly(acrylic acid) to create grafts of poly(methyl methacrylate) on 400 nm polystyrene particles. The Armes group[36,37] also reported the synthesis of a polyelectrolyte initiator for the *in situ* adsorption onto silica nanoparticles and subsequent ATRP, utilizing a variety of monomers to increase the particle dispersion properties.

We have synthesized an anionic PPE (**P1**) to assemble LbL films, as shown in preceding chapters. The post-polymerization reaction for converting **P1** to a PPE macroinitiator, **P2**, is shown in Figure 6.2. **P2** can then be LbL assembled onto silica particles (d = 0.6 μm) after initial adsorption of a cationic polyelectrolyte such as poly(ethyleneimine) (PEI) to create initiator-functionalized particles. Grafting via ATRP can be carried out from the surfaces of the **P2**-coated particles with functionalized acrylates (Figure 6.3), and in this chapter we will investigate the surface-initiated ATRP of glycidyl methacrylate (GMA) and 2-hydroxyethyl methacrylate (HEMA). The reactive epoxide repeat unit of p(GMA) has been used for post-polymerization modification and surface conjugation to biomolecules.[40,41] HEMA is a nonionic and hydrophilic monomer used frequently in biomedical applications. Both have been utilized as chromatographic supports as well, due to their strong resistance to hydrolysis, low degree of swelling in water and organic solvents, and the high density of hydroxyl and diol groups.[42]

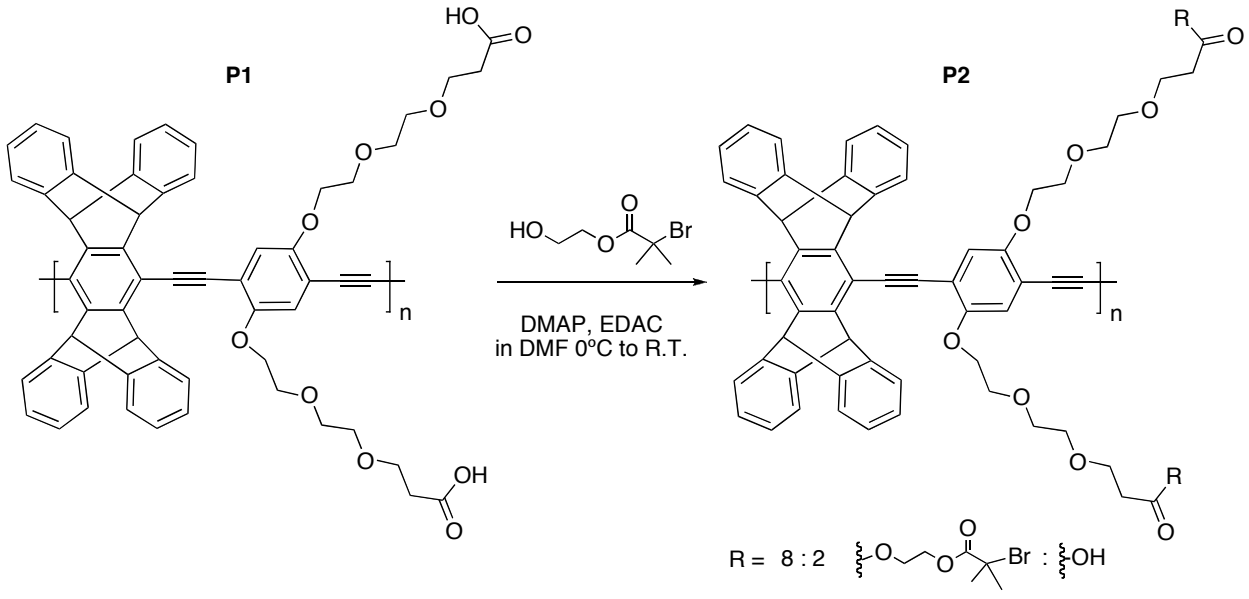

Figure 6.2. Synthesis of PPE macroinitiator **P2** from reaction of **P1** with 2-hydroxyethyl 2-bromo-2-methylpropionate (**1**).

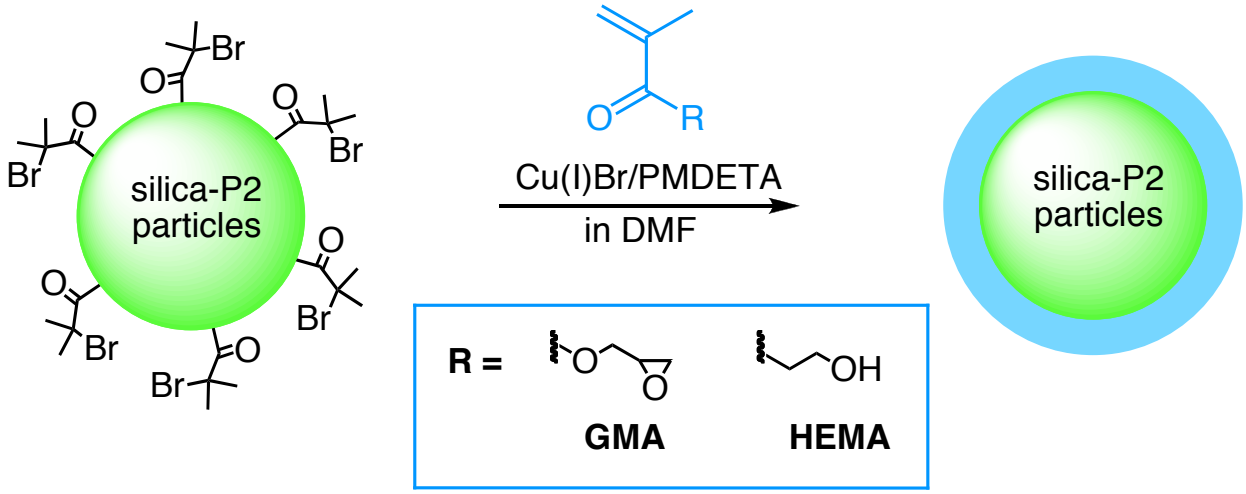

Figure 6.3. ATRP grafting of glycidyl methacrylate (GMA) and 2-hydroxyethyl methacrylate (HEMA) from **P2**-coated particles.

6.2 Results and Discussion

6.2.1 Synthesis and characterization of PPE macroinitiator

The choice of ATRP initiators is dependent on the monomers being used. In general, α-bromopropionates are good initiators for the ATRP of acrylates due to their structural resemblance[2] and have been used extensively in the ATRP of methacrylates. 2-hydroxyethyl 2-bromo-2-methylpropionate (**1**) was prepared according to a literature procedure[43] with the reaction of ethylene glycol and slow addition of 2-bromoisobutyryl bromide. Post-polymerization esterification reaction of **P1** with 2-hydroxyethyl 2-bromo-2-methylpropionate with catalytic DMAP and EDAC in DMF forms **P2**, with an 80% inclusion of initiator groups indicated by the ^{1}H NMR integration ratio of the bridgehead protons of the pentiptycene units and the methyl protons of the bromoinitiator (Chapter 6 Appendix). The molecular weight of **P1** cannot be ascertained directly, due to its ionic character and inability to elute from the GPC. **P2**, however, can be eluted, and based on PS standard, a molecular weight of $M_n = 6.5 \times 10^4$ g/mol (PDI =

1.5) was obtained by GPC analysis. Grazing angle attenuated total internal reflectance - Fourier transform infrared spectroscopy (GATR-FTIR) measurements also confirm the transformation of **P1** to **P2** (Figure 6.4), with the 1730 cm^{-1} stretch corresponding to the ester carbonyl groups in **P2** and the reduction in the O–H bends (3200–3500 cm^{-1}) from the $–CO_2H$ groups. Both polymers have the same spectroscopic behavior in DMF solution, indicating no significant chemical changes in the conformation after conversion of 80% of the carboxylic acid groups to initiator groups (Figure 6.5).

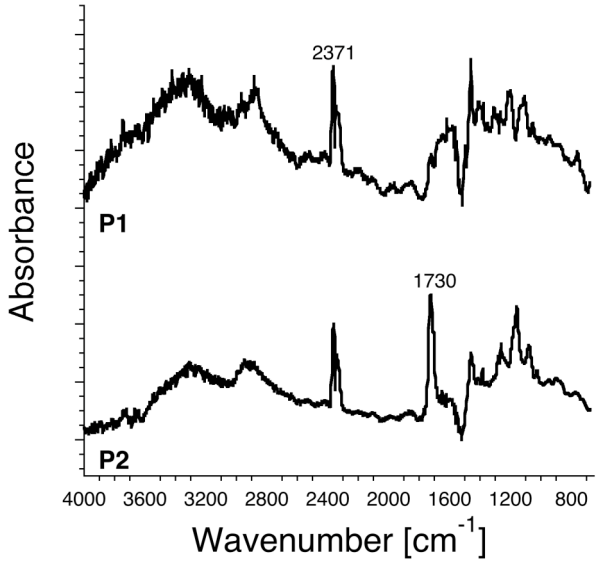

Figure 6.4. GATR-FTIR spectra of **P1** and **P2**.

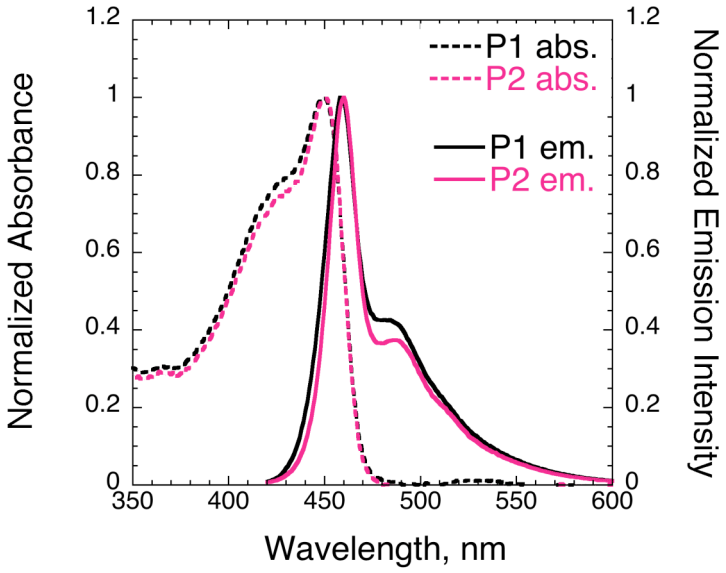

Figure 6.5. Normalized solution absorption and emission spectra of **P1** and **P2** in DMF.

6.2.2 Layer-by-layer adsorption of PPE macroinitiator onto silica particles

Adsorption via layer-by-layer assembly was first monitored on glass substrates with UV/Vis absorbance spectroscopy to observe a linear buildup of **P2** (alternating with PEI), consistent with the behavior of other structurally similar PPE polyelectrolytes synthesized in our group (see Chapters 2 and 3). In spite of **P2** having less charge density than the polymers tested in Chapter 3, the optical density of 4-bilayer films composed of **P2** (O.D. = 0.13) is much more similar to that of **P1** (O.D. = 0.17) than the macrocycle-incorporated anionic PPE (O.D. = 0.1) and the control polymer (O.D. = 0.055) (see Chapter 3 for absorbance spectra), indicating the regularity of the copolymer and the resultant material that the post-polymerization modification produces.

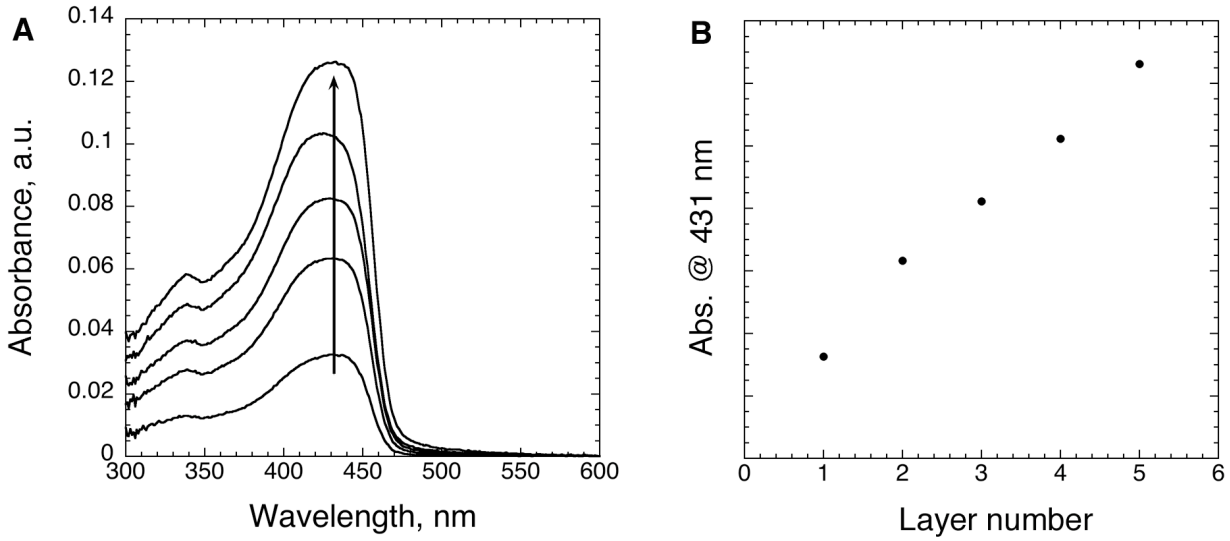

Figure 6.6. (A) UV/Vis absorption spectra of **P2** adsorption (alternating with PEI) on glass slides (arrow indicates increasing number of bilayers); (B) Peak absorption at 431 nm versus number of **P2** layers.

Coating on silica particles (d = 0.6 μm) from a DMF solution of **P2**, after initial adsorption of PEI, was achieved using the procedure for depositing polyelectrolytes described in Chapter 2 and Chapter 3 with 15-minute adsorption times. Confocal laser scanning microscopy (Figure 6.7 (a)) confirms the fluorescence of the **P2**-coated particles. The fluorescence image shows the dispersion of the particles in solvent, and the image reflects the movement of the particles while being observed. Transmission electron microscopy (TEM) images of dried deposited particles confirm the non-aggregating behavior of the **P2**-coated particles and the uniformity of the films (Figure 6.7).

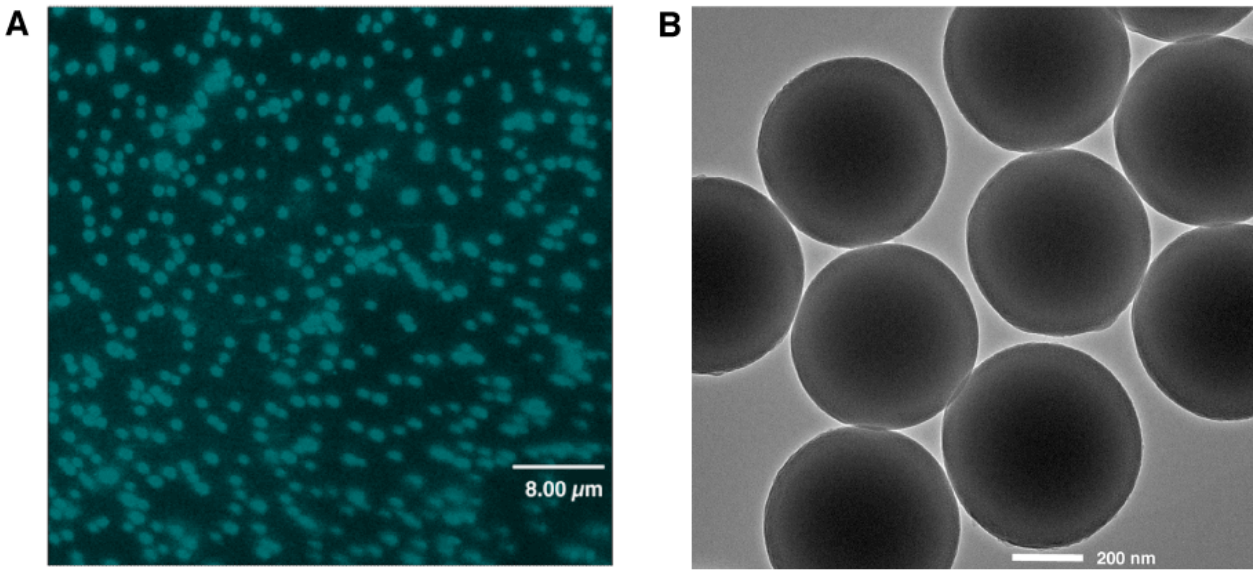

Figure 6.7. (A) Confocal and (B) TEM microscopy of **P2**-coated particles.

6.2.3 Surface-initiated ATRP grafting from PPE-coated particles

The **P2**-coated particles were dispersed in DMF, a good solvent for solubilizing the initiator groups and for conducting ATRP of methacrylates.[44] We chose GMA as a suitable monomer for grafting because of the versatility of direct coupling reactions afforded with the reactive epoxide side groups and the relatively high reactivity of GMA for ATRP compared to other methacrylates.[19,45] The reaction with GMA was optimized using a Cu(I)Br/PMDETA catalyst system at 50ºC for 5, 10, and 18 hours in air-free conditions. The particles were recovered after the reaction with repeated centrifugation and sonication in dichloromethane to remove residual monomer and catalyst. It is critical to remove all the catalyst, since the presence of copper quenches the fluorescence of the PPE. Complete copper removal can be achieved with a wash of 1 M NH_4OH solution due to the ability of ammonia to act as a ligand for the copper (II) salts. Since the treatment with NH_4OH also opens the epoxide ring, the wash

step was carried out as a final step after conjugation reactions. The resultant particles grafted with P(GMA) are more difficult to disperse and gel-like when dried.

The morphology was examined by TEM, and the images in Figure 6.8 show a clear modification of the surface after reaction for 5 hours. The particle coatings are rather rough and not as smooth as observed for the silica-**P2** initiator particles. At longer times (10 hours), free polymer also begins to form, and even encapsulates aggregates of particles (18 hours). The presence of clumped particles, especially at long reaction times, and the difficulty in dispersing the particles even after sonication treatment leads us to the conclusion that the particles are aggregated with the grafting of P(GMA). The presence of free polymer in solution may be attributed to the mechanical breakup of the grafted polymers with repeated sonication steps.

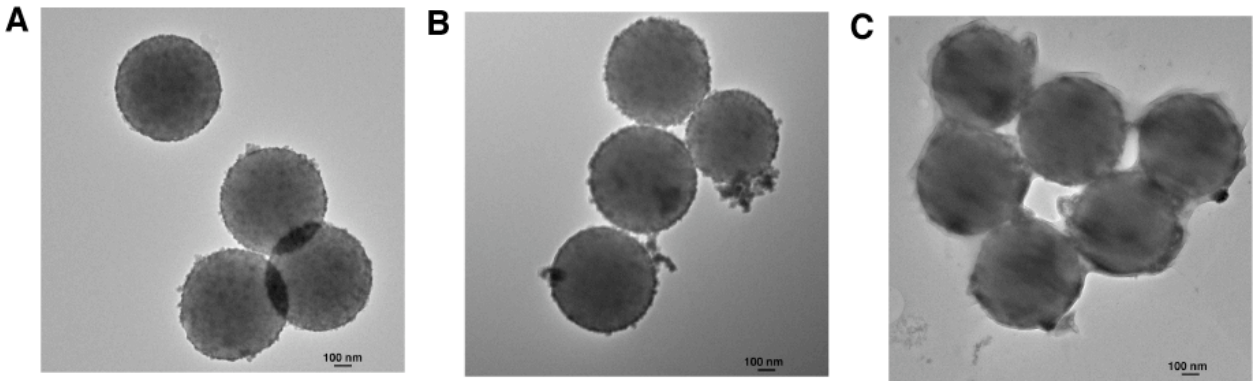

Figure 6.8. TEM images of **P2**-coated particles with GMA at (A) 5, (B) 10, and (C) 18 hours reaction time at 50ºC.

The relative amount of grafted P(GMA) can be examined with thermogravimetric analysis (TGA). Figure 6.9 shows the weight retention after heating the samples from 30ºC to 600ºC under nitrogen. TGA was not conducted on the sample reacted for 18 hours, due to the large amount of free polymer and the presence of aggregation indicated from the TEM images. The initial **P2**-coated particles (Figure 6.9 (a)) show no significant decomposition, but with the

grafted **P2**-coated particles (Figure 6.9 (b & c)) there is a clear mass loss in the range of 250–300ºC, indicating the decomposition of P(GMA). At time = 10 hours (Figure 6.9 (c)), the mass loss is significant in comparison to the initial **P2**-coated particles (Figure 6.9 (a)).

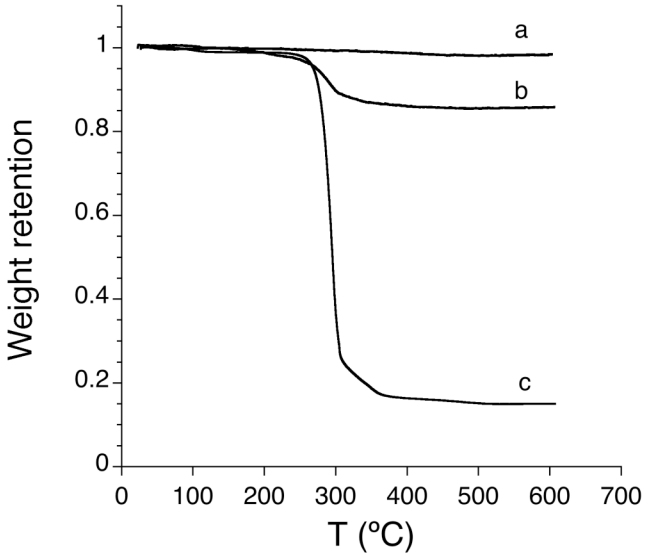

Figure 6.9. TGA curves of (a) silica-**P2**-initiator particles and silica-**P2**-P(GMA) particles after (b) 5 hours and (c) 10 hours reaction times.

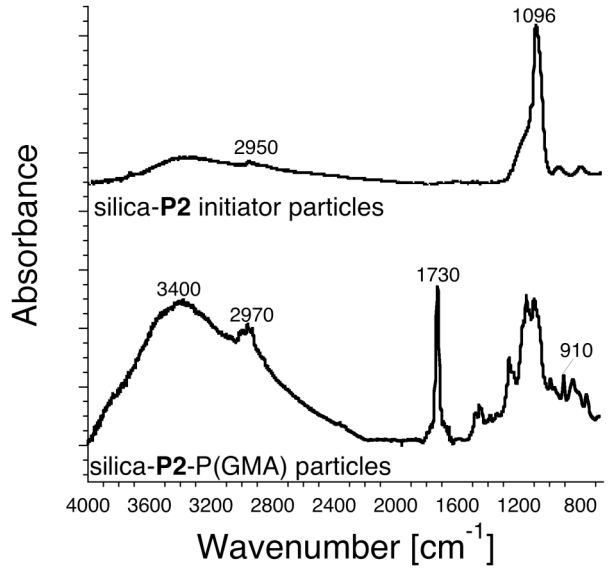

Figure 6.10. GATR-FTIR of the silica-**P2**-initiator particles and silica-**P2**-P(GMA) particles (10 hours reaction time).

GATR-FTIR also confirms P(GMA) on the surface of the particles (Figure 6.10). The absorption peak at 1096 cm^{-1} of the silica-**P2** initiator particles is attributed to the silanol (Si–OH) stretch, and is quite dominant due to the relatively thin bilayer of PEI/**P2** adsorbed on the surface. **P2** is not particularly IR active when coated on the silica particles due to the relative ratio of the two materials; however, a small alkyl C–H stretch from **P2** can be observed near 2950 cm^{-1}. Upon reaction with GMA for 10 hours, new peaks are observed at 1730 cm^{-1} and 910 cm^{-1} corresponding to carbonyl and epoxide groups, and at 2970 cm^{-1} attributed to the methylene groups of the grafted P(GMA). Rinsing with 1 M NH_4OH removes the copper catalyst but also opens the ring through ammonolysis, generating primary amines and –OH groups (broad peak at 3400 cm^{-1}) on the grafted particles. It will be necessary for further desired reactions with the epoxide groups to be conducted prior to rinsing with 1 M NH_4OH and removal of the catalyst.

The resultant silica-**P2**-P(GMA) particles are not completely dispersable in organic solvents, and this is most likely attributed to the hydrophobic properties of the P(GMA) layer. Under similar conditions, we proceeded with grafting of HEMA from the **P2**-coated particles. HEMA is a hydrophilic methacrylate monomer, but a relatively less reactive monomer than GMA, and so a longer reaction time (15 hours) at 75ºC was necessary to achieve grafting.

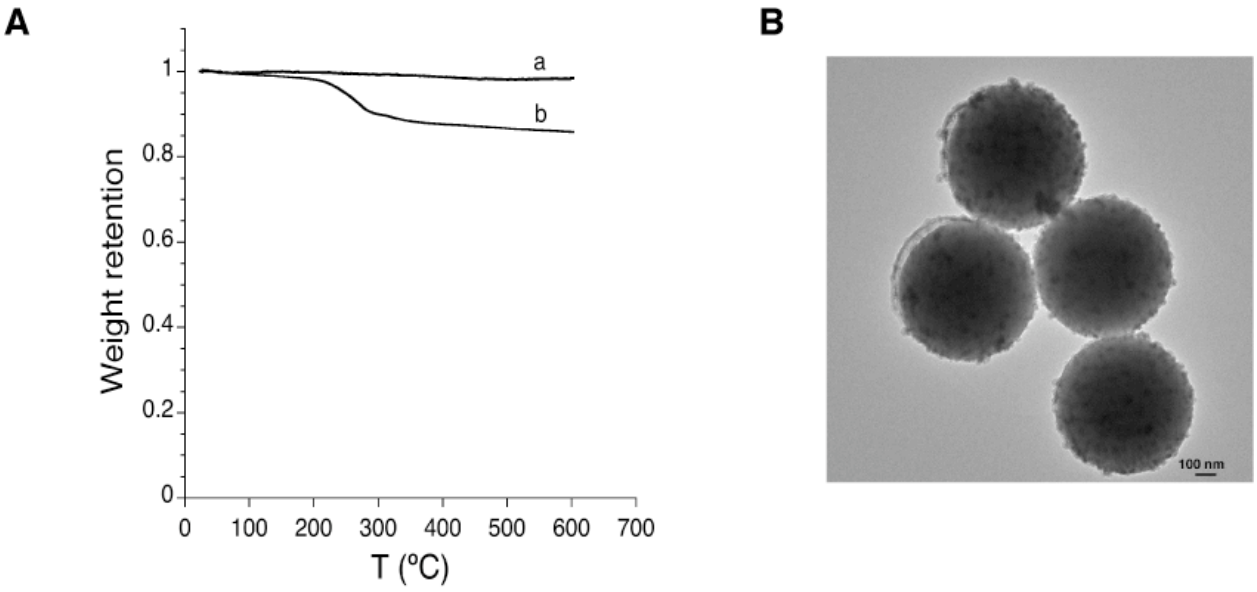

Figure 6.11. (A) TGA curve of (a) silica-**P2**-initiator particles and (b) silica-**P2**-P(HEMA) particles and (B) TEM image of silica-**P2**-P(HEMA) particles.

Figure 6.11 shows the TGA curve and the TEM morphology of the silica-**P2**-P(HEMA) particles. The 15% mass loss for the particles is comparable to that of the silica-**P2**-P(GMA) after 5 hours reaction time. These particles can be easily dispersed in both organic solvents and aqueous buffers, in contrast to the silica-**P2**-P(GMA) due to the hydrophilicity of the grafted P(HEMA).

In order to impart solubility and also have functionality for further conjugation or crosslinking reactions, copolymers of GMA and HEMA were grafted from the **P2**-coated particle surface. A relative monomer molar ratio of 0.25 : 0.75 GMA : HEMA was used in the polymerization. It should be noted that since GMA has a higher reactivity than HEMA,[19] the actual ratio is most likely higher in GMA content. Due to the content of HEMA, a longer reaction time (20 hours at 50°C) was necessary with the same catalyst system. The resulting silica-**P2**-P(HEMA-co-GMA) particles are similar to the silica-**P2**-P(HEMA) particles in their

dispersion ability. The mass loss as measured by TGA (Figure 6.12 (A-b)) is 20%, slightly larger than that of the grafted homopolymers. The increased amount of material is most likely attributed to the longer reaction time. Two inflection points can be observed from the TGA trace of (Figure 6.12 (A-b)), and could be due to the subtle difference in decomposition temperatures of P(GMA) and P(HEMA). The TEM image in Figure 6.12 (B) confirms the grafting of the copolymer from the particle surface, with similar morphology as the particles grafted with the homopolymers.

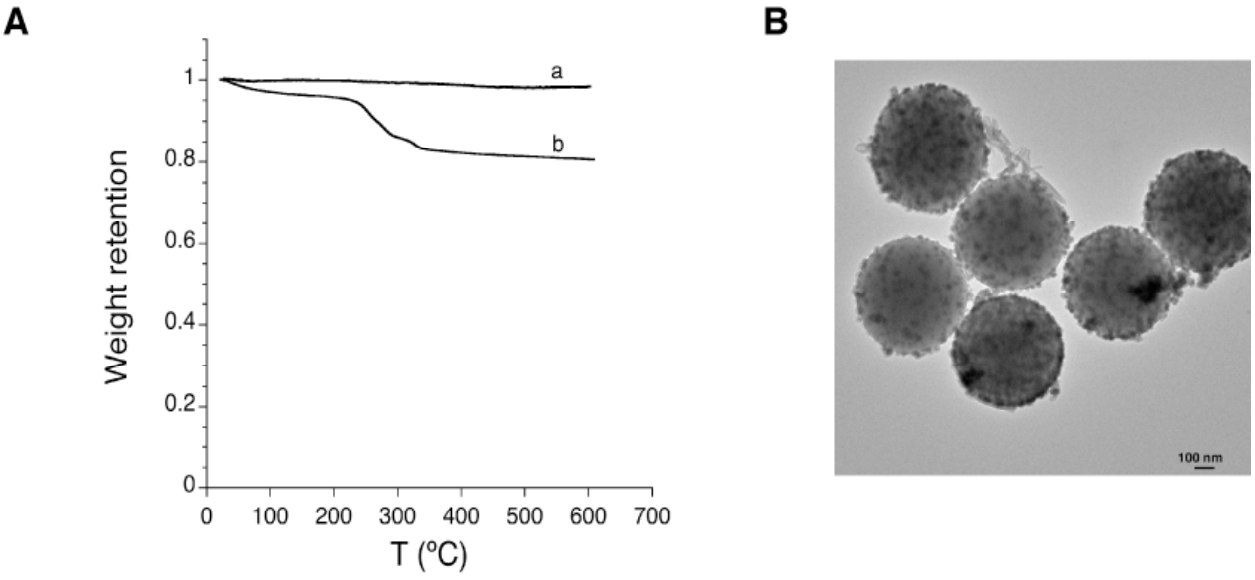

Figure 6.12. (A) TGA curve of (a) silica-**P2**-initiator particles and (b) silica-**P2**-P(HEMA-co-GMA) particles and (B) TEM image of silica-**P2**-P(HEMA-co-GMA) particles.

Table 6.1 summarizes the various reaction conditions in regards to mass increase calculated from TGA and particle diameter, compared to the initiator particles. Particle diameter was measured from 10 different particles using ImageJ, an image analysis software program obtained from the National Institute for Health.[46] The mass increase for the silica-**P2**-P(HEMA-co-GMA) is the largest of the three grafting conditions, although not significantly greater than

that of the homopolymer grafts. Statistically, the mean diameters of all the grafted particles are similar and are larger than the mean diameter measured of the silica-**P2** initiator particles. The estimated mean graft length from image analysis is 30 nm, as compared from the mean radius of the three grafting conditions minus the mean radius of the initiator particles. The calculated length of the grafts is similar to other reports of polymer grafting of particles using ATRP.[35] Dynamic light scattering of these particles could also measure the increase in diameter upon polymer grafting, but was not conducted due to the level of aggregation in solution observed with confocal microscopy. The volume calculated from the particle diameter increases by 40% after grafting, much larger than the mass increase (15-20%), indicating the roughness of this grafted layer.

particles	Mass increase (%)	Mean diameter (μm)
Si-P2	2	0.57 ± 0.03
Si-P2-P(GMA): 5 hr. rxn.	15	0.64 ± 0.01
Si-P2-P(HEMA)	15	0.64 ± 0.03
Si-P2-P(HEMA-co-GMA)	20	0.63 ± 0.02

Table 6.1. Mass increase (%) and mean diameter (μm) after particle surface-initiated ATRP of grafts.

6.2.5 Biofunctionalization of polymer-grafted PPE particles

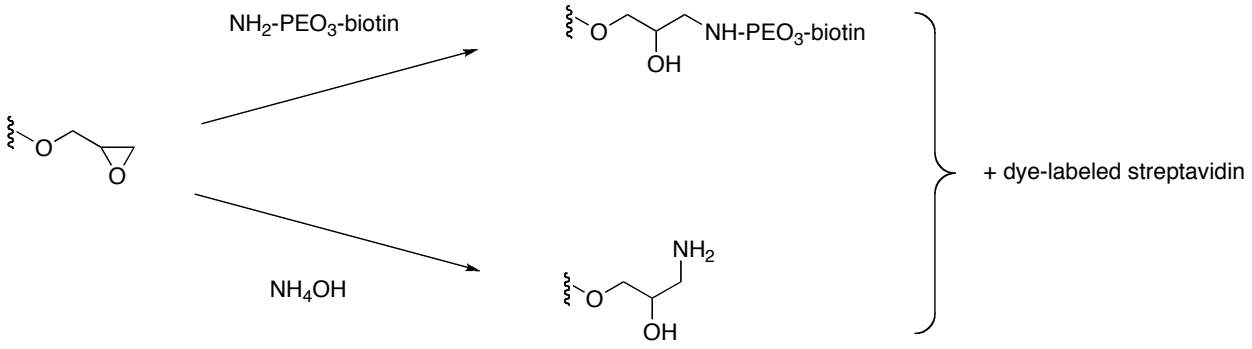

Figure 6.13. Reaction of grafted epoxide groups for biotinylated and unbiotinylated particles for assay with dye-labeled streptavidin.

To investigate further conjugation onto the polymer-grafted particles, we chose a model biological system, the streptavidin-biotin interaction,[47] commonly used in the development of biological assays due to the large free energy of association (K_{assoc} ~10^{15} M^{-1}) with the non-covalent tetrameric binding and the stability over a wide range of temperature and pH.[48,49] The dried silica-**P2**-P(HEMA-co-GMA) particles were resuspended in ethanol and reacted in neutral conditions with an amine-PEO_3-biotin at room temperature for 20 hours. After washing excess reagent and treating with 1 M NH_4OH to remove residual catalyst and quench any unreacted epoxide groups, the particles were assayed for their ability to bind to Texas Red®-labeled streptavidin. As a control, silica-**P2**-P(HEMA-co-GMA) particles treated with 1 M NH_4OH were also tested (Figure 6.13). After incubation with the dye-labeled streptavidin for 1 hour, the particles treated with amine-PEO_3-biotin became dark red and the untreated particles showed no color change. Excitation at 364 nm and 543 nm with confocal laser scanning microscopy,

respective wavelengths for **P2** and the dye, confirmed the specific binding of Texas Red®-labeled streptavidin to the treated particles (Figure 6.14). Spectral information was obtained with the individual excitation wavelengths by scanning the images (xyλ scan) across the specified wavelength range. The peak that arises at 612 nm with λ_{ex} = 364 nm could also be attributed to energy transfer between the PPE and Texas Red®,[50] although it is difficult to quantify this behavior due to the broad overlapping adsorption peak of the PPE. The particles, while readily dispersable, still display aggregation behavior, even in suspension. Further investigation with ATRP grafting of other hydrophilic or ionic monomers may yield particles that are less susceptible to aggregation.

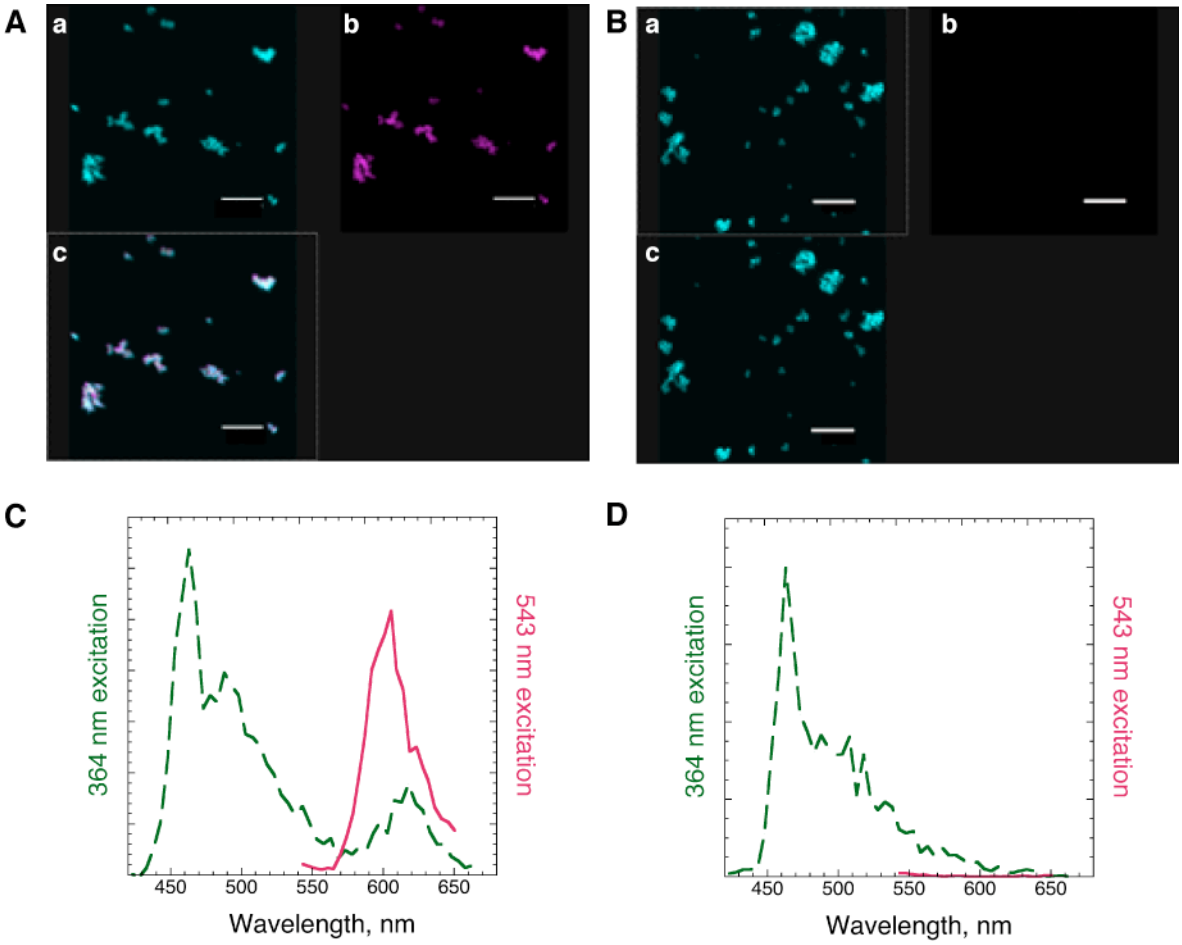

Figure 6.14. Confocal images of (A) biotinylated silica-**P2**-P(HEMA-co-GMA) particles and (B) control particles with PMT channels at (a) 440–480 nm and (b) 580–620 nm. Image (c) is overlap of (a) & (b). Scale bar corresponds to 8 μm. Corresponding spectra (C & D) taken at specified excitation wavelength using a xyλ scan.

6.2.6 Polymer-grafted PPE particles as particle sensors

The ability to bind streptavidin specifically is a step forward for translating the grafted particles into the particle sensors described in Chapter 1. Current work is in collaboration with Jeewoo Lim, a graduate student in the Swager Group, and Dr. Filip Swirski of the Harvard

Medical School to utilize the fluorescent particles in flow cytometry studies. The epoxide groups can bind to lysine-terminated peptide substrates for urokinase, an extracellular serine protease that is an important therapeutic target in cancer and cardiovascular disease,[51] due to its antithrombotic activity. The peptide substrate has a quencher on the unbound end, such as LysDNP (Chapter 1), the methyl viologens (Chapter 3), or the dendritic quenchers (Chapter 4). Future work in the Swager Group to identify and implement dyes that can interact with PPEs through energy transfer may yield even greater sensitivity for these assays, since a new long wavelength emission can be detected with greater signal-to-background. The grafted polymer serves as an anchor for the peptide substrate and will prevent quenching of the PPE-coated particle prior to the assay. The length of the grafts is 30 nm, which should provide adequate distance for the localized quencher to not interact with the PPE, but still keep the substrate close to the PPE for a fast quenching response. Once the substrate is cleaved, the quencher is liberated in solution and should interact with the PPE through favorable hydrophobic interactions designed with the quencher. The analysis of the peptide substrate employed is important for predicting solubility and noncovalent interactions before and after cleavage. Grafting thickness, polymer composition, and subsequent crosslinking of the grafts may also need to be optimized to prevent the pre-assay quenching as well as facilitating quencher diffusion after activation.

6.3 Conclusions

The post-polymerization modification of a PPE polyelectrolyte yields a PPE macroinitiator capable of adsorption onto surfaces via electrostatic layer-by-layer assembly. Characterization of the PPE macroinitiator shows similar processing properties as the polyelectrolyte precursor, and initiator surfaces can be created via layer-by-layer assembly. This method encourages exploration of other substrates for surface-initiated ATRP, such as the europium-incorporated

polystyrene microspheres (Chapter 3) to utilize the internal reference method for quantifying interactions. Grafting of polymers composed of HEMA and GMA monomers can be achieved via surface-initiated ATRP from the PPE-macroinitiator coated silica particles (d = 0.6 μm). Other acrylate monomers should also be able to be ATRP-grafted from the particle surface, or from polymer-grafted particles to create interesting block copolymers. Grafted polymers having ionizable groups may improve the dispersability properties of the particles. Crosslinking of the coating can also be achieved with dual reactive monomers such as addition of diacrylates or post-graft formation such as reaction with diamines. Bioconjugation is also possible with the P(HEMA-co-GMA)-grafted particles, as demonstrated with the dye-labeled streptavidin and biotinylated particles. This platform shows promise for creating activatable particles for biosensor applications.

6.4 Experimental Section

Materials

Unless noted, all chemicals and solvents were used as received. *N,N*-dimethylformamide (HPLC grade, ≥ 99.9%), diisopropylamine (≥ 99.5%), 4-dimethylaminopyridine, ethylene glycol, *N,N,N',N',N*-pentamethyldiethylenetriamine (PMDETA, 99%), and Triton® X-100 were obtained from Sigma-Aldrich. Ammonia (27% in water (w/w)) and toluene were obtained from Mallinckrodt. Copper(I) iodide (Sigma-Aldrich) and $Pd(PPh_3)_4$ (Strem) were kept in nitrogen glovebox. Diethynylpentiptycene was purchased from ICx Nomadics, Inc. 2-Bromoisobutyryl bromide and 1-ethyl-3-(3-dimethylaminopropyl)carbodiimide hydrochloride (EDAC, stored at 0ºC) were obtained from Alfa Aesar. Copper(I) bromide (99.999%, Sigma-Aldrich) was kept in a desiccator under vacuum. Glycidyl methacrylate (GMA, min. 98.5%, Polysciences) and 2-hydroxyethyl methacrylate (HEMA, 97%, Alfa Aesar) were flushed through an activated neutral

alumina column to remove inhibitor and stored at 0°C until polymerization. Polyethyleneimine (PEI, M_n = 60,000 g/mol) was obtained from Sigma-Aldrich as a 50% (w/v) aqueous solution. Silica particles (d = 0.6 μm, 10% solids, Bangs Laboratories), EZ-link amine-PEO_3-biotin (Pierce Technologies), and bovine serum albumin (Sigma-Aldrich) were stored at 0ºC. Texas Red®-labeled streptavidin was prepared in 1 mg/mL aliquots in Tris buffer (20 mM, pH 7.4) and stored at -40ºC until use. Glass slides for monitoring film adsorption were used as received from VWR. All water used in experiments was obtained from a Millipore Milli-Q purification system.

Methods

^{1}H and ^{13}C NMR spectra were recorded on a Varian Inova instrument in deuterated solvents (Cambridge Isotopes Laboratories).

Polymer molecular weights were determined by gel permeation chromatography (GPC) measurements using a Hewlett Packard series 1100 GPC system equipped with a diode array detector (254 nm and 450 nm) and a refractive index detector running at 1.0 mL/min. in DMF. Molecular weights are reported relative to polystyrene (Polysciences) as standard.

To monitor the layering process, glass slides (pre-coated with PEI/PSS/PEI) were dipped in a 1 mg/mL **P2** in DMF solution for 15 minutes, followed by water rinse and drying with nitrogen stream. UV/Vis absorbance spectra were recorded on a Cary-50 UV/Vis spectrometer, using glass-PEI/PSS/PEI as the blank. Slides were then dipped in PEI for 15 minutes, rinsed with water, and dipped with **P2** for subsequent layers. Layer numbers indicate the number of PPE layers deposited, alternating with PEI.

Thermal gravimetric analysis (TGA) was performed using a Seiko Dual TG/DTA 320 Thermal Analyzer with samples in an aluminum pan under nitrogen atmosphere and heated from 30ºC to 600ºC at 10ºC/minute.

Grazing angle attenuated total reflectance (GATR)-Fourier transform infrared spectroscopy (FTIR) measurements were made using a GATR accessory with a Ge crystal and fixed 45º incident angle (Harrick Scientific) attached to a Nicolet Magna 860 FTIR Spectrometer. Samples for GATR-FTIR were deposited directly onto a germanium crystal and sandwiched with gold substrate under pressure in air atmosphere.

Transmission electron microscopy (TEM) was performed on a JEOL 200CX at an operating voltage of 200V. Samples for TEM were prepared by allowing drop-casted ethanol solutions on Formvar®-coated copper grids (Ladd Research) to evaporate in ambient air and coating with carbon prior to imaging. Image analysis was performed using ImageJ, a public domain software developed at the National Institute for Health. Mean particle diameters (with reported standard error) were obtained from 10 separate particles from acquired TEM images.

Confocal microscopy images were taken on a Leica TCS-SP2 confocal laser scanning microscope using Ar 360 nm, ArKr 488 nm, and GreNe 543 nm at 40% laser power as the excitation sources and a 63x/1.4 oil immersion lens. Samples for confocal were deposited on glass slides from solution and covered with glass coverslips (no. 1 1/2).

Synthesis of P1

P1 has been synthesized and reported earlier.[52] A typical procedure is as follows. To a 25 mL Schlenk tube, 84.5 mg of 1,4-diiodo-2,5-bis(17-carboxy-3,6,8,12,15-pentaoxaheptadecyloxy)benzene (0.12 mmol) and 61.1 mg of diethynylpentiptycene (0.13 mmol) were added, and subsequently evacuated and backfilled with argon three times. The tube was transferred to the glovebox and catalytic amounts of CuI and $Pd(PPh_3)_4$ were added. The sealed tube was transferred to air atmosphere, and 3 mL of the solvent mixture (5 : 4 : 1 (v/v) *N*-methylpyrrolidine : toluene : diisopropylamine, degassed for 30 minutes with nitrogen) was added under argon pressure for complete solubility of the starting materials. The tube was

completely sealed and heated in an oil bath at 70ºC. The solution turned from a milky white color to a yellow solution within 1 hour of heating. The solution was further heated for 22 hours, after which the solution was bright yellow and fluorescent green under UV illumination. The tube was then removed from heat and opened to the air. Ethyl acetate was added to precipitate the reaction mixture, and centrifuged to collect a yellow solid, dried *in vacuo* (130 mg, 95% yield). ^{1}H NMR (δ in ppm, 500 MHz, DMF-d_7) 7.72 (broad s, 2H), 7.11 (broad m, 8H), 6.43 (broad s, 8H), 4.82 (broad s, 4H), 4.35 (broad s, 4H), 3.77–3.79 (broad m, 8H), 3.64–3.68 (broad m, 8H), 2.49 (broad m, 4H).

Synthesis of PPE macroinitiator (P2)

To prepare 2-hydroxyethyl 2-bromo-2-methylpropionate,[43] ethylene glycol (2.68 mL, 48.1 mmol) was added to a 500 mL round-bottom flask. Diethyl ether (120 mL) and pyridine (5.19 mL, 65.6 mmol) were then added and the solution was stirred at room temperature. 2-bromoisobutyryl bromide was dissolved in a separate 20 mL portion of diethyl ether and added dropwise with syringe to the flask over a 20-minute period. After stirring at room temperature for 20 hours, the reaction mixture was filtered and extracted with ether/water. The organic portion was dried over magnesium sulfate and evaporated to yield the crude product as oil. Column chromatography with silica running 25 : 75 hexane : ethyl acetate as eluent yielded the purified product (**1**) as a clear oil (3.2 g, 35%). ^{1}H NMR ((δ in ppm, 500 MHz, $CDCl_3$) 4.43 (s, 1H), 4.32 (t, 2H, J = 5 Hz), 3.88 (t, 2H, J = 5 Hz), 1.96 (s, 6H). ^{13}C NMR (δ in ppm, 125 MHz, DMF-d_7) 177.3, 149.3, 149.2, 147.2, 138.5, 134.9, 126.8, 120.5, 112.7, 83.5, 70.1, 66.7, 47.3, 40.8, 34.6, 20.1, 6.5. ^{13}C NMR (δ in ppm, 125 MHz, $CDCl_3$) 172.1, 67.5, 60.9, 56.0, 30.8.

P1 (0.122 g, 0.13 mmol), **1** (60.5 mg, 0.29 mmol), and DMAP (7.9 mg, 0.065 mmol) were added to a 250 mL round-bottom flask, and subsequently the flask was purged and backfilled

with argon. DMF (120 mL) was added and the flask was placed in an ice bath, stirring at 0ºC, before the addition of EDAC (55 mg, 0.29 mmol). The reaction mixture was kept stirring at 0ºC for 1 hour, and then stirred at room temperature for 14 hours. The solvent was partially evaporated, and was filtered to remove solid material. The filtrate was precipitated into acetone to recover a yellow solid, washed several times in acetone and dried *in vacuo* to yield the recovered product, **P2** (76 mg, 60%). ^{1}H NMR (δ in ppm, 500 MHz, DMF-d_7) 7.73 (broad s, 2H), 7.12 (broad m, 4H), 6.44 (broad s, 4H), 4.85 (broad s, 4H), 4.36 (broad s, 8H), 3.24–3.80 (broad m, 16H), 2.92–2.96 (m, 4H), 2.74–2.80 (m, 4H), 1.89 (m, 6H). Ratio of the integration of the broad signal centered at 4.85 ppm for the bridgehead protons and the signal for the methyl protons at 1.89 ppm indicates ~80% inclusion of initiator groups into the polymer backbone. ^{13}C NMR (δ in ppm, 125 MHz, DMF-d_7) 181.1, 176.8, 173.3, 169.1, 154.2, 149.2, 144.9, 138.4, 120.9, 118.1, 114.6, 90.6, 68.3, 56.6, 54.0, 47.2, 39.9, 33.6, 26.8, 20.1, 4.9. GPC (UV) M_n = 6.5×10^4 g/mol, PDI = 1.5.

Preparation of silica-P2-initiator particles

Solutions with concentrations of 1 mg/mL in water or DMF were prepared with PEI and **P2**, respectively. In a 1.5 mL centrifuge tube, 100 μL of the silica particle solution was added with 900 μL of water. The tube was centrifuged for 4 minutes at 14,500 RPM to settle the particles. The supernatant was removed and replaced with 1 mL of PEI solution, sonicated with a probe sonicator (Misonix) for 10 seconds at 3.5 W (RMS) to fully disperse the particles, and vortexed at high speed for 15 minutes. The tube was then centrifuged, and the PEI solution was removed. Water (1 mL) was added, followed by sonication and centrifugation, to wash the particles. This step was repeated twice before the next adsorption step. **P2** solution (1 mL) was adsorbed in the same manner as the previous PEI step, with sonication and vortexing

followed by the two wash steps. The coated particles were then stored in aqueous solution at 0ºC until used for subsequent reactions.

ATRP of GMA from silica-P2-initiator particles

P2-coated particles (20 mg) were resuspended with sonication in DMF (1 mL) to make a 2 wt.% particle solution. A separate flask containing GMA monomer and the flask containing the particle solution were both degassed with nitrogen for 30 minutes. In a 25 mL Schlenk flask, Cu(I)Br (14.6 mg, 0.10 mmol) and PMDETA (21.3 μL, 0.10 mmol) were added, and the flask was evacuated and backfilled with argon three times. GMA (1 mL, 10.2 mmol) was then added via degassed syringe, followed by addition via cannulation of the particle solution (1 mL). The flask was sparged with argon, sealed and stirred at 50ºC. After specific reaction times (t = 5, 10, 18 hrs.), the reaction was removed from heat and exposed to air to stop the polymerization. Dichloromethane was added, and the solution was centrifuged for ~5 minutes to settle the particles. The supernatant was removed, and the particles were subjected to further washing with dichloromethane through sonication and centrifugation to remove any unattached polymer. The GMA-**P2**-coated particles were dried and stored *in vacuo* prior to characterization.

ATRP of HEMA from silica-P2-initiator particles

A similar procedure as described for GMA was used for ATRP of HEMA from **P2**-coated particles. Cu(I)Br (14.6 mg, 0.10 mmol) and PMDETA (21.3 μL, 0.10 mmol) were added to a 25 mL Schlenk flask and evacuated/backfilled with argon three times. Degassed HEMA (1.24 mL, 10.2 mmol) and **P2**-coated particles in DMF (2 wt.%, 1 mL) were added to the flask via syringe. After sparging with argon, the flask was sealed and stirred at 75ºC for 15 hours.

ATRP of HEMA-co-GMA from silica-P2-initiator particles

Cu(I)Br (14.6 mg, 0.10 mmol) and PMDETA (21.3 μL, 0.10 mmol) were added to a flask, evacuated/backfilled with argon three times. GMA (0.25 mL, 2.55 mmol) and HEMA (0.93 mL, 7.65 mmol) were added, followed by particle solution (2 wt. %, 1 mL), as previously described, and the flask was heated at 50ºC for 20 hours.

Biotinylation of silica-P2-P(HEMA-co-GMA) particles and streptavidin assay

Dried silica-**P2**-P(HEMA-co-GMA) particles (5 mg) were resuspended in ethanol (3 mL) and added to a 20 mL glass vial with stirbar. In a separate vial, a solution of amine-PEO_3-biotin (10 mg) in ethanol (3 mL) was prepared and subsequently added to the particles. The solution was allowed to stir at room temperature for 20 hours. The particles were then centrifuged and rinsed thoroughly with several rinses of ethanol, followed by 1 M NH_4OH. The particles were dried overnight *in vacuo*.

Biotinylated and control particles (silica-**P2**-P(HEMA-co-GMA) treated only with 1 M NH_4OH) were both resuspended in 1 mL Tris buffer in separate centrifuge tubes. To a 1 mg/mL solution of Texas Red®-labeled streptavidin in Tris buffer, BSA (2 mg) and Triton X-100 (0.4 μL) were added to decrease nonspecific binding. 50 μL of the streptavidin solution was added to both the biotinylated and control particles, and the tubes were vortexed at high speed in the dark at room temperature. After 1 hour, the tubes were centrifuged for 4 minutes at 14,500 RPM, and the supernatant was removed. The biotinylated particles were dark red, and the control particles were yellow in color. Repeated rinses with ethanol were performed to remove unbound reagent before imaging.

6.5 References

(1) Kamigaito, M.; Ando, T.; Sawamoto, M. *Chem. Rev.* **2001**, *101*, 3689-3745.

(2) Matyjaszewski, K.; Xia, J. *Chem. Rev.* **2001**, *101*, 2921-2990.

(3) Kato, M.; Kamigaito, M.; Sawamoto, M.; Higashimura *Macromolecules* **1995**, *28*, 1721-1723.

(4) Wang, J. S.; Matyjaszewski, K. *J. Am. Chem. Soc.* **1995**, *117*, 5614-5615.

(5) Fischer, H. *J. Polym. Sci. Part A* **1999**, *37*, 1885.

(6) Advincula, R. A., ed. *Polymer Brushes*; Wiley-VCH: Weinheim, 2004.

(7) Ejaz, M.; Yamamoto, S.; Ohno, K.; Tsujii, Y.; Fukuda, T. *Macromolecules* **1998**, *31*, 5934-5936.

(8) Husseman, M., Malmstrom, E.E., McNamara, M., Mate, M., Mecerreyes, D., Benoit, D.G., Hedrick, J.L., Mansky, P., Huang, E., Russell, T.P., Hawker, C.J. *Macromolecules* **1999**, *32*, 1424-1431.

(9) Radhakrishnan, B.; Ranjan, R.; Brittain, W. J. *Soft Matter* **2006**, *2*, 386-396.

(10) Li, D.; Jones, G. L.; Dunlap, J. R.; Hua, F.; Zhao, B. *Langmuir* **2006**, *22*, 3344-3351.

(11) El Harrak, A.; Carrot, G.; Oberdisse, J.; Jestin, J.; Boué, F. *Polymer* **2005**, *46*, 1095-1104.

(12) Perruchot, C.; Khan, M. A.; Kamitsi, A.; Armes, S. P.; von Werne, T.; Patten, T. E. *Langmuir* **2001**, *17*, 4479-4481.

(13) Huang, X.; Wirth, M. J. *Anal. Chem.* **1997**, *69*, 4577-4580.

(14) von Werne, T.; Patten, T. E. *J. Am. Chem. Soc.* **2001**, *123*, 7497-7505.

(15) Pyun, J.; Jia, S.; Kowalewski, T.; Patterson, G. D.; Matyjaszewski, K. *Macromolecules* **2003**, *36*, 5094-5104.

(16) Mori, H.; Seng, D. C.; Zhang, M.; Müller, A. H. E. *Langmuir* **2002**, *18*, 3682-3693.

(17) Jayachandran, K. N.; Takacs-Cox, A.; Brooks, D. E. *Macromolecules* **2002**, *35*, 4247-4257.

(18) Bontempo, D.; Tirelli, N.; Masci, G.; Crescenzi, V.; Hubbell, J. A. *Macromol. Rapid Commun.* **2002**, *23*, 417-422.

(19) Zheng, G.; Stöver, H. D. H. *Macromolecules* **2003**, *36*, 1808-1814.

(20) Guerrini, M. M.; Charleus, B.; Vairon, J.-P. *Macromol. Rapid Commun.* **2000**, *21*, 669-674.

(21) Zheng, G.; Stöver, H. D. H. *Macromolecules* **2002**, *35*, 7612-7619.

(22) Nuß, S.; Böttcher, H.; Wurm, H.; Hallensleben, M. L. *Angew. Chem. Int. Ed.* **2001**, *40*, 4016-4018.

(23) Ohno, K.; Koh, K.; Tsujii, Y.; Fukuda, T. *Angew. Chem. Int. Ed.* **2003**, *42*, 2751-2754.

(24) Farmer, S. C.; Patten, T. E. *Chem. Mater.* **2001**, *13*, 3920-3926.

(25) Hu, F.; Neoh, K. G.; Cen, L.; Kang, E.-T. *Biomacromolecules* **2006**, *7*, 809-826.

(26) Liu, T.; Jia, S.; Kowalewski, T.; Matyjaszewski, K.; Casado-Portilla, R.; Belmont, J. *Langmuir* **2003**, *19*, 6342-6345.

(27) Liu, T.; Jia, S.; Kowalewski, T.; Matyjaszewski, K.; Casado-Portilla, R.; Belmont, J. *Macromolecules* **2006**, *39*, 548-556.

(28) Qin, S.; Qin, D.; Ford, W. T.; Resasco, D. E.; Herrera, J. E. *J. Am. Chem. Soc.* **2004**, *236*, 170-176.

(29) Yao, Z.; Braidy, N.; Botton, G. A.; Adronov, A. *J. Am. Chem. Soc.* **2003**, *125*, 16015-16024.

(30) Kong, H.; Gao, C.; Yan, D. *J. Am. Chem. Soc.* **2004**, *126*, 412-413.

(31) El Harrak, A.; Carrot, G.; Oberdisse, J.; Eychenne-Baron, C.; Boué, F. *Macromolecules* **2004**, *37*, 6376-6384.

(32) Piech, M.; Bell, N. S. *Macromolecules* **2006**, *39*, 915-922.

(33) Chen, G.; Huynh, D.; Felgner, P. L.; Guan, Z. *J. Am. Chem. Soc.* **2006**, *128*, 4298-4302.

(34) Cheng, Z.; Zhu, X.; Shi, Z. L.; Neoh, K. G.; Kang, E. T. *Ind. Eng. Chem. Res.* **2005**, *44*, 7098-7104.

(35) Fulghum, T. M.; Patton, D. L.; Advincula, R. C. *Langmuir* **2006**, *22*, 8397-8402.

(36) Vo, C.-D.; Schmid, A.; Armes, S. P.; Sakai, K.; Biggs, S. *Langmuir* **2007**, *23*, 408-413.

(37) Chen, X. Y.; Armes, S. P.; Greaves, S. J.; Watts, J. F. *Langmuir* **2004**, *20*, 587-595.

(38) Zheng, G.; Stöver, H. D. H. *Macromolecules* **2002**, *35*, 6828-6834.

(39) Kizhakkedathu, J. N.; Brooks, D. E. *Macromolecules* **2003**, *36*, 591-598.

(40) Kim, Y.-G.; Lee, C.-S.; Chung, W.-J.; Kim, E.-M.; Shin, D.-S.; Kim, J.-H.; Lee, Y.-S.; Chung, J.; Kim, B.-G. *Biotechnol. Lett.* **2006**, *28*, 79-84.

(41) Pirrung, M. C. *Angew. Chem. Int. Ed.* **2002**, *41*, 1276-1289.

(42) Müller, E. *Chem. Eng. Technol.* **2005**, *28*, 1295-1305.

(43) White, M. A.; Johnson, J.A.; Koberstein, J.T.; Turro, N.J. *J. Am. Chem. Soc.* **2006**, *128*, 11356-11357.

(44) Yu, W. H.; Kang, E. T.; Neoh, K. G. *Langmuir* **2004**, *20*, 8294-8300.

(45) Krishnan, R.; Srinivasan, K. S. V. *Macromolecules* **2004**, *37*, 3614-3622.

(46) Downloaded from http://rsb.info.nih.gov/ij/.

(47) Green, N. M. *Methods in Enzymology* **1990**, *184*, 51-67.

(48) Wilcheck, M.; E.A., B. *Methods in Enzymology* **1990**, *184*, 5-13.

(49) Diamandis, E. P.; Christopoulos, T. K. *Clin. Chem.* **1991**, *37*, 625-636.

(50) Zheng, J.; Swager, T. M. *Chem. Comm.* **2004**, 2798-2799.

(51) Andreasen, P. A.; Kjøller, L.; Christensen, L.; Duffy, M. J. *Int. J. Cancer* **1997**, *72*, 1-22.

(52) Wosnick, J. H.; Liao, J. H.; Swager, T. M. *Macromolecules* **2005**, *38*, 9287-9290.

Appendix for Chapter 6:

NMR Spectra

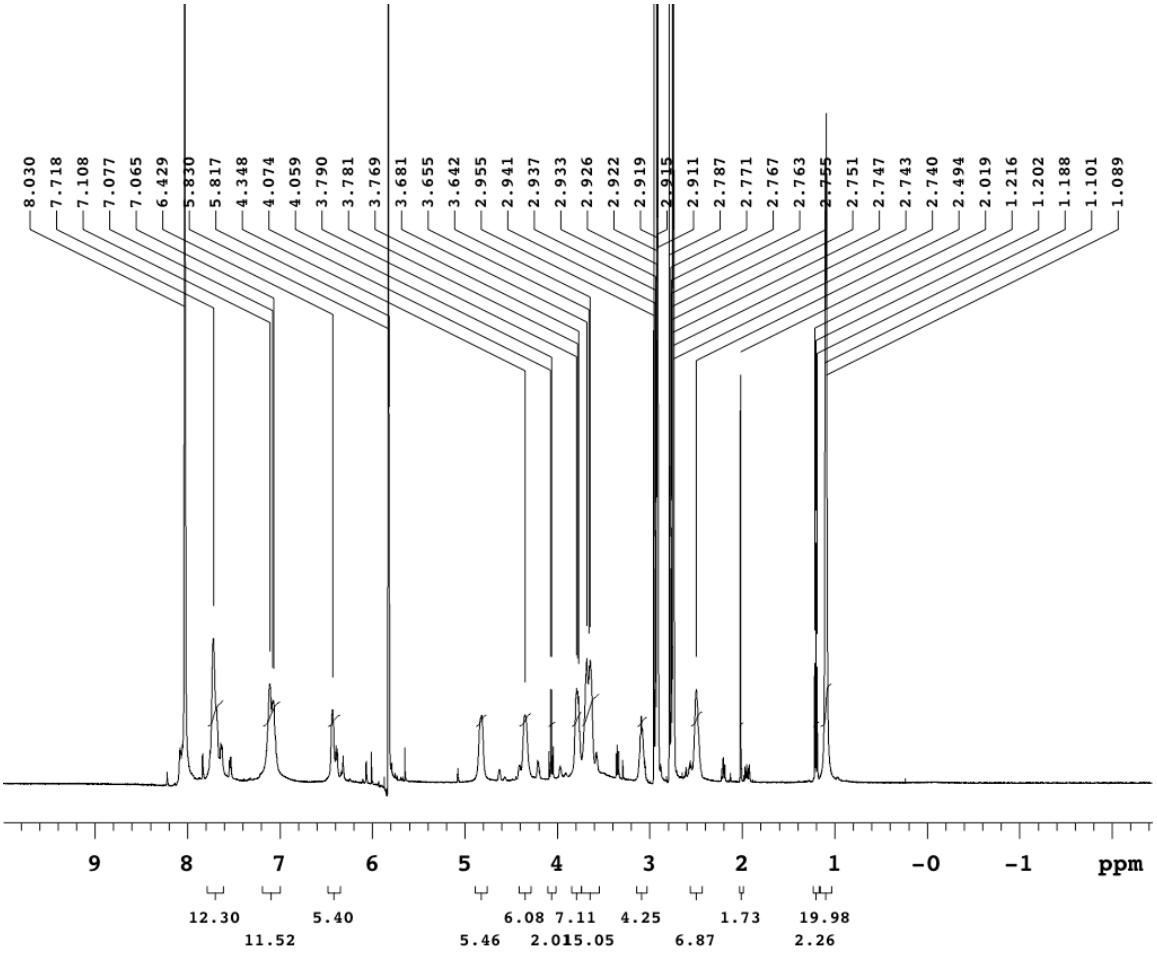

Appendix 6.1. ^{1}H NMR of **P1** in DMF-d_7 (500 MHz).

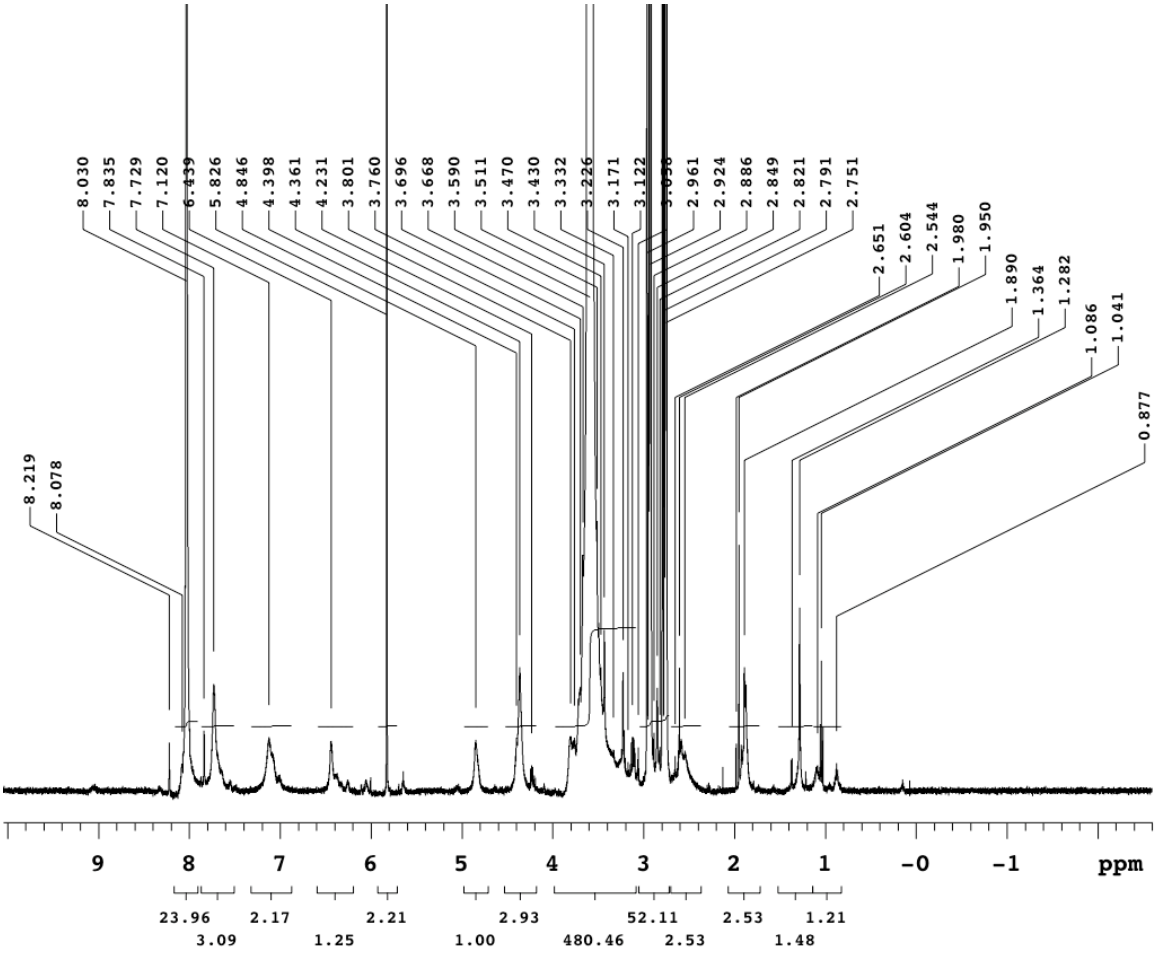

Appendix 6.2. ^{1}H NMR of **P2** in DMF-d_7 (500 MHz).

Chapter 7:

ATRP Grafting in Solution:

Prospects for Nanostructured Materials

7.1 Introduction

The synthesis of a poly(phenylene ethynylene) (PPE) macroinitiator was described in Chapter 6 for surface-initiated atom transfer radical polymerization (ATRP). We will show in this chapter that grafting via atom transfer radical polymerization (ATRP) of 2-hydroxyethyl methacrylate (HEMA) is possible from the PPE macroinitiator in solution. This introduces prospects of nanostructure formation due to the covalent attachment of a hydrophilic polymer to the hydrophobic conjugated polymer backbone to create an amphiphilic graft copolymer.

7.1.1 Amphiphilic graft copolymers

Amphiphilic polymers have been studied extensively due to their properties at the oil-water interface and have shown wide commercial utility as polymer surfactants. While most of the work for creating polymer nanostructures such as micelles and vesicles with amphiphilic polymers has been with block copolymers, graft copolymers are also capable of self-assembly. Figure 7.1 illustrates the difference between amphiphilic block and graft copolymers. Compared with block copolymers, graft copolymers can form micelles at lower concentrations,[1,2] due to the combination of intra- and intermolecular association. The ability to distribute functionality along the polymer backbone provides unique opportunities to alter the physical and chemical properties as well. For example, crosslinked and hollowed nanostructures[3-5] have been made for potential biomedical applications. Cylindrical micelles have also be formed from these "molecular bottlebrushes" as templates for inorganic nanoparticle formation.[6-8]

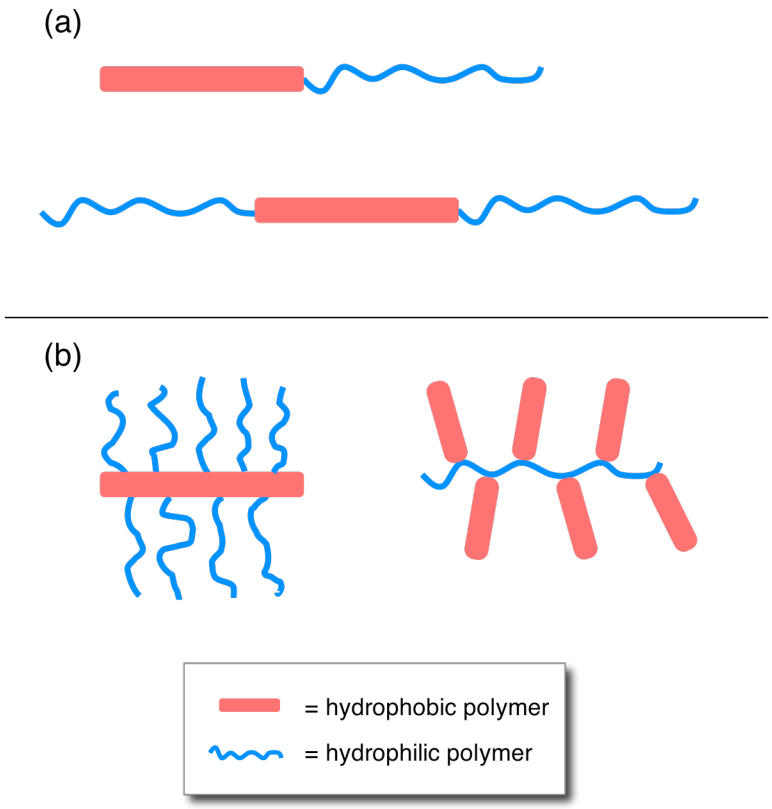

Figure 7.1. Amphiphilic (A) block and (B) graft copolymers.

7.1.2 ATRP as a method to create PPE-based amphiphilic graft copolymers

Side-chain grafting of PPEs has been utilized for increasing solubility and providing material compatibility with other polymeric systems, as well as minimizing aggregation effects and improving the photophysical properties in the solid state. Atom transfer radical polymerization (ATRP), as introduced in Chapter 6, provides a controlled method to synthesize graft copolymers,[9,10] and was previously demonstrated in our group for the grafting of polystyrene[11] and oxadiazole[12] from PPEs for optoelectronic applications. Bunz and coworkers have also synthesized graft copolymers with PPEs utilizing nitroxide-mediated radical

polymerization (NMRP) for polystyrene and polyoxazoline grafting[13] or using monomers with polyester side chains and proceeding with coupling conditions,[14] but the resultant materials in both cases were particularly polydisperse (range of PDI = 3.1–5.3).[13,14]

Amphiphilic copolymers synthesized from conjugated macromolecules have primarily been of the block copolymer type. Rod-coil amphiphilic block copolymers composed of conjugated oligomers[15,16] and polymers have been used to create self-assembled nanostructures in polar media, primarily for electronic and optoelectronic applications. A coil-rod-coil amphiphilic block copolymer was synthesized by Kuroda and Swager utilizing di-*tert*-butylnitroxide derivative end caps on nonionic water-soluble PPES for NMRP of *N*-isopropylacrylamide, demonstrating the use of the grafted copolymers as thermal precipitation assays.[17]

Amphiphilic graft copolymers, however, have not been synthesized with PPEs as the backbone in a comb-type morphology, and has not been explored in depth for use in biological applications. Interfacial activity has been studied to understand the aggregation observed with amphiphilic side chains,[18,19] but has not yet been conducted with polymeric side chains. PPEs are generally considered to be flexible rods[20,21] and are particularly hydrophobic in solution, especially in polar environments such as methanol or water. The encapsulation of the hydrophobic backbone by hydrophilic polymer grafts can be advantageous for associating hydrophobic quenchers or dyes in sensory schemes in polar solvents, similar to the “molecular tweezer” effect described by Balazs and coworkers,[22] and thus could be explored as potential biosensors. In addition, the amphiphilic graft copolymer could be used as a compatibilizer to create hydrophilic and protein-resistant surfaces on hydrophobic and water-insoluble conjugated polymer films, extending the scope of polymers that could be implemented as biosensors.

7.2 Results and Discussion

7.2.1 Synthesis of PPE-P(HEMA) graft copolymer

We are interested in moving towards the implementation of nonionic conjugated polymers in biosensing platforms,[23] in order to incorporate an even greater variety of polymers developed in our group. One method of achieving this goal is through ATRP grafting of hydrophilic polymers from the polymer backbone, to create amphiphilic graft polymers that can perform well in polar solvents. Initial attempts for synthesizing a nonionic PPE macroinitiator were made using a copolymer composed of the diethynylpentiptycene and a dialkoxy diiodomonomer with pendant hydroxyl groups, similar to the comonomer used by Breen et al.[11] This polymer was not readily soluble in organic solvents, and thus complete conversion to the PPE macroinitiator and subsequent ATRP reactions in solution were not possible.

The ionic PPE macroinitiator, described in Chapter 6, was used to demonstrate the synthesis of amphiphilic PPE graft copolymers in the present chapter. **P2** is readily soluble in DMF, a good solvent for ATRP reactions.

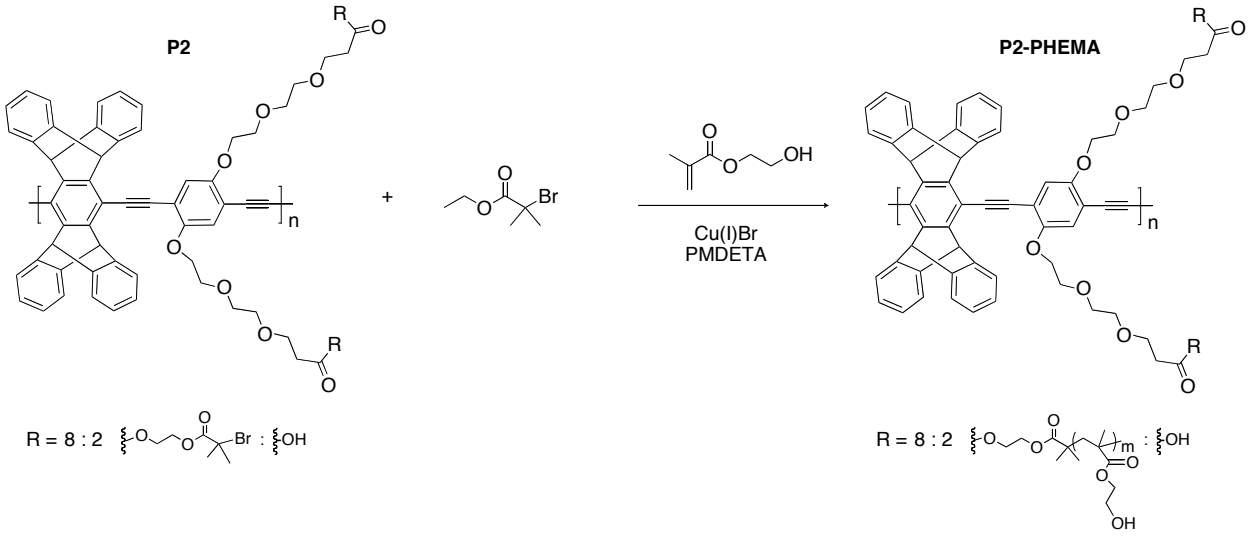

Figure 7.2. Synthesis of **P2-P(HEMA)** graft copolymer.

Figure 7.2 shows the ATRP conditions using the Cu(I)Br/PMDETA catalyst system in DMF for the synthesis of **P2-P(HEMA)**. A small molecule initiator, ethyl α-bromoisobutyrate, was added to the polymerization along with the **P2** macroinitiator. This method of a "sacrifical initiator" is often used in surface-initiated polymerization for controlled chain growth.[24] Typically, there is a low concentration of initiating groups at the surface to prevent surface termination events. The addition of sacrificial initiator allows for a sufficient concentration of persistent radicals to be generated in order to provide a controlled grafting reaction. Others have also added excess of the persistent radical species (Cu(II)) to the precursor solution as an alternative to the sacrificial initiator procedure.[25] In our case, the sacrificial initiator compensates for the limited amount of **P2** material for reaction as well as ensuring the generation of the persistent radical. It is observed that when ATRP is performed from a multifunctional initiator such as **P2**, radical coupling of the propagating chains is likely to occur because of the high local concentration of radicals, resulting in gelation,[26] and similar to surface-initiated polymerization, this termination effect has been prevented through the addition of a deactivator or by diluting the reaction mixture. The products resulting from the small molecule initiator can be separated by molecular weight versus the grafted copolymer at the end of the polymerization. Future experiments should be conducted without the sacrificial initiator to ensure the PPE macroinitiator is independently capable of controlled polymerization via ATRP.

7.2.2 Characterization of PPE-P(HEMA) graft copolymer

The resultant **P2-P(HEMA)** is a viscous translucent solid, as compared to the powdery characteristics of **P2**. The polymer is soluble in DMF as well as methanol, a solvent that usually precipitates nonionic PPEs from solution. ^{1}H NMR (Chapter 7 Appendix) in methanol shows

only the proton signals from the grafted P(HEMA), indicating the ability of the grafts to encapsulate and "solubilize" the PPE backbone. The molecular weight of the backbone is much smaller in comparison to the grafts, and thus solubilization in a good solvent for the backbone, such as THF, is not possible for NMR analysis.

The solvent character of **P2-P(HEMA)** has an effect on the fluorescent properties, as the P(HEMA) grafts enable the PPE to be solubilized and exhibit emissive properties characteristic of pentiptycene-incorporated PPEs in methanol (Figure 7.3). This method provides an "encapsulation" of the hydrophobic backbone through post-polymerization reactions, and could be implemented for rendering conjugated polymers soluble in polar solvents. The solubility in Tris buffer was assessed, but it was found that **P2-P(HEMA)** formed a turbid solution and was aggregated due to the insolubility of P(HEMA) in water. Formation of a block copolymer from the P(HEMA) with a water-soluble polymer would generate water-soluble nanostructures, with the conjugated polymer located at the core. The quantum yield for **P2-P(HEMA)** in methanol is much less than the quantum yield in DMF (Table 7.1), and is attributed to aggregation of the **P2** backbone in the poor solvent conditions leading to self-quenching of the fluorescence. The flexibility of the P(HEMA) grafts is translated to the flexibility of the PPE backbone, contributing to rotations that may disrupt the conjugation in solution. Future nanostructured materials should address how to control microenvironments to prevent the occurrence of this deleterious effect. Depositing **P2-P(HEMA)** as a film may "freeze" the conformation of the **P2** and provide a greater quantum yield than that measured in methanol.

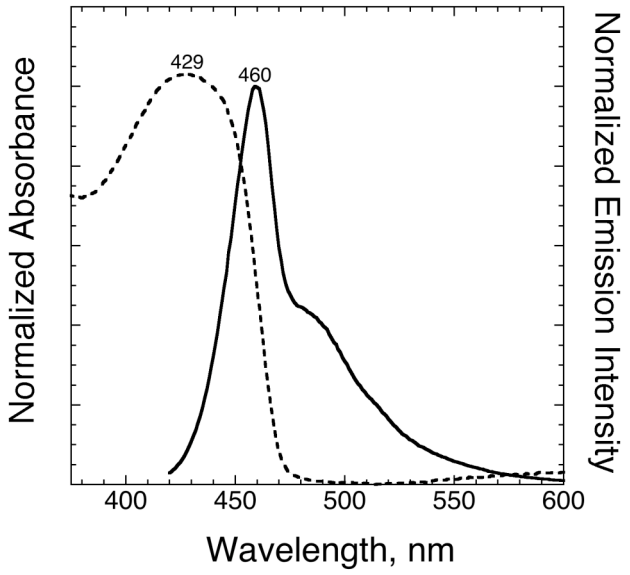

Figure 7.3. Normalized UV/Vis absorbance and fluorescence spectra of **P2-P(HEMA)** in methanol.

Polymer	Φ_F in DMF	Φ_F in MeOH
P2	0.5	---
P2-P(HEMA)	0.5	0.1

Table 7.1. Relative quantum yields (Φ_F) based on coumarin 6 in ethanol as standard.

The GPC traces shown in Figure 7.4 shows the faster elution time of **P2-P(HEMA)** versus **P2** in DMF, indicating an increase in molecular weight from the grafted copolymer. The GPC trace of **P2-P(HEMA)** shows a minor peak at 27 minutes, most likely due to traces of oligomers of **P2**. The molecular weights and polydispersities of **P2** and **P2-P(HEMA)** are listed in Table 7.2. The molecular weight of the grafts cannot be analyzed directly using GPC; however, the molecular weight increase from the grafted P(HEMA) is significant in comparison to **P2**, confirming the grafting reaction occurred from the macroinitiator. The calculated

molecular weight of the P(HEMA) grafts from M_n values determined from GPC is 330 kDa, corresponding to ~2,500 repeat units. Compared to the **P2** backbone, composed of ~70 repeat units, the polymer grafts are much larger and are the dominant component at a given weight. The synthesis of shorter P(HEMA) grafts with respect to the PPE may improve the solution luminescent properties since less flexibility will be imparted to the backbone. The polydispersity slightly increases from 1.5 to 1.9, indicating the distribution of graft composition of **P2-P(HEMA)**. This may be due to the random distribution of initiator groups of the precursor **P2**, which itself does not have a very low polydispersity. Polymerization of HEMA is initiated with the macroinitiator and sacrificial initiator, leading to a possible random distribution of grafts from the PPE backbone due to the chains formed in solution. For self-assembly processes, the uniformity of the grafted copolymers is critical for formation of the desired nanostructure. Future studies should thus be conducted by well-defined synthesis of PPE macroinitiators and without the sacrificial initiator in order to achieve more uniform and controlled grafting for self-assembly studies. Varying the reaction conditions could test the living nature of the grafting via ATRP to verify the ability of the PPE macroinitiator to produce controlled polymer grafts.

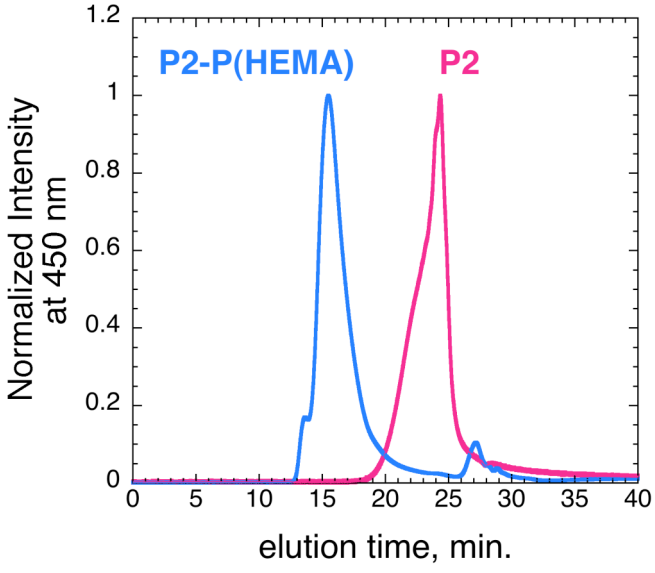

Figure 7.4. GPC (UV) traces of **P2** and **P2-P(HEMA)**, eluted in DMF.

Polymer	M_n (kDa)	PDI
P2	65	1.5
P2-P(HEMA)	390	1.9

Table 7.2. Number-average molecular weights (M_n) and polydispersities (PDI) of **P2** and **P2-P(HEMA)** measured from GPC (UV), based on PS standard.

The thermal behavior was monitored by differential scanning calorimetry (DSC). **P2-P(HEMA)** displays a broad second-order transition that is intermediate of the homopolymer glass transition (T_g) values, corresponding to the T_g associated with the distribution of grafted P(HEMA) on the PPE (Figure 7.5, Table 7.3). The lower transition observed for the grafted polymer indicates the greater mobility of the **P2** backbone achieved with the flexible P(HEMA) grafts. The intermediate T_g further confirms the covalent linkage between the grafts and the PPE, since the two phases otherwise would be immiscible. Another transition for **P2-P(HEMA)** is observed around 180ºC; however, it is unclear whether this peak is a melting point associated with P(HEMA) or a glass transition associated with **P2**. Dynamic mechanical analysis could provide another method of observing the thermal transitions, but was not performed due to insufficient amounts of material.

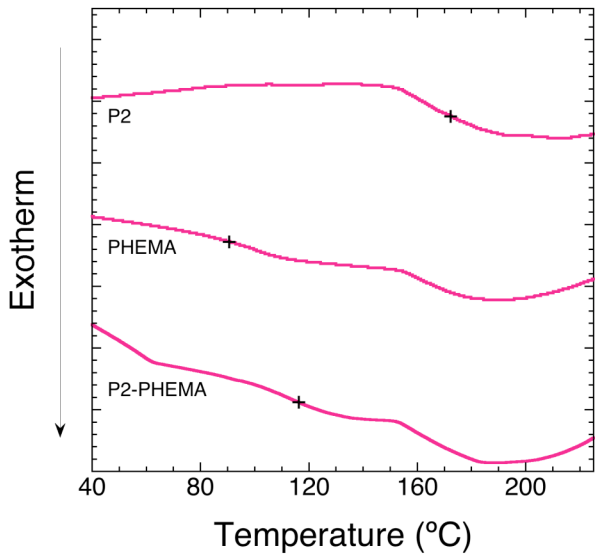

Figure 7.5. DSC cooling curves for **P2**, P(HEMA), and **P2-P(HEMA)**. Crosses indicate T_g values.

Polymer	T_g (ºC)
P(HEMA)	89
P2	157
P2-P(HEMA)	109

Table 7.3. T_g values of P(HEMA), **P2** and **P2-P(HEMA)** observed from DSC curves.

7.2.3 Future prospects of amphiphilic PPE copolymers

The initial intention of the **P2-P(HEMA)** synthesis was to test the ability of the PPE macroinitiator to perform ATRP in solution. The material properties that resulted from grafting hydrophilic polymers from the PPE backbone generated new ideas for creating self-assembled nanostructures. The amphiphilic polymer, as synthesized in this study, could serve as a compatibilizer and be prepared as a blend with water-insoluble conjugated polymers to form an

insulating barrier against the environment and solubilize the materials in polar solvents. Grafting of functional acrylates using ATRP is feasible to incorporate biological targets, as shown in Chapter 6, and also can be used to crosslink the formed nanostructures. The particles that have been developed in this thesis are rather large (d = 0.2 – 5 μm) and are limited to bioassays for extracellular targets. The smaller nanostructures that can be formed with self-assembly (<100 nm) create opportunities for cell-based studies due to cellular uptake of the smaller sized particles, increasing the scope of targets that can be assayed with the particle sensors.

7.3 Conclusions

The synthesis of an amphiphilic graft copolymer composed of a PPE backbone and P(HEMA) grafts was conducted utilizing a PPE macroinitiator and a small molecule initiator. Characterization was performed using NMR, GPC, absorbance and fluorescence spectroscopy, and DSC to confirm the grafting of P(HEMA) from the PPE macroinitiator. Further studies should be conducted without the use of the small molecule initiator to test the robustness of the PPE macroinitiator and also to improve the uniformity of the grafts. Controlling the length and the distribution of hydrophilic grafts from a hydrophobic PPE will prove useful for self-assembled nanostructures. Future work in developing these nanostructures has potential for creating interesting sensory schemes for biological imaging and diagnostics.

7.4 Experimental Section

Materials

N,N-dimethylformamide (HPLC grade, ≥ 99.9%), *N,N,N',N',N*-pentamethyldiethylenetriamine (PMDETA, 99%), and ethyl α-bromoisobutyrate (EBriB, 98%) were obtained from Sigma-Aldrich. Copper(I) bromide (99.999%, Sigma-Aldrich) was kept in a desiccator under vacuum. 2-hydroxyethyl methacrylate (HEMA, 97%, Alfa Aesar) was flushed through an activated neutral alumina column to remove inhibitor and stored at 0°C until polymerization. P(HEMA) for DSC measurements was purchased from Sigma-Aldrich in crystalline form with average M_v ~300,000 g/mol.

Methods

Synthesis of **P2** was described in Chapter 6. Degassing solvents and monomers were performed prior to reaction for 30 minutes with nitrogen gas. ^{1}H NMR spectra were recorded on a Varian Inova instrument in deuterated solvents (Cambridge Isotopes Laboratories). All spectroscopic measurements were performed with dilute solutions (O.D. < 0.1) in a 1-cm pathlength quartz cuvette. Absorbance was measured using a Cary 50 UV-Vis spectrophotometer, corrected for solvent baseline. Fluorescence spectra were measured on a Jobin Yvon SPEX Fluorolog-τ2 or -τ3 fluorometer. Relative quantum yields (Φ were measured by the gradient method, with 5 separate measurements at different concentrations (O.D. < 0.1), and calculated based on the quantum yield of coumarin 6 in ethanol as standard (Φ = 0.78). The molecular weights were determined by gel permeation chromatography (GPC) measurements using a Hewlett Packard series 1100 GPC system equipped with a diode array detector (254 nm and 450 nm) and a refractive index detector running at 1.0 mL/min. in DMF. Molecular weights are reported relative to polystyrene (Polysciences) as standard. Differential

scanning calorimetry (DSC) experiments were performed in aluminum pans under nitrogen atmosphere on a TA Instruments DSC Q10 heating/cooling from 30ºC to 250ºC for two complete cycles at a ramp rate of 20ºC/min. The glass transition temperature (T_g) is reported from the second order transitions of the second cooling cycle.

Synthesis of P2-P(HEMA)

P2 (4.3 mg, 3.5 μmol of initiator groups) was added to a 25 mL Schlenk tube. Cu(I)Br (5.0 mg, 0.035 mmol), PMDETA (8.7 mg, 0.035 mmol), and EBriB (3.4 mg, 0.017 mmol) were added to the tube, and then evacuated and backfilled with argon three times. Degassed DMF (1 mL) was added via purged syringe, followed by addition of degassed HEMA (0.4 mL). The flask was sealed and heated at 75ºC in an oil bath. After 16 hours, the solution had turned from an initial dark green color to a turquoise color, and was viscous. The reaction mixture was precipitated and washed several times in diethyl ether. A sticky solid was obtained after centrifugation. The solid was redissolved in DMF and flushed through an activated neutral alumina column to remove the catalyst. Solvent was removed by rotavap and the final product was dried *in vacuo* to yield the final product as a yellow translucent solid (240 mg). ^{1}H NMR (δ in ppm, 500 MHz, CD_3OD) 4.02 (broad s, 2H), 3.74 (broad s, 2H), 1.92 (broad m, 1H), 1.08 (broad s, 1H), 0.91 (broad s, 2H). GPC (UV) $M_n = 3.9 \times 10^5$ g/mol, PDI = 1.9.

7.5 References

(1) Pitsikalis, M.; Woodward, J.; Mays, J. W.; Hadjichristidis, N. *Macromolecules* **1997**, *30*, 5384-5389.

(2) Israelachvili, J. N. *Intermolecular and Surface Forces*; Academic Press: London, 1985.

(3) Cheng, C.; Qi, K.; Khoshdel, E.; Wooley, K. L. *J. Am. Chem. Soc.* **2006**, *128*, 6808-6809.

(4) Breitenkamp, K.; Emrick, T. *J. Am. Chem. Soc.* **2003**, *125*, 12070-12071.

(5) Lee, H. J.; Yang, S. R.; An, E. J.; Kim, J.-D. *Macromolecules* **2006**, *39*, 4938-4940.

(6) Zhang, M.; Müller, A. H. E. *J. Polym. Sci., Part A: Polym. Chem.* **2005**, *43*, 3461-3481.

(7) Djalali, R.; Yi, S.-Y.; Schmidt, M. *Macromolecules* **2002**, *35*, 4282-4288.

(8) Zhang, M.; Drechsler, M.; Müller, A. H. E. *Chem. Mater.* **2004**, *16*, 537-543.

(9) Börner, H. G.; Beers, K.; Matyjaszewski, K.; Sheiko, S. S.; Möller, M. *Macromolecules* **2001**, *34*, 4375-4383.

(10) Cheng, G.; Böker, A.; Zhang, M.; Krausch, G.; Müller, A. H. E. *Macromolecules* **2001**, *34*, 6883-6888.

(11) Breen, C. A.; Deng, T.; Breiner, T.; Thomas, E. L.; Swager, T. M. *J. Am. Chem. Soc.* **2003**, *125*, 9942-9943.

(12) Breen, C. A.; Rifai, S.; Bulovic, V.; Swager, T. M. *Nano Lett.* **2005**, *5*, 1597-1601.

(13) Wang, Y.; Wilson, J. N.; Smith, M. D.; Bunz, U. H. F. *Macromolecules* **2004**, *37*, 9701-9708.

(14) Wang, Y.; Erdogan, B.; Wilson, J. N.; Bunz, U. H. F. *Chem. Comm.* **2003**, 1624-1625.

(15) Hulvat, J. F.; Sofos, M.; Tajima, K.; Stupp, S. I. *J. Am. Chem. Soc.* **2005**, *127*, 366-372.

(16) Mori, T.; Watanabe, T.; Minagawa, K.; Tanaka, M. *J. Polym. Sci., Part A: Polym. Chem.* **2005**, *43*, 1569-1578.

(17) Kuroda, K.; Swager, T. M. *Macromolecules* **2004**, *37*, 716-724.

(18) Breitenkamp, R. B.; Tew, G. N. *Macromolecules* **2004**, *37*, 1163-1165.

(19) Kim, J.; Swager, T. M. *Nature* **2001**, *411*, 1030-1034.

(20) Cotts, P. M.; Swager, T. M.; Zhou, Q. *Macromolecules* **1996**, *29*, 7323-7328.

(21) Samorí, P.; Severin, N.; Müllen, K.; Rabe, J. P. *Adv. Mater.* **2000**, *12*, 579-582.

(22) Pan, T.; Balazs, A. C. *Langmuir* **1993**, *9*, 3402-3407.

(23) Joly, G. D.; Geiger, L.; Kooi, S. E.; Swager, T. M. *Macromolecules* **2006**, *39*, 7175-7177.

(24) Husseman, M.; Malmström, E. E.; McNamara, M.; Mate, M.; Mecerreyes, D.; Benoit, D. G.; Hedrick, J. L.; Mansky, P.; Huang, E.; Russell, T. P.; Hawker, C. J. *Macromolecules* **1999**, *32*, 1424-1431.

(25) Matyjaszewski, K.; Miller, P. J.; Shukla, N.; Immaraporn, B.; Gelman, A.; Luokala, B. B.; Siclovan, T. M.; Kickelbick, G.; Vallant, T.; Hoffman, H.; Pakula, T. *Macromolecules* **1999**, *32*, 8716-8724.

(26) Östmark, E.; Harrisson, S.; Wooley, K. L.; Malmström, E. E. *Biomacromolecules* **2007**, *8*, 1138-1148.

(27) Clark, A. P.-Z.; Cadby, A. J.; Shen, C. K.-F.; Rubin, Y.; Tolbert, S. H. *J. Phys. Chem. B* **2006**, *110*, 22088-22096.

Appendix for Chapter 7:

NMR Spectra

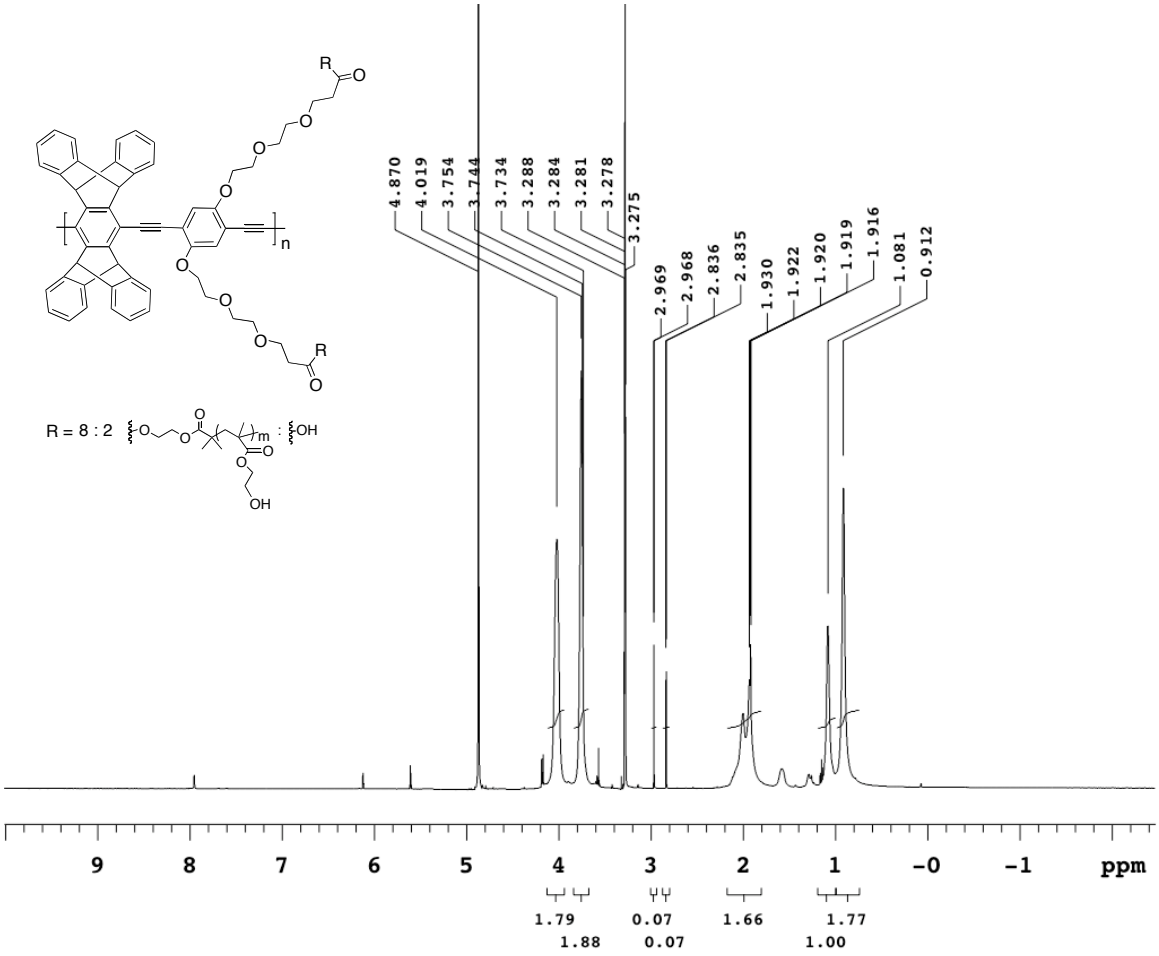

Appendix 7.1. ^{1}H NMR of **P2-P(HEMA)** in CD_3OD (500 MHz).

Curriculum Vitae

b. December 12, 1979 in Hoboken, NJ

EDUCATION

Massachusetts Institute of Technology
Cambridge, MA
Ph.D. in Materials Science & Engineering, June 2007
Concentration: Program for Polymer Science & Technology (PPST)

Rutgers University
New Brunswick, NJ
Bachelor of Science with Highest Honors in Biomedical Engineering, May 2002
Ranked 1st in major
GPA: 3.98/4.0

RESEARCH EXPERIENCE

M**assachusetts Institute of Technology**
Institute for Soldier Nanotechnologies
Cambridge, MA November 2002–June 2007
Advisor: Professor Timothy M. Swager, Department of Chemistry

- Developed a conjugated polymer particle sensor with potential application for cancer detection and high-throughput screening.
- Implemented a ratiometric method for measuring particle sensory response.
- Synthesized core-shell particles with surface-initiated atom transfer radical polymerization (ATRP) of functional acrylates for encapuslation and bioconjugation.

Ethicon, Inc. (a Johnson & Johnson company)
Somerville, NJ January 2002–August 2002

- Performed chemical reactions of new adhesive monomers as materials for next generation wound care products and assisted with patent literature search.
- Exploratory project expanded into a full project with the addition of one full-time scientist.

W.M. Keck Center for Collaborative Neuroscience
New Jersey Center for Biomaterials
Piscataway, NJ June 2001–May 2002

- Developed method on deconvolution microscope for measuring cell-adhesion properties of Green Fluorescent Protein macrophages on PEG copolymer library to screen as candidates for regenerative spinal cord biomaterial therapies.

TEACHING EXPERIENCE

Rutgers University Learning Resource Center
New Brunswick, NJ March 2000–June 2002

- Certified as Level 1-Tutor (group and one-on-one) in Calculus (I–V), Systems Physiology, and Statics.

Project BECK/Success in the Sciences
Piscataway, NJ June 2000–June 2002
- Prepared and taught weekly recitations in Systems Physiology for underrepresented undergraduate students pursuing medical careers at Rutgers University.

PUBLICATIONS

Wosnick, J. H.; **Liao, J. H**.; Swager, T. M. "Layer-by-layer Poly(phenylene ethynylene) Films on Silica Microspheres for Enhanced Sensory Amplification" Macromolecules 2005, 38, 9287-929.

Liao, J.H.; Swager, T.M. "Quantification of Amplified Quenching for Conjugated Polymer Microsphere Systems" Langmuir 2007, 23, 112-115.

Swager, T.M. ; **Liao, J.H.** "Emissive Compositions With Internal Standard and Related Techniques" PCT Filing (10/05/06).

PRESENTATIONS

Materials Research Society Meeting
Boston, MA December 2006
Oral Presentation: "Conjugated Polymer Particle Systems: Establishing Fidelity and Sensitivity Through Film Architecture for Monitoring Enzyme Activity"

Gordon Research Conference on Organic Thin Films
Newport, RI July 2006
Poster Presentation: "Conjugated Polymers as Biosensors: Improving Sensitivity with Film Architecture"

Materials Research Society Meeting
Boston, MA December 2005
Poster Presentation: "Amplified Quenching of Poly(phenylene ethynylene) Thin Films in Aqueous Environment for Biosensing Applications"

Congressional Visits Days
Washington, D.C. March 2006
Represented MIT student population and met with legislators on Capitol Hill to discuss new initiatives proposed for funding in science and engineering in the Federal Budget.

AWARDS

Recipient of National Science Foundation Graduate Fellowship Award, 2002–2005
Outstanding Achievement Award in Biomedical Engineering, June 2002
Edward J. Bloustein Distinguished Scholar, June 1998
Presidential Award of Academic Excellence, June 1998

MEMBERSHIPS

Golden Key Honor Society
Tau Beta Pi Honor Society
Materials Research Society
American Chemical Society

Acknowledgements

I am so grateful for all the support from people who really helped me throughout my time at MIT. I have so many fond memories, and here I'd like to share a few that stand out.

My first year at MIT was great. So much fun to learn polymer physics with David Nguyen, Ben Larman, Nick Tsui, Grace Kim, and of course having falafel lunch on the steps afterwards! Meeting Drew Satorius, Neil Kumar, and Nick Conway made those years so much fun too. DMSE socials are the best! Spending time with my PPST classmates made getting through quals a much easier and fun time. Lin Han really pushed me to memorize all the information, and Daeyeon Lee I really looked up to.

Of course, part of research is finding your research home. Joining the Swager group was such a delight. When it fits, you really know! I really have to thank Nate Vandesteeg and Debbie Mascaro for introducing me to the group and providing initial advice. Meeting Tim for the first time, I was impressed with his extreme enthusiasm and interest in research, and his affable and outgoing personality. I am deeply indebted to his kindness and his ever-persevering attitude about science! I thank him especially for shepherding me through the trials of graduate school and being a cheerleader when I needed it most. He has truly been a great advisor and mentor, and I will miss him as my boss.

And his research group reflects that.

My first meeting of Swagerites was with Jordan Wosnick and Gigi Bailey, both of whom I owe so much gratitude. I had the pleasure with working with Jordan on the layer-by-layer films and microspheres, which I inherited and continued for the rest of my thesis research. Jordan was always very generous with his knowledge, and it was clear that he was an expert in so many areas, both in and out of the lab. I really thank him for all of his positive encouragement, even since leaving the lab, with research and job searching. Gigi was positivity all the way, and continues to be a shining source. I am happy to have worked alongside her sunny personality, sharing benchspace and officespace, for just being able to turn to her and show my true silly self at times and for her to understand that. She is truly one of the nicest people I know, always willing to extend herself to help others. It was so natural and fun to brainstorm and to work together on the dendrimer quenching project.

Juan Zheng helped me with any contraption I wanted to build in the lab. We would scour the drawers together looking for toothpicks, epoxy, plastic, whatever, to make practical lab tools. I will always strive to be as neat and meticulous as Juan! I really had a great time with her discussing culture or just laughing at silliness and watching funny movies. I am so grateful for her friendship and support over the years. Her and Josh are two peas in a pod. I will forever buy them growing toys. Soon Josh will know more Chinese than me!

Kenichi Kuroda really helped me become acclimated to the laboratory. Even though he was already writing his thesis and on his way out, he was willing to help me out with my setting up. I enjoyed his humor, his humility, and his kind spirit. Only a few months we spent as labmates, but I learned this from him. He also showed me how to make gels for a class assignment in the most amusing way, and it was my first introduction into free radical polymerization. I am grateful for his continued enthusiasm and encouragement for my endeavors in polymer science.

Vanessa Perez and Rob Eaton, I shared benchspace with them in my first year. Although they didn't stay long in the group, I enjoyed the times we spent together. I'll never forget when Vanessa showed me her ring. Her and Paul are so much fun and such a great match!

As a young Swagerite, I really looked up to all the senior students. I thought Karen and Phoebe were so cool! Sam and John, they were both very knowledgeable and helpful with any questions I had, and just great to be around. It was so amazing to discover that Sam and my Nick both went to the same high school! Youngmi was so quiet when I first met her, but I soon realized how sweet and caring she was and continues to be. I always enjoy seeing and talking with her, and can't believe she has been a mom for so long. Paul Byrne, always so quiet, but always so nice. Ah, it was always a bit sad when someone graduated.

But of course, there are the people who you came with. The year I joined the group, these guys were also the new "freshmen". Andrew Satrijo, what a great guy. I am so happy we are both defending and starting work on the same day! He has really been a buddy with everything, and it has been great to share so many similar struggles together, especially when we became senior students. Thesis writing and job search help, and just someone great to talk to, I really owe to the support of Andrew. I feel so honored to DJ at him and Liz's wedding! The basement guys, Changsik Song and Zhihua Chen, although I rarely see them, when I do it is filled with smiles. Jean Bouffard, you are an extraordinary chemist! I enjoy your impeccable taste in fine cuisine, film, and of course music!

Postdocs often passed through our lab, and it was so great to learn of their experiences around the world. Paul Kouwer, the tall Dutchman, so cordial and full of life. I thank him for all his help and encouragement with my chemistry and all of my endeavors. He and Suzanne were the loveliest and the tallest couple (even taller than Gigi and Curtis!) to be around. Nick and I will visit in Holland as promised! Koushik Venkatesan, still here! I remember the first few days he came, so quiet and subdued, but soon the Koushik we know and love came out full force! I am always so grateful of his kindness and enthusiasm, providing a shoulder to lean on whenever needed and of course, fresh coffee in the a.m.! Lars Geiger and Guy Joly, I have to thank them both for providing me with the viologen quenchers and with helpful discussions on research throughout a pivotal time in my thesis research. And of course, soon-to-be Professor Anne McNeil! I have enjoyed so many wonderful hours with her running along the Charles, going to exercise classes, and just going to lectures together, discussing anything and everything. She has always strove to be part of what is important to so many people, and I know she will be an excellent advisor! I remember her very first week coming to my thesis proposal and giving some great feedback on my project. I am especially thankful for her support and advice as I struggled with my research and job search.

To the entire Swager group, I am so thankful for each and every day of creating a wonderful work environment. I wish everyone the best of luck in finishing strong! To the second years, Fei, Trisha, Julian, and Eric – just knowing you a short time, but I know you will be an amazing class! Thanks to Fei for practicing Chinese with me! And to Brett and Jeewoo – go team bio! Thank you especially to Becky Bjork, for keeping the lab in such tip-top shape, and being such a great person to sit next to! I enjoy your enthusiasm for life and am thankful for all the help you have given both in and out of the lab. Thank you to Kathy Sweeney, for being so sweet and helpful for setting up appointments, getting signatures, and helping me find a good thesis room!

I am also thankful for all the mentoring I have received throughout my years. Early thoughts for being an engineer were supported by my high school Physics teacher, Mr. Puglise, who gave me a copy of Feynman's lectures when I graduated. Who knew I would come to MIT then? I was happy to work alongside Dr. Hongbo Liu, who gave me my first experience in industry as well as providing impetus to pursue materials chemistry as a graduate student. At MIT, I am deeply thankful for the professors that have stood out and have taught me a great deal, and as such I selected my committee comprised of these great minds. I have enjoyed our collaboration with the Weissleder group at MGH, meeting Ralph and the other outstanding members, who remind me how much biology I have truly forgotten.

Thanks to all of my friends outside my lab that I have spent such good times with over the years. Grace Kim, I especially need to thank for helping me go through so many ups and downs in grad school and in life. I love her enthusiasm and positive energy, and I will miss grabbing lunch and chatting with her. I wish her all the best in finishing up here! To Katherine, Natalie, and Abby, my NY girls always on the run, but always there to support me and cheer me on. Janny, Arnel, and Jalil, I will be in Cali soon! And to Cantabrigians, Jonathan and the G-stone family, I will really miss you. Thanks for cultivating my music interest over the years! Sharie and Dave, thanks for being so awesome to live with in these final years of school. Sharie – we are Jersey girls forever! Jenny and Nick, my fellow chemists! When can we have Cuban again? Li – you are such a lovely spirit and such a great friend to talk to through all the transitions I have made here.

And in spite of not being so nearby, my family has supported me so much. I am inspired by my grandparents' stories and the challenges they have overcome to live in prosperity. I must learn Chinese much better to communicate and express to them how I sincerely feel. I am forever indebted for the love and encouragement of my mother and father, and my sister, even being so physically far apart over the years. As life brings many challenges, I feel blessed to be together with them in spirit. It is always a pleasure to reunite and spend time together! To my mom, I am officially now a doctor! Thank you for teaching me to have fun with everything I do, but still maintain discipline. To my dad, thank you for always supporting my decisions and bearing through my early childhood days to nurture and then help me grow as an independent person. I am happy that I make you so proud. This one really is for you and for our family. Thank you especially to Ruth, my one and only little sister, who never lets me forget that I always liked school and that science guy on TV that I don't even remember. I am so thankful for her, teaching me how not to write in the passive voice, and reminding me that I remind her of a "mad scientist"! I am so proud of her journalistic passion and enduring spirit.

Especially, I am thankful for Nick being a part of my school life. Our friendship began in my first year at MIT, and was cultivated through the early years with fun times. Thank my lucky stars, it grew into something so amazing! I am so happy to share with him my passions, my struggles, and my vision for life. Who knew there was someone so in tune with me? Thank you to Nick for helping to motivate me to accomplish this in my life. I look forward to being your strength in your future endeavors, and will always be smiling back at you.